Improvement in burning velocity models for hydrogen in the gas explosion simulator FLACS

By

Hui Huang

Master of Science Thesis in

Process Safety Technology

Department of Physics and Technology

University of Bergen

04.2021

Acknowledgments

First and foremost, I would like to thank my supervisor, Professor Bjørn Johan Arntzen, for his guidance on the topic of burning velocity, patience explanation of all my questions related to thesis build-up, detailed discussion, and quick feedback on study work.

I want to acknowledge Melodia Lucas Perez from Gexcon AS for her support, valuable discussions, help in the implementations of FLACS simulation and thesis writing. Furthermore, I would like to extend a big thank you to Wanchun Liu from Gexcon AS, who has contributed with problem-solving when FLACS has not worked as desired.

I would like to express gratitude to Professor Trygve Skjold and Pawel Jan Kosinski for their lessons on explosion hazards in the process industry and fluid mechanics, giving me background knowledge relative to this thesis.

Finally, I would like to give sincere thanks to my parents, and local friends in Bergen for their encouragement, support to maintain me in the fight for all these times.

Abstract

The properties of hydrogen differ significantly from hydrocarbons, such as methane and propane. Due to the low ignition energy, wide flammability range, high thermal diffusivity, and significantly higher burning velocity, hydrogen-air combustion has a higher potential risk of transferring into hydrogen explosions resulting from pressure build-up during the combustion process. The magnitude of the pressure rise depends strongly on the combustion rate, which can be determined by burning velocities that describe factors such as the reactivity of the fuel-air mixtures and properties of the reactive flow.

The CFD tool FLACS is used for engineering calculations related to process safety applications, such as consequence modelling for gas explosions in industrial facilities. The burning velocity models utilized in FLACS are validated with the extensive large-scale experiments of hydrocarbons, and therefore the simulations results are highly representative and reliable for hydrocarbons. In contrast, the simulation for mixtures involving hydrogen is less appropriate due to hydrogen´s unique physicochemical properties. Consequently, modelling burning velocities for hydrogen combustion can be improved to simulate hydrogen explosions with better accuracy.

This research focuses on constructing representative models for thermal conductivity, thermal diffusivity, Lewis number, and chemical time scale for gas mixtures. These models shall be used in prediction models for laminar and turbulent burning velocities utilized in FLACS to simulate gas explosions. The models are validated against experimental values for burning velocities.

Based on this thesis´s work, the models for laminar and turbulent burning velocities as a function of thermal diffusivity, Lewis number effect, and chemical time scale result in better prediction values with higher accuracy. In present FLACS, the turbulent burning velocity in hydrogen explosions is a function of laminar burning velocity and a Lewis number correction. In the new model for turbulent burning velocity, the dependence of Lewis number is avoided, which would be critically important for predicting turbulent burning velocities for mixtures of hydrogen and hydrocarbons and at elevated pressures.

Contents

Nomenclature

Latin letters

A	Pre-exponential factor	$[s^{-1}]$, $[m^3/mol \cdot s]$
A_{Le}	Correction constant for Le calculation	-
c	Molar concentration	$[mol/m^3]$
C_1, C_2	First and second constant for λ calculation	-
C_3, C_4	First and second constant for C_p calculation	-
C_K	Constant for estimation of K	-
C_p	Specific heat capacity at constant pressure	$[J/kg \cdot K]$
C_{QL}	Constant for estimation of S_{QL}	-
C_{ST}	Constant for estimation of S_T	-
D	Mass diffusivity	$[m^2/s]$
F	Fuel	-
K	Karlovitz strain rate	-
Le	Lewis number (dimensionless)	-
l_I	Integral length scale	$[m]$
m	Mass fraction	-
M	Molecular weight	$[g/mol]$
Ma_{sr}	Markstein number	-
n	Mole fraction	-
O	Oxidant	-
P	Pressure	$[Pa]$
R	Universal gas constant or flame radius	$[J/K \cdot mol]$ or $[m]$
Re_T	Turbulent Reynolds number	-
S_f	Flame speed	$[m/s]$
S_g	Flow velocity of unburned gases	$[m/s]$
S_L	Laminar burning velocity	$[m/s]$
S_{QL}	Quasi-laminar burning velocity	$[m/s]$
S_T	Turbulent burning velocity	$[m/s]$
S_u	Laminar burning velocity	$[m/s]$
T	Temperature	$[K]$
T_A	Activation temperature	$[K]$
T_i	Initial temperature	$[K]$
T_P	Product temperature	$[K]$
u'	Turbulent velocity fluctuation	$[m/s]$
v	Volume fraction	-
V	Volume	$[m^3]$
w	Reaction rate	$[s^{-1}]$
$\dot{w}$	Reaction rate in terms of concentration	$[mol/s]$
x	Mole/volume fraction	-
y	Mass fraction	-

Greek letters

α	Thermal diffusivity	$[m^2/s]$
β_z	Zeldovich number	-
ρ	Density	$[kg/m^3]$
λ	Thermal conductivity	$[W/m\,k]$
ν	Kinematic viscosity	$[m^2/s]$
τ_c	Chemical timescale	$[s]$
ϕ	Equivalence ratio	-

Subscript

A	Abundant reactant
D	Deficient reactant
i	ith species
L	Laminar
P	products
T	Turbulent
$actual$	Actual mixture
eff	Effective
mix	Mixture
$pred$	Prediction
$stoich$	Stoichiometric mixture
z	Zeldovich

Superscript

α	Power exponent for temperature
β	Power exponent for pressure, exponent of K in S_T
0	Reference conditions
Max	Maximum
St	Stoichiometry

Abbreviations

AIT	Auto Ignition Temperature
CFD	Computational Fluid Dynamic
CNG	Compressed Natural Gas
ER	Equivalence Ratio
FLACS	Flame Acceleration Simulator
IEA	International Energy Agency
LFL	Lower Flammability Limit
LPG	Liquefied Petroleum Gas
MIE	Minimum Ignition Energy
MIT	Minimum Ignition Temperature
NTP	Normal temperature and pressure
MP	Monitor Point
UFL	Upper Flammability Limit

List of Figures

List of Tables

1 INTRODUCTION

This chapter presents the motivation, objective, and organization of this thesis.

1.1 Motivation of the thesis

With expanding population and industrial activities, global energy consumption has grown rapidly over the past centuries. The rising demand for fuel, such as coal, oil, and natural gas, brands the trends of higher living standards and longer livelihoods. However, a sharp rise in fossil fuel consumption leads to increasingly emit greenhouse gases resulting from global climate change and other health & environmental challenges. A better system of clean energy transitions such as emission reduction should be in-depth promotion to cope with these challenges. Apart from the replacement of fossil fuel that emits greenhouse gases with renewable sources such as solar and wind, hydrogen can be another approach because it produces no direct emissions of pollutants or greenhouse gases. As International Energy Agency (IEA) reported in 2019, the demand for pure hydrogen has grown more than threefold in the past 43 years between 1975 and 2018, and the demand is rising continually.

Hydrogen is the most abundant element in the universe, and it exists in a gaseous form at room temperature and atmospheric pressure. As an energy carrier, it has various usages in four sectors mainly today, including industry (e.g., oil refining), transport (e.g., hydrogen fuel cell electric vehicles), buildings (e.g., hydrogen heating boiler) and power generation (e.g., hydrogen gas turbine). All these usages are implemented by hydrogen combustion. As an exothermic chemical reaction, hydrogen combustion has a high potential risk of transition into an explosion resulting from pressure build-up during combustion process. The magnitude of the pressure rise depends strongly on the rate of combustion, which can be determined by factors such as the reactivity of the fuel-air mixtures, and properties of the reactive flow.

Laminar burning velocity (S_L) is a physicochemical property of premixed fuel-oxidant mixtures resulting from the combined influence of the mixture diffusivity, exothermicity, and reactivity (Forman, 1984; Law, 2010). Turbulence forms under laminar flame propagation,

and it strongly affects the burning velocity, which is transferred from laminar to turbulent. Hence, turbulent burning velocity (ST) dominants the combustion rate. Consequently, considering burning velocities (both laminar and turbulent) of hydrogen-air combustion is very important for determining the combustion rate and further determining the consequences of explosion related to the hydrogen combustion. In contrast with hydrocarbons, the consequences of explosion relative to hydrogen-air mixtures are much more severe. The hazard primarily comes from its low ignition energy, a wide range of flammability, high thermal diffusivity, extremely fast burning velocities, and the considerable amount of energy released when hydrogen burns and explodes (Astbury, 2008). Hydrogen safety considerations must be accounted for in the process industry, where hydrogen is used as an energy carrier.

FLACS (Flame Acceleration Simulator) is a commercial computational fluid dynamic (CFD)-based tool specializing in the modelling of gas explosion for process safety and risk assessment. The combustion models utilized in FLACS are validated with extensive large-scale natural gas experiments, and therefore the simulations for hydrocarbons are highly representative and reliable. Whereas the simulation for mixtures involving hydrogen is less accurate because of, e.g., inappropriate Lewis number correction applied for hydrogen. Therefore, models for combustion related to hydrogen should be improved in FLACS to simulate hydrogen explosions with better accuracy.

1.2 Objectives of the thesis

The thesis's work focuses on constructing representative models for thermal conductivity, thermal diffusivity, Lewis number, and chemical timescale for gas mixtures. These models shall be used in improved models for laminar and turbulent burning velocities used in the CFD code FLACS to simulate gas explosions. This thesis's primary focus will be on hydrogen-air mixtures at a range of hydrogen concentrations and initial pressures and temperatures. The models are validated against experimental values for burning velocities.

1.3 Organization of the thesis

This thesis's remainder details the procedure of modelling build-up for laminar burning velocity and turbulent burning velocity, results of the new model application, and conclusions reached.

Chapter 2 collects and organizes fundamental theories and previous studies relating to laminar burning velocity and turbulent burning velocity. The basic concept of the burning velocity model utilized in FLACS also includes in this chapter.

Chapter 3 detail builds up mathematical models related to determining laminar burning velocity and turbulent burning velocity in the hydrogen-air mixture—the relative parameters specified separately for the laminar burning velocity model and the turbulent burning velocity model.

Chapter 4 presents the laminar burning velocity models testing for hydrogen-air combustion at ambient conditions. A representative SL prediction model is selected and utilized to calibrate the S_T model, which is then estimated by thermal diffusivity, chemical time scale, turbulent fluctuation velocity, and turbulent integral length scale for comparison with the FLACS model and experimental data from preview work. Results obtained with discussion.

Chapter 5 provides conclusions reached in this study as well as suggestions for future work.

2 BASIC THEORY

This chapter presents the relevant basic concepts of combustion properties, laminar and turbulent burning velocities, and burning velocity model in FLACS.

2.1 Combustion

Combustion, in nature, is a chemical reaction between a fuel and an oxidant to form oxidized products. External energy must be supplied to initiate the combustion, and once it starts, the released heat may provide energy to make combustion self-sustaining. Combustion is usually accompanied by the generation of heat and light, resulting in a flame. The flame can be classified into a premixed flame that is generated by initiating a well-mixed fuel and oxidant before combustion and a non-premixed flame caused by combustion that coincides with the mixing of fuel and oxidant.

This thesis focuses on premixed combustion since gas explosion occurs after the mixing of fuel and oxidant. Four requirements should mainly be fulfilled for premixed combustion to occur. They are the presence of fuel, oxidant, proper mixture concentration, and ignition.

2.1.1 Fuel

All types of substances that carry energy in physical or chemical form can be chosen as the fuel used in the combustion process. Based on the substance's physical state, fuel can be classified into three categories: gaseous fuels, liquid fuels, and solid fuels. Examples for these three categories are listed in Table 2.1.

Table 2.1: Examples for fuel corresponding to each category (Law, 2006)

Fuel type	**Representative components**
Gaseous fuel	Light hydrocarbons (e.g., methane), hydrogen, CNG, etc.
Liquid fuel	Heavy hydrocarbons (e.g., naphtha), LPG, ethanol, etc.
Solid fuel	Wood, coal, carbon, metals, etc.

2.1.2 Oxidant

A substance that can oxidize other chemical species can be chosen as an oxidant. The typical oxidant used in a combustion process is oxygen, either pure oxygen or oxygen in the air. According to the CRC Handbook of Chemistry and Physics (97th edition, 2016-2017), dry air in Earth's atmosphere comprises 78.09% nitrogen, 20.95% oxygen, 0.93% argon, 0.04% carbon dioxide, and small amounts of other gases by volume. This thesis assumes that normal air contains 79 vol% nitrogen and 21 vol% oxygen, no CO2 and water vapor in the normal air, and argon is nitrogen. In FLACS, the composition of the air is 79.05 vol% nitrogen and 20.95 vol% oxygen.

2.1.3 Mixture composition

Premixed combustion undergoes alone with fuel concentration in oxidant lying within well-defined bounds. If the mixture gases' fuel concentration is lower than the bound, the mix between the fuel and the oxidant is too weak to ignite. Meanwhile, if the fuel concentration is above the bound, the mix is too ¨fat¨ to spark. Combustion can be generally distinguishable by the content of the fuel. The representative terms relative to this requirement are flammability limits and equivalence ratio.

Flammability limits

Flammability limits refer to lower flammability limit (LFL) and upper flammability limit (UFL). LFL is the minimum concentration of a flammable gas that will propagate flame when exposed to an ignition source. UFL is the maximum concentration of the fuel for flame propagation. The range of LFL and UFL differ for various gasses and is defined by experimental determination. By contrast, the lower flammability limit is usually the ¨more important¨ limit or the critical parameter determining if the combustion is in progress.

Equivalence ratio

The equivalence ratio, ϕ, is defined as the actual fuel-air ratio to the combustion's stoichiometric fuel-air ratio. Accordingly, as shown in Equation (2.1), the equivalence ratio can be calculated under mass basis, volume basis, or mole basis.

$$\phi = \frac{(m_{fuel}/m_{air})_{actual}}{(m_{fuel}/m_{air})_{stoich}} = \frac{(v_{fuel}/v_{air})_{actual}}{(v_{fuel}/v_{air})_{stoich}} = \frac{(n_{fuel}/n_{air})_{actual}}{(n_{fuel}/n_{air})_{stoich}} \quad (2.1)$$

The equivalence ratio higher than one represents excess fuel in the mixture that would be required for complete combustion, irrespective of the fuel and air being used. The equivalence ratio less than one represents a deficiency of fuel or equivalently excess air in the mixture. The fuel-air mixture, therefore, can be classified into three categories, as shown in Table 2.2.

Table 2.2: Fuel-air mixtures classified by ER

Fuel-air mixture	**Equivalence ratio (ER)**
Lean	$\phi < 1$
Stoichiometric	$\phi = 1$
Rich	$\phi > 1$

2.1.4 Ignition

Ignition occurs due to local heating of combustible mixtures to the point where a sufficiently large volume reaches the auto-ignition temperature (AIT) of the fuel, and chemical reactions are initiated (Astbury et al., 2007). Ignition is a process of providing energy that is required to trigger combustion. A portion of the combustible mixtures is heated first to a sufficiently high temperature such that adjacent un-combusted layers also react. Each point of the burning layer serves as an ignition source for the next adjacent layer, and so on.

Minimum ignition energy (MIE) and minimum ignition temperature (MIT) are two basic sensitivity ignition parameters. The former one is the minimum energy that is required to ignite a fuel-oxidant mixture successfully. The latter is the lowest temperature at which a fuel must be heated to initiate combustion or combustion to self-sustain. They differ for various gasses and are defined by experimental determination.

2.2 Properties of Hydrogen

Hydrogen combustion occurs where gaseous hydrogen oxidizes to produce water vapor with the release of chemically bound energy into heat. The total chemical reaction for this process involves a sequence of elementary reactions, many related to atoms or radicals, which are short-lived species with high reaction rates. The overall chemical Equation under stochiometric condition can be expressed as follows

$$2H_2(g) + O_2(g) + \frac{79}{21}N_2(g) \rightarrow 2H_2O(g) + \frac{79}{21}N_2(g) + heat \qquad (2.2)$$

According to Risto (1997), the hydrogen-air gas explosion can be expressed as a rapid increase of pressure (pressure build-up) resulting from an expansion of energy which is produced by the combustion of premixed hydrogen and air. Pressure build-up depends strongly on combustion properties determined by the physical and chemical properties of the fuel.

Physical properties of hydrogen

Diatomic molecules form hydrogen with the formula H2. At normal temperature and pressure (NTP), hydrogen is a colorless, odorless, tasteless, and non-toxic gas. At atmospheric pressure, hydrogen is a liquid when the temperature is below its boiling point, that is -252.76 ℃ (20.39 K), and it is a solid for temperature lower than -259.16 ℃ (13.99 K).

The molecule of hydrogen exists in two forms distinguished by the relative rotation of the individual's nuclear spin atoms in the molecule (spin isomers). As shown in Figure 2.1, molecules with spins oriented in the same direction (parallel rotation) are ortho hydrogen, and molecules with spins in the opposite direction (anti-parallel rotation) are para hydrogen.

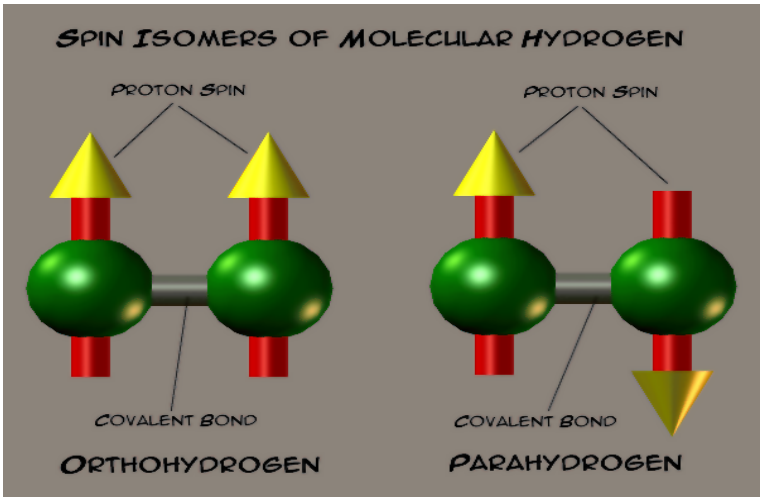

Figure 2.1: Ortho- and para hydrogen (Jim Farris, 2010)

Normal hydrogen is a mixture of these two forms, and the temperature determines the equilibrium quantities of each form. Normal hydrogen is formed by 75% ortho hydrogen and 25% para hydrogen at room temperature and above. The para hydrogen ratio increases with the decrease of temperature and a dramatic increase trend observed for temperatures lower than 160 Kelvin, as shown in Figure 2.2.

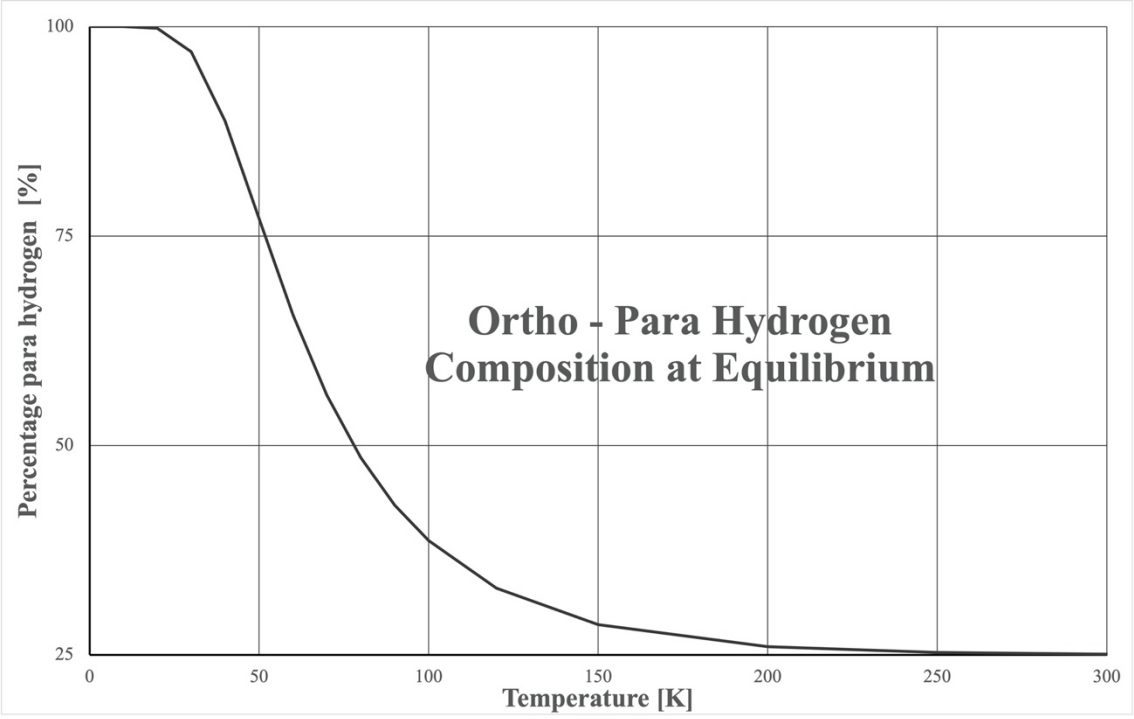

Figure 2.2: Percentage para hydrogen (Woolley et al., 1948)

Due to the difference of para hydrogen content in normal hydrogen, the specific heat capacity and thermal conductivity of hydrogen will vary when temperature decreases to its normal boiling point. Thus, the different thermal diffusivity patterns and specific heat capacity obtained for normal hydrogen during temperature decreasing.

As a result of small molecular weight (2.016 g/mol) and a low viscosity ($8.948 * 10^{-6}\ Pa \cdot s$, at NTP), hydrogen can permeate through materials and pass through smaller leak paths as compared to other gases. Hydrogen gas would escape faster through the leakage comparing with other gases. For example, for the same size of leak path, hydrogen would leak about 2.8 times faster than methane (Cracknell, et al., 2002).

Hydrogen is approximately 14 times less dense than air at NTP, and it has greater diffusivity than other gases. If a leak occurs, hydrogen has a higher propensity to diffuse and form an ignitable mixture with ambient air. The high molecular diffusivity of the hydrogen into the air improves the mixture uniformity and combustion efficiency. In an unconfined area, the hydrogen-air mixture would easily dilute to a level below the lower flammability limit and cannot ignite by any ignition sources. However, the mixture can accumulate in confined areas (both partially and fully), and combustion can be initiated by available ignition sources (Maha, 2020).

Hydrogen has high buoyancy, affecting flame propagation and acceleration for hydrogen-air combustion (Middha, 2010). Hydrogen possesses a higher tendency for a flame to propagate upwards than downwards, resulting from the buoyancy effect. Buoyancy exerts an upward force on the cold reactants propagate into hot combustion products leading to flame instabilities and enhanced flame acceleration.

Chemical properties

The flammability range for hydrogen is between 4% and 75% by volume of concentration in the air (Lewis and von Elbe, 1987). Generally, the flammability range widens with higher temperatures and falls with pressure (up to 20 bars) for hydrogen (Taylor, 1991). Figure 2.3 shows the dependence of flammability limits on temperature. The range of limits linearly increase with temperature from 20 degrees Celsius to 400 degrees Celsius at atmospheric pressure. Meanwhile, Figure 2.4 shows the dependence of flammability limits on pressure.

The pressure dependence of the flammability limits shows a remarkable anomaly. The LFL increases with increasing initial pressure up to 50 bars at temperature equals 20 ℃. The UFL decreases for initial pressure lower than 20 bars or higher than 50 bars. It increases for initial pressure ranges between 20 bars and 50 bars.

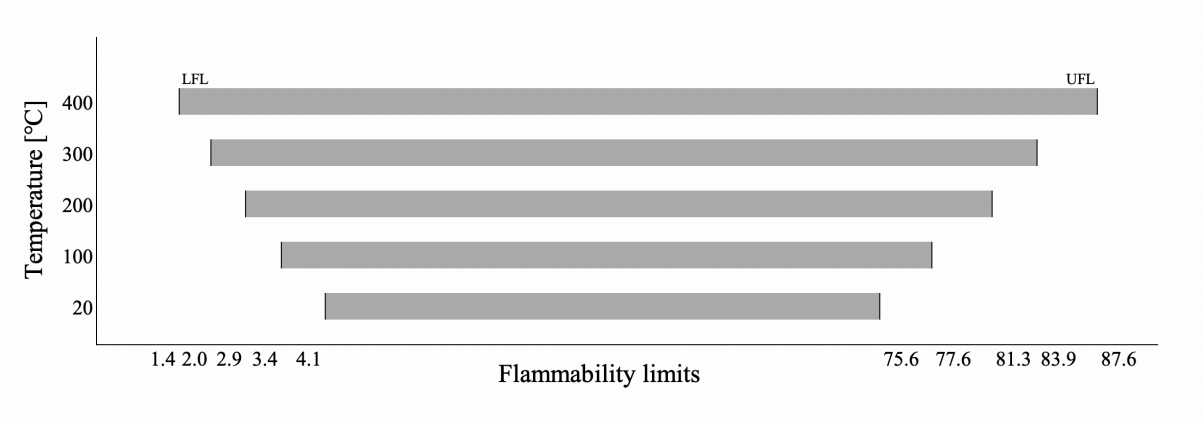

Figure 2.3: Flammability limits dependence on temperature (Gasse, 1992)

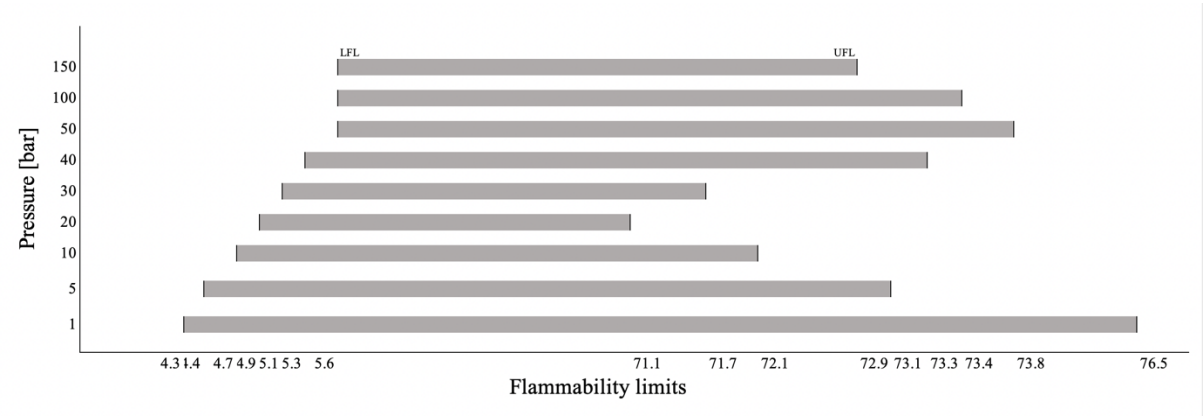

Figure 2.4: Flammability limits dependence on pressure (Schroeder, 2003)

The minimum autoignition temperature for hydrogen is 520 K. It is relatively lower than that of methane, that is 540 K. The ignition energy for hydrogen is relatively low, and it is about one order of magnitude lower than other fuels, e.g., methane. The minimum ignition energy for hydrogen is about 0.011- 0.017 mJ if the mixture is ignited by an electric spark (Bjerketvedt, et al., 1997). It is much lower compared with that of methane, 0.28 mJ. Hydrogen is extremely sensitive to ignition than the other flammable materials regarding its lower ignition energy and minimum ignition temperature. The mass-related energy density of

hydrogen is very high. One kilogram of hydrogen contains 142 MJ, which is approximately 2.5 times more energy than is contained in 1 kilogram of natural gas (Maher, 2020).

Hydrogen has a burning velocity about seven times faster than that of natural gas, which gives higher product temperature and smaller quenching gap (e.g., 0.64 mm for a stoichiometric hydrogen-air mixture at NTP), and a higher tendency of transition between combustion and explosion for a hydrogen-air mixture. According to Biennial Report on Hydrogen Safety (HySafe, 2007), a stoichiometric burning hydrogen-air mixture's maximum product temperature is 2400K observed at an equivalence ratio slightly higher than one at 25 ℃ and 1 atm. The laminar burning velocity of the stoichiometric hydrogen-air mixture would be about 2.2 m/s, and the maximum burning velocity, that is about three m/s, comes with a hydrogen concentration in 42 vol% or $ER = 1.7$.

2.3 Laminar burning velocity

As one of the most critical parameters of a combustible mixture, the burning velocity describes flame propagation rate. After combustion is initiated, the flame front starts propagating outwardly through the unburned mixtures. Depending on flame flow conditions, flame propagation can either be laminar or turbulent. Laminar flame in practical cases is formed first. The laminar burning velocity (SL) can be defined, following Law (2006), as the velocity at which a laminar, steady, plane, unstretched, adiabatic flame freely propagates relative to the unburned premixed gas in the direction normal to the flame front. A one-dimensional combustion model can be derived for the laminar burning velocity determination. Eckhoff (2016) illustrated the laminar burning velocity (S_u) for a planar laminar flame as a function of flame speed (S_f) and unburned gas flow velocity (S_g), as shown in Figure 2.5. S_f is defined as the rate of the flame front propagation relative to an absolute reference point. The flow velocity of unburned gases describes the unburned gas's moving rate ahead of the flame (Bjerketvedt, et al., 1997).

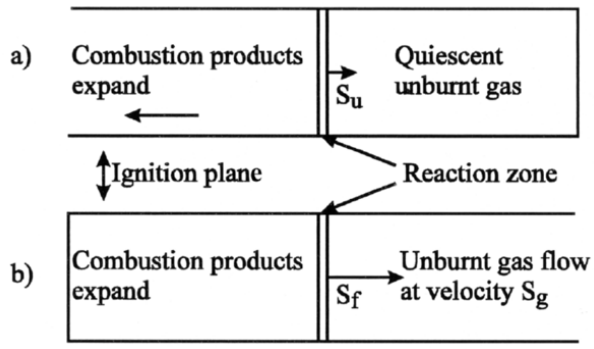

Figure 2.5: One-dimensional tube system for modelling premixed fuel-air combustion with a plane laminar flame (Eckhoff, 2016)

The combustion undergoes at constant pressure and is specified as idealized adiabatic with no heat loss, no buoyancy, and no interference by the wall of the tube. Suppose the gas mixture is ignited in the open end of the tube (2.5 a). In that case, the combustion products will propagate freely into the tube's left side's ambient atmosphere. The magnitude of the laminar burning velocity will be the same as the magnitude of flame speed observed to the tube wall. Suppose the ignition occurs in the closed end of the tube (2.5 b). In that case, the combustion products will propagate in the same direction of flame propagation from the left to the right side of the tube. The laminar burning velocity will be the difference between flame speed and flow velocity of unburned gases. Therefore, the laminar burning velocity can be obtained either directly from the experimental measurement or extracted from measurements with proper data processing. Accurate measurement and prediction of laminar burning velocity are important for characterizing premixed combustion properties of fuel and calibration of turbulent combustion models.

2.3.1 Experimental measurement for laminar burning velocity

Extensive experiments have been carried out to investigate and determine the laminar burning velocity for gaseous mixture combustions since the first recorded estimation of a methane-air flame's burning rate in 1815 by Sir Humphrey Davy (Taylor,1991). Generally, the experimental measurement of laminar burning velocity can be categorized either in propagating flames or in the stationary flame (Rallis and Garforth, 1980). Different methods

have been utilized relative to these two approaches, and examples of the methods are shown in Table 2.3.

Table 2.3: Different methods for laminar burning velocity measurement

Measurement approach	**Corresponding methods**
Propagation flames	Tube; soap bubble; spherical bomb
Stationary flames	Bunsen burner; flat flame burner

The research on the measurement of the laminar burning velocity in hydrogen-air mixture can be traced back to 1889 when Michelson measured the laminar burning velocity in hydrogen-air mixtures at room temperature and atmospheric pressure on the inner surface of a Bunsen burner. In the past century, quantitative experiments have been carried out to measure the values of laminar burning velocities for hydrogen-air mixtures. The S_L resulted from experiments differs with various measurement methods. The discrepancies have also been observed in the experiments utilizing the same method. The experimental data shown in *Table 2.4* represent these discrepancies in the maximum laminar burning velocity (S_L^{max}) and laminar burning velocity for the stoichiometric mixture (S_L^{st}) in hydrogen-air mixtures for two different measurement methods at room temperature and atmospheric pressure.

Table 2.4: Experimental data on measured laminar burning velocities in hydrogen-air mixtures at room temperature and atmospheric pressure

Method	Author	Year	H_2 vol%	S_L^{st} $[cm/s]$	S_L^{max} $[cm/s]$
Burner	Michelson	1889	15.3 – 74.6	217	281
	Jahm	1934	30 – 75	187	267
	Fine	1956	28 – 62	193	304
	Heimel	1956	28 – 57	206	297
	Senior	1961	17.4 – 33	200	-
	Gunther and Janisch	1972	15 – 70	282	355
	Koroll, Kumar, Bowles	1993	8 – 70	250	340
	Pareja and co-authors	2010	25 – 56	236	316
Spherical bomb	Manton and Milliken	1956	30 – 70	232	300
	Iijima and Takeno	1986	17.4 – 62.7	238	298
	Dowdy, Smith, Taylor	1990	9 – 68	213	286
	Faeth and co-authors	1998	16 – 56	210	246
	Law and co-authors	2000	14 – 63	190	282
	Verhelse and co-authors	2005	11 – 30	224	-
	Kuznwraov and co-authors	2012	10 – 70	209	287
	Krejci and co-authors	2013	17– 68	218	284

100 cm/s difference has been obtained for the experimental value of S_L^{max} and S_L^{st} presented in Table 2.4 both between two methods and within the same method. For example, the lowest value of S_L^{max} is 246 cm/s resulting from spherical bomb method, while the highest is 355 cm/s given by the burner method. The lowest and highest values of S_L^{st} are 187 cm/s and 282 cm/s, respectively resulting from the burner method. Practically it is unfeasible to direct implementation of the SL definition for its measurement since it requires creating an infinite and perfectly planar flame. Under the experimental procedure, the flame will be affected by non-quiescent unburned gases resulting from thermal expansion, the interaction between flame and wall, and buoyancy effects (Lewis and von Elbe,1934). Data processing would be another reason for the discrepancies. For example, the stretch correction model is probably the most critical effect on laminar burning velocities derived from spherical bomb methods

(Egolfopoulos et al., 2014). The laminar burning velocity is an essential parameter of the flame since it is practically needed to assess various flame phenomena such as flame stabilization and turbulent flame propagation (Tse et al., 2000). The experimental measurement results validate detailed reaction mechanisms, simplified kinetic models, and corrected prediction model results.

2.3.2 Numerical prediction model for laminar burning velocity

Theoretically, it is possible to model the laminar burning velocity. Thermal theories, diffusion theories, and comprehensive theories are used initially to model laminar flame propagation (Turns, 1999). The first two theories predict the laminar burning velocity as a function of thermal diffusivity or mass diffusion of the unburned mixtures and reaction rate with many assumptions and easy reaction mechanisms. The comprehensive theories determine laminar burning velocity through the steady-state comprehensive mass, species, and energy conservation equations with a complete reaction mechanism for the fuel-oxidant system, specifying the energy release.

From detailed theoretical analysis, both thermal and comprehensive theories, the dependence of laminar burning velocity on thermal diffusivity and reaction rate can be expressed as follows (Glassman et al., 2014)

$$S_L = (\alpha * \frac{\dot{\omega}}{\rho})^{1/2} = (\frac{\lambda}{\rho * C_p} * \frac{\dot{\omega}}{\rho})^{1/2} \tag{2.4}$$

where α, λ, ρ, C_p and $\dot{\omega}$ specify the thermal diffusivity, thermal conductivity, density, specific heat capacity at constant pressure and reaction rate in terms of concentration, respectively. The first four parameters are the properties of unburned gas mixtures. The last one refers to the overall reaction rate for fuel-oxidant system. The laminar burning velocity can also be expressed with the chemical time scale, τ_c, that presents the reactivity of the chemical reaction. The chemical time scale is inversely proportional to reaction rate. The expression for chemical time scale can be presented as

$$\tau_c = \omega^{-1} = (\dot{\omega}/\rho)^{-1} \tag{2.5}$$

Combining with Equation (2.4), S_L can be modelled according to

$$S_L = (\alpha * {\tau_c}^{-1})^{1/2} \tag{2.6}$$

Based on the study of Law (2006), the reaction rate can be determined with expression as

$$\omega = k(T) * \prod_{i=1}^{N} c_i^{n_i} \tag{2.7}$$

where c_i is the molar concentration of species i. n_i is the power exponent coefficient to the i^{th} species. It indicates the influence of the concentration of the i^{th} reactant on the reaction rate. $k(T)$ is the reaction rate coefficient, and it can be estimated following Arrhenius approximation as

$$k\ (T) = A * e^{[-E_a/(R*T_P)]} \tag{2.8}$$

with A is the pre-exponential factor, E_a is the activation energy, and R is the universal gas constant. T_P refers to the product temperature. With $T_a = E_a/R$, reaction rate for fuel-oxidant system can be instead represented with the activation temperature (T_a) as

$$\omega = A * c_F^{n_F} * c_O^{n_O} * e^{(-T_a/T_P)} \tag{2.9}$$

where subscripts F and O refer to fuel and oxidant, respectively. The two expressions for laminar burning velocity mentioned above are suitable for the condition of unity Lewis number, Le, which is a measure of the relative influence of thermal to mass diffusion of the deficient reactant ($Le = \alpha/D$). However, there will be a deviation of Lewis number from the unity on account of the flame propagation process resulting from the thermal-diffusive instability (Law, 2006). Thus, Lewis number should be included into the numerical model of laminar burning velocity for a complete description of flame propagation, and the Equation (2.6) can be modified as

$$S_L = (\alpha * Le * {\tau_c}^{-1})^{1/2} \tag{2.10}$$

2.3.3 Effect parameters on laminar burning velocity

As an experimental measurement parameter, the laminar burning velocity depends highly on the initial experimental conditions, such as pressure, temperature, and mixture composition of the unburned gases. The laminar burning velocity depends strongly on the type of fuel and oxidant tested in the experiments. Distinctive physical and chemical properties concerning the using fuel and oxidant specify the laminar burning velocity. The relations between S_L and these dependent parameters help validate and modify numerical prediction models to improve the accuracy of estimation results.

Initial temperature and pressure

Generally, laminar burning velocity magnitudes rapidly with an increase of initial temperature and slightly with the pressure change. The dependence on initial temperature and pressure of laminar burning velocity can be quantified by the empirical correlations between S_L, T and p. The total correlation for temperature dependence and pressure dependence can be expressed in the form as

$$\frac{S_L}{S_L^0} = (\frac{T}{T^0})^{\alpha} * (\frac{p}{p^0})^{\beta} \tag{2.11}$$

where S_L^0 denotes the laminar burning velocity at reference conditions of temperature (T^0) and pressure (p^0), and S_L the laminar burning velocity at arbitrary conditions of temperature (T) and pressure (p). The superscripts α and β are power exponents coefficients to temperature and pressure. These two power exponents are extracted from the experiments demonstrating the effect of temperature and pressure on the burning velocity. Therefore, they vary with the experimental method and the way chosen to process experimental data. For example, Liu and MacFarlane (1983) proposed linear correlations below and above the maximum of the burning velocity in hydrogen-air mixtures as a function of x_{H2} with the junction value of $\alpha = 1.571$. Iijima & Takeno (1986) measured the effects of temperature and pressure on the laminar burning velocity in hydrogen-air mixtures with ER varied from 0.5 to 4.0 at temperature between 291 K to 500 K and pressure between 0.5 atm to 25 atm. Two correlation equations presented for α and β as follows

$$\alpha = 1.54 + 0.026 * (\phi - 1) \quad (2.12)$$

$$\beta = 0.43 + 0.003 * (\phi - 1) \quad (2.13)$$

FLACS represents the dependence of laminar burning velocity in hydrogen-air mixtures on the initial temperature and pressure with values of 1.574 and -0.035, respectively.

Equivalence ratio and fuel concentration

The laminar burning velocities increase on the lean side of the mixture and decrease on the rich side of the mixture. Generally, the maximal laminar burning velocity is slightly on the rich side, where the highest product temperature is obtained at room temperature and atmospheric pressure. Based on the study of Dirrenberger et al. (2011), the laminar burning velocity for methane, propane, and ethane peaks at $ER = 1.1$. For hydrogen, the maximum laminar burning velocity was obtained for $ER \approx 1.7$, as shown in Figure 2.6. The dependence of S_L on hydrogen fraction by volume is also presented in this figure. All the symbols refer to the experimental data of laminar burning velocities in hydrogen-air mixtures measured at room temperature and atmospheric pressure. The laminar burning velocity is a vital function of hydrogen concentration varying from a maximum value of around three m/s at 42 vol% hydrogens to less than two cm/s near the lower flammability limit at four vol% hydrogens.

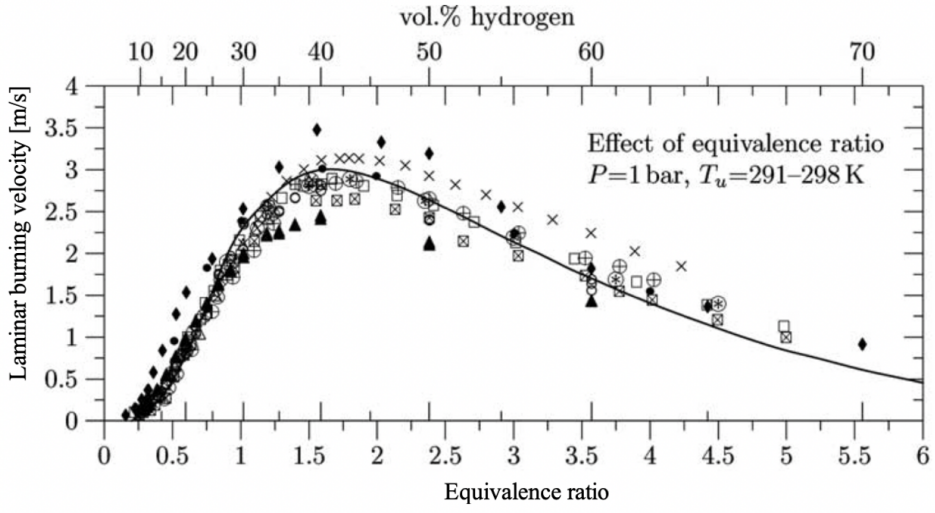

Figure 2.6: The laminar burning velocity of hydrogen-air mixtures depend on volumetric hydrogen concentrations and equivalence ratios (Dahoe, 2005)

Product temperature

The product temperature is the temperature that reached the state of chemical equilibrium in a chemical reacting system of combustion, and the energy balance determines it. For a fixed type of work interaction between the system and the surrounding environment, an adiabatic system has the highest product temperature since there is no energy loss from the system to the surrounding environment. All the energy released from the chemical reaction is used to heat the products. The product temperature exerts a dominant influence on the laminar burning velocity through the reaction rate, as illustrated in Equations (2.9). The higher the product temperature, the higher the laminar burning velocity. At ambient condition, the maximum product temperature for stoichiometric mixtures of methane-air is 2210 K, and for stoichiometric mixtures of hydrogen-air is 2400 K (Glassman et al., 2014). At ambient condition, the maximum laminar burning velocity for stoichiometric methane-air flames is around 36 cm/s, and for stoichiometric hydrogen-air flames is around 300 cm/s (Hermanns, 2007).

Pre-exponential factor and activation temperature

Figure 2.7 shows the effect of the pre-exponential factor, A, on laminar burning velocity as a function of hydrogen mole fraction. Two values of pre-exponential factor utilized with one order of magnitude difference. The pre-exponential factor is linearly related to the reaction rate or chemical time scale, as illustrated in Equation (2.8) or Equation (2.9). With a higher value of pre-exponential factor utilized in a chemical reaction, the laminar burning velocity would increase, resulting from the rise of the chemical reaction rate.

Figure 2.8 shows the effect of activation temperature, T_A, on laminar burning velocity as a function of hydrogen mole fraction. Two values of activation temperature utilized with a 3000 K difference. Activation temperature is exponentially related to the laminar burning velocity as illustrated in Equation (2.9). A higher value of activation temperature required by the chemical reaction would lower the magnitude of laminar burning velocity since more energy should be added to the system to break bonds between molecules involving in the chemical reaction. A slower reaction undergoes as the result of the higher temperature barrier, and flame propagation slows down.

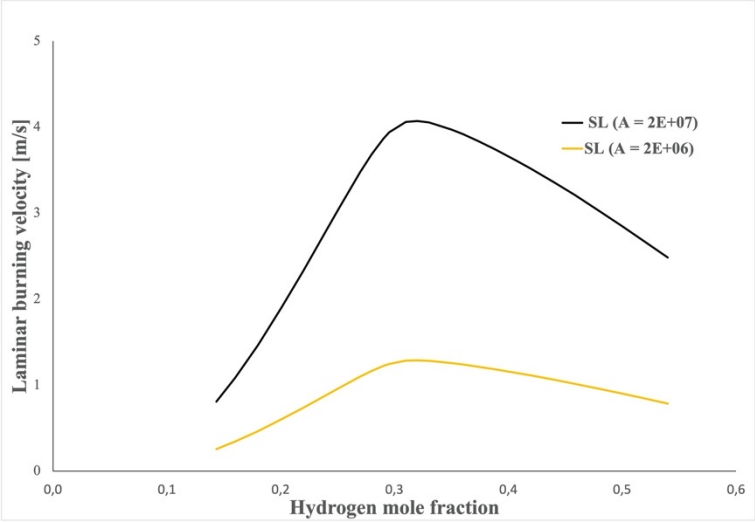

Figure 2.7:The effects of the pre-exponential factor on laminar burning velocity

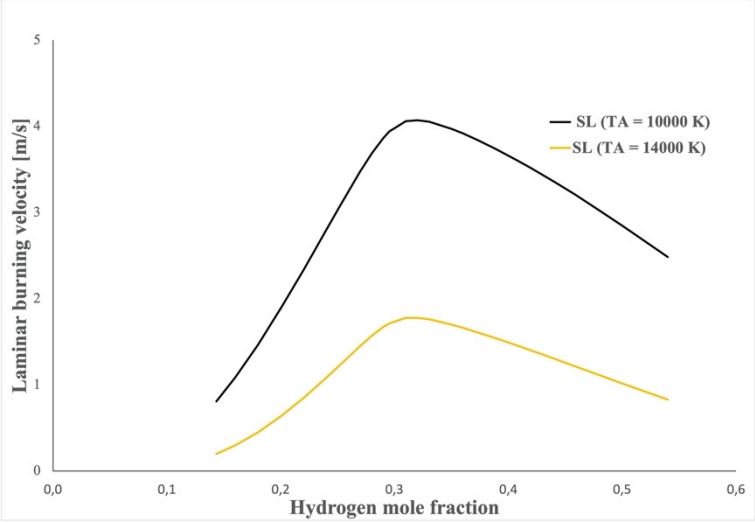

Figure 2.8: The effects of the activation temperature on laminar burning velocity

Lewis number

Lewis number represents the thermal-diffusive effects on laminar burning velocity. If $Le < 1$, i.e., the mass diffusivity of the reactant is larger, more reactant diffused to the flame front, initiated, and combusted. The reaction rate increases with increased reactants involving in combustion which further leads to the rise of thermal-diffusive instability. Stretch and

curvature enhanced due to the formation of cellular flame and laminar burning velocity increased. If $Le > 1$, i.e., that the thermal diffusivity is larger than mass diffusivity, and thermal-diffusive instability decreases. The flame front tends stable, and the laminar burning velocity is reduced. The Lewis number varies with mixture composition. Hiksen (2018) presents that instability of reaction zone observed when the lighter component of a mixture is deficient. For a fuel-air system where fuel is heavier than air, i.e., propane-air mixtures, the thermal-diffusive instability observed in the fuel-rich side and Lewis number is smaller than one. In the fuel-air system where fuel is lighter than air, i.e., hydrogen-air mixtures, the thermal-diffusive instability is observed in the fuel-lean side, and Lewis number is smaller than one here.

Oxygen concentration

At room temperature and atmospheric pressure, the thermal diffusivity of oxygen is higher than that of nitrogen. The laminar burning velocity for fuel-air mixtures increases with enrichment of oxygen content in the air, and it peaks with fuel-pure oxygen mixtures. The laminar burning velocity decreases with the dilution of oxygen content in the air. For example, the maximum laminar burning velocity in enriched $H_2/O_2/N_2$ ($O_2 = 90\ vol\%$) mixtures is 8.5 m/s at ambient conditions, while the maximum laminar burning velocity in diluted $H_2/O_2/N_2$ ($O_2 = 12.5\ vol\%$) mixtures is 1.2 m/s at ambient conditions (Lewis and von Elbe, 1987). More oxygen would be involved in the reaction if the oxygen concentration enlarged. The laminar burning velocity would peak at a higher ER value due to the increased eaction rate.

2.4 Turbulent burning velocity

Under the influence of flow turbulence, the laminar flame is transferred to a turbulent flame where turbulent burning velocity dominates the rate of flame propagation. Unlike laminar burning velocity, which depends only on the thermal and chemical properties of the gas mixtures, the turbulent burning velocity depends on the characteristics of the flow and the physicochemical properties of the gas mixtures. A universally accepted definition is not yet available for turbulent burning velocity, possibly due to the flame front's arbitrary definition for the turbulent flame, which is highly wrinkled. In energy conversion devices, such as

engines, the burning velocity should express the rate of formation of burned gas. In contrast, in explosion hazards, a more useful burning velocity expresses the rate at which the leading edge of a propagating flame entrains unburned mixtures. Flame fronts can be defined to express either of these burning velocities, whereas the flame front's corresponding definition can be quite different between these two burning velocities (Bradley, 2002). Considerable scatters of the experimental data related to turbulent burning velocity for premixed gas mixtures are shown in Figure 2.9 (Bradley et al., 1992). The turbulent burning velocity data extracted from Abedel-Gayed et al. (1987), and based on this figure, different turbulent burning velocities were observed under the same turbulent fluctuation velocity (u') with obvious scatters. One of the main reasons would be the different measurements corresponding to these two flame front definitions (Abdel-Gayed et al.,1988).

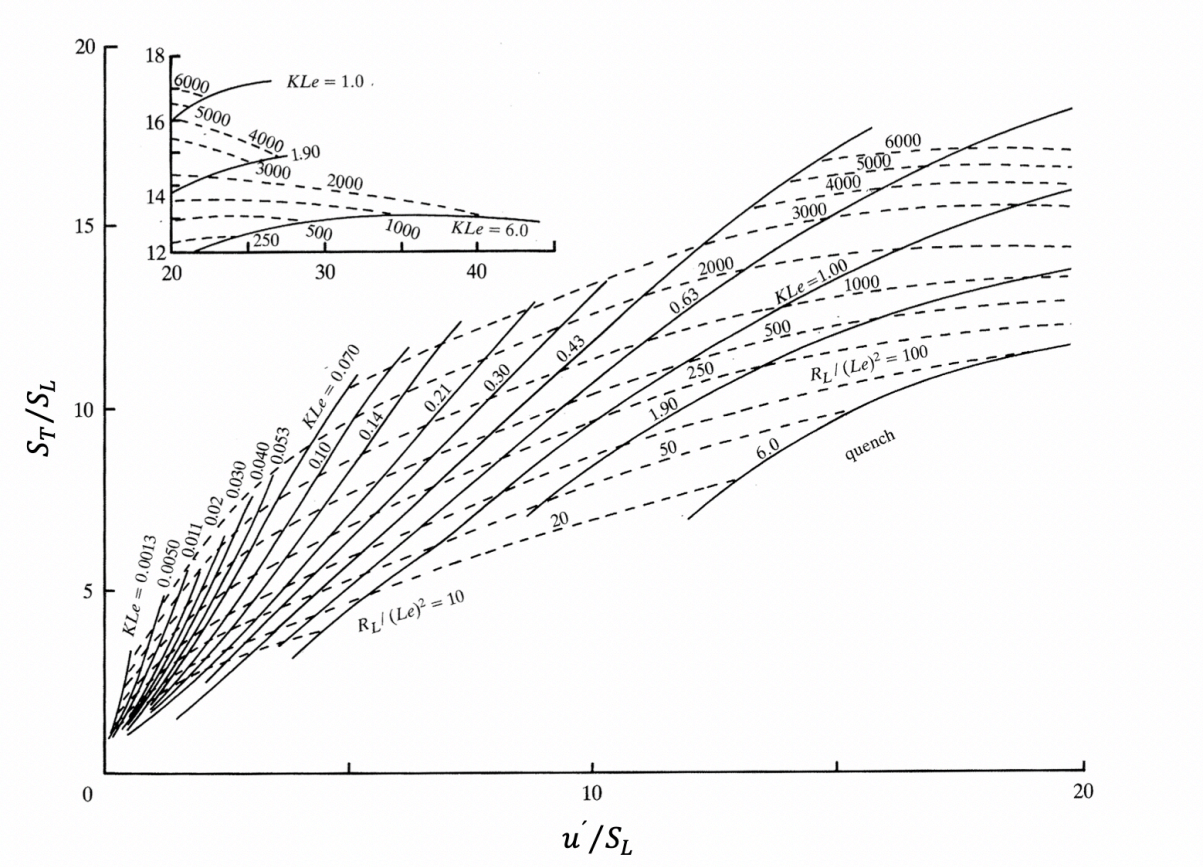

Figure 2.9: Normalized turbulent burning velocities versus normalized turbulent fluctuation velocities (Bradley et al., 1992)

Models for turbulent burning velocities prediction

Experimental research has been devoted to understanding the turbulent flow field's characteristics in premixed turbulent combustion and achieving good models for predicting turbulent burning velocity, incorporating turbulence effects on flame propagation. One of the main approaches is the flamelet model, which assumes that turbulent premixed combustion can be represented by an array of laminar flame structures with a finite thickness embedded in a turbulent flow field (Bradley et al., 1992).

The first flamelet model was presented by Damköhler (1947). He divided the effect of turbulence into two regimes, defined by the laminar flame thickness. He concluded that turbulence will always enhance the burning velocity, either due to an enlarged flame area by wrinkling of the flame front or increasing the rate of heat and active species transport.

The flamelet models for turbulent burning velocity can be divided into two categories. The first one gives the turbulent burning velocities as a function of flame wrinkling, which is determined by the turbulent fluctuation velocity (u'). This flamelet model is valid only for a small stretch rate. Bray (1990) presented an empirical expression related to this category as follows

$$S_T = C_{ST} * u' * K^{-\beta} \tag{2.14}$$

where C_{ST} the constant in expression for turbulent burning velocity equals 0.875. S_T refers to turbulent burning velocity, u' the turbulent fluctuation velocity. β, with a value of 0.392, is the power exponent for K, which is the Karlovitz strain rate represents the stretch rate of the flame, and can be evaluated with a correlation in the form as follows

$$K = C_K * \left(\frac{u'}{S_L}\right)^2 * Re_T^{-0.5} \tag{2.15}$$

where C_K the constant in expression for K equals 0.157 in the model of Bray (1990). Re_T represents the Reynolds number associated with indicating the intensity of turbulence (turbulent Reynolds number). The higher the Reynolds number, the higher flow turbulence. It can be estimated according to

$$Re_T = \frac{u' * l_I}{\nu} \tag{2.16}$$

where l_I refers to the integral length scale representing the time for a turbulent eddy to turn over. ν is the kinematic viscosity. The turbulent Reynolds number measures the relative importance of inertial forces compared to viscous forces in the flame flow. At low turbulent Reynolds numbers, laminar flow occurred and was dominated by viscous forces. The laminar flow is characterized by smooth, constant fluid motion. At high turbulent Reynolds numbers, turbulent flow occurred and was dominated by inertial forces that tend to produce chaotic eddies, vortices, and other flow instabilities. The expression for predicting turbulent burning velocity, as shown in Equation (2.14), is valid for $K < 0.3$ following the illustration of Bray (1990) as the predictions agreed well with the experimental data.

In the second category relative to the flamelet models for predicting turbulent burning velocities, the effects of stretch on the burning velocities have been considered. Bradley et al. (1992) presented an empirical expression related to this category utilizing Lewis number to represent the sensitivity of the flame to the stretch due to the thermo-diffusive effects as follows

$$S_T = C_{ST} * u' * (K * Le)^{-\beta} \tag{2.17}$$

where $C_{ST} = 0.88$ and $\beta = 0.3$ in this model. K represents the Karlovitz strain rate and can be evaluated with the same correlation as shown in Equation (2.15). Le represents the Lewis number effect. The correlation of turbulent burning velocity in terms of $K * Le$ is shown in Figure 2.9 with solid lines.

Another approach to representing the flame's sensitivity to the stretch is the Markstein number, which indicates how the burning velocities of flamelets in turbulent premixed combustion respond to the rate of flame stretch. The flamelets in mixtures characterized by negative Markstein numbers appear to have higher burning velocities than mixtures with positive Markstein numbers (Bradley et al., 2005). Bradley et al. (2011b) and Bradley et al. (2013) updated correlations of turbulent burning velocity in terms of $K * Ma_{sr}$ instead of K as shown in Equation (2.14). C_{ST} and β were expressed in terms of Markstein number as follows

$$C_{ST} = 0.023 * (30 - Ma_{sr}) \text{ and } \beta = 0.0103 * (Ma_{sr} - 30) \quad Ma_{sr} > 0 \qquad (2.18)$$

$$C_{ST} = 0.085 * (7 - Ma_{sr}) \text{ and } \beta = -0.0075 * (Ma_{sr} + 30) \quad Ma_{sr} < 0 \qquad (2.19)$$

with $C_K = 0.25$ in the expression for K (Equation (2.15)), and $Le = 1$. Ma_{sr} refers to the strain rate Makstein number, and it is a function of mixture concentration, ER, initial temperature, and pressure. Combined with Equation (2.18) and Equation (2.19), the expression for predicting turbulent burning velocity, as shown in Equation (2.14), is valid for $K > 0.05$.

2.5 Burning velocity model in FLACS

As a computational fluid dynamics (CFD) software, the FLACS has been developed by Christian Michelsen Institute, Christian Michelsen Research, and Gexcon AS since the 1980s. It has now developed into a tool for ventilation, dispersion, explosion, and fire simulation in complex industrial processes, starting as a tool for simulating gas explosions offshore.

The combustion modelling utilized in FLACS assumes combustion undergoes with one-step reaction kinetic, and the flame in an explosion can be regarded as a collection of flamelets. The combustion modelling consists of four parts, including a burning velocity model. The burning velocity model comprises three sub-models describing laminar burning velocity, quasi-laminar burning velocity, and turbulent velocity separately (Gexcon, 2019).

Laminar burning velocity model

The flame's initial state is laminar, and the flame front is smooth and governed by molecular diffusion. The model describes the laminar burning velocity as a function of gas mixtures, concentration, temperature, pressure, the oxygen concentration in air, and inert diluents. For each fuel, the laminar burning velocity at different equivalence ratios is tabulated.

Quasi-laminar burning velocity model

Shortly after the laminar stage, the burning velocity is enhanced, resulting from flame instabilities and wrinkling, and the flame becomes quasi-laminar. The quasi-laminar burning velocity is calculated by multiplying an enhancement factor with laminar burning velocity. The enhancement factor is a function of flame radius and gas mixture. The quasi-laminar burning velocity is defined as follows

$$S_{QL} = S_L * (1 + C_{QL} * R^{1/2}) \tag{2.20}$$

S_{QL} is the quasi-laminar burning velocity, R is the flame radius, and C_{QL} is the adjustment factor depending on parameters related to the gas mixtures and the ignition point´s geometry location. The typical values of this adjustment factor are between 2 and 8 (Arntzen, 1998).

Turbulent burning velocity model

After a transition period, the flame eventually reaches the turbulent stage. The model describes turbulent burning velocity as a turbulence parameter, which are turbulent velocity fluctuations and length scale. Two expressions utilizing in FLACS for calculating the turbulent burning velocity are derived from an empirical expression by Bray (1990) as shown in Equation (2.14). Combined with Equation (2.15) and Equation (2.16), the turbulent burning velocity can be expressed as follows

$$S_T = 1.81 * u^{'0.412} * S_L^{0.784} * l_I^{0.196} * \nu^{-0.196} \tag{2.21}$$

This expression is satisfactory at high turbulent intensities, and it is not valid for large values of K or low values of $u^{'}$. Based on this expression $S_T \rightarrow 0$ when $u^{'} \rightarrow 0$. In practice, the laminar burning velocity dominants flame propagation when turbulent fluctuation velocity is infinitely close to 0, and the turbulent burning velocity will be infinitely close to laminar burning velocity. Arntzen (1998), therefore made a correlation by adding the product of Equation (2.21) and the square root of $u^{'}/S_L$ to the laminar burning velocity. The turbulent burning velocity, therefore, can be expressed as follows

$$S_T = 0.96 * u'^{0.912} * S_L^{0.784} * l_I^{0.196} * \nu^{-0.196} + S_L \quad (2.22)$$

This expression is only used for low values of the turbulent fluctuation velocity.

Burning velocity model with correction of Lewis number and Markstein number

Standard versions of FLACS do not apply Lewis number-dependent corrections for any other fuel-air mixtures' burning velocity than hydrogen. Figure 2.10 shows the Lewis number correction for hydrogen-air mixtures from FLACS-CFD 20.1 (Solid squares) together with the uncorrected values of laminar burning velocities from FLACS-CFD 20.1 (Hollow squares).

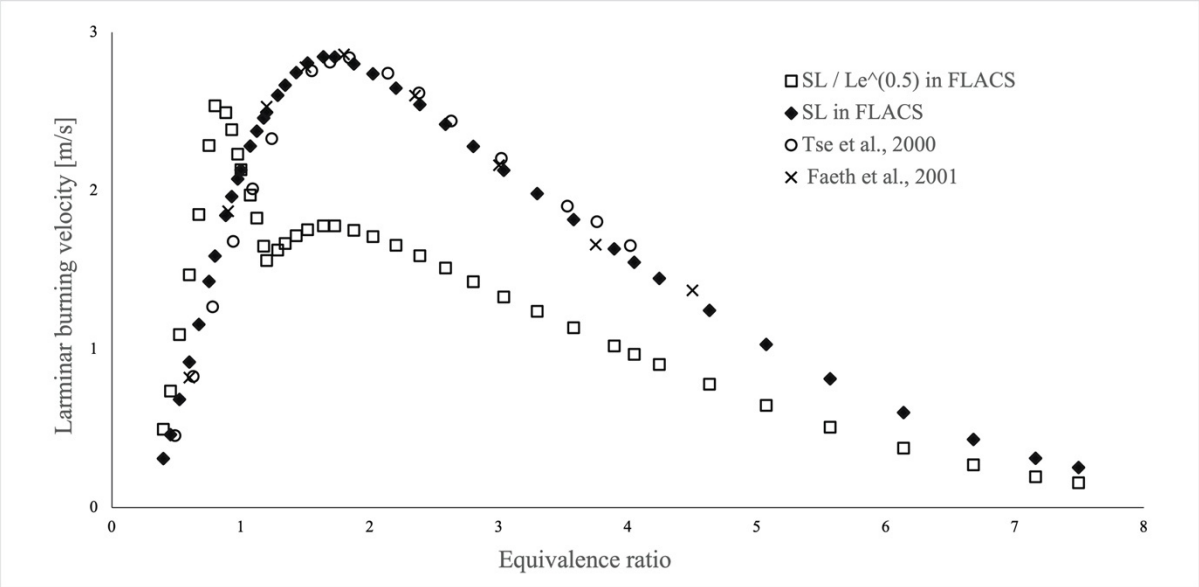

Figure 2.10: Laminar burning velocities comparison
with Le-correction or without Le-correction

Figure 2.11 shows the Lewis number utilized in FLACS as a function of equivalence ratio. In general, the burning velocity of hydrogen-air mixtures is corrected by the root of Le with a numerical value of 1.6 for $ER \leq 0.8$ and with a numerical value of $1 / 1.6$ for $ER \geq 1.2$. For ER ranges from 0.8 to 1.2, the numerical value for Le-correction decreases from 1.6 to $1 / 1.6$.

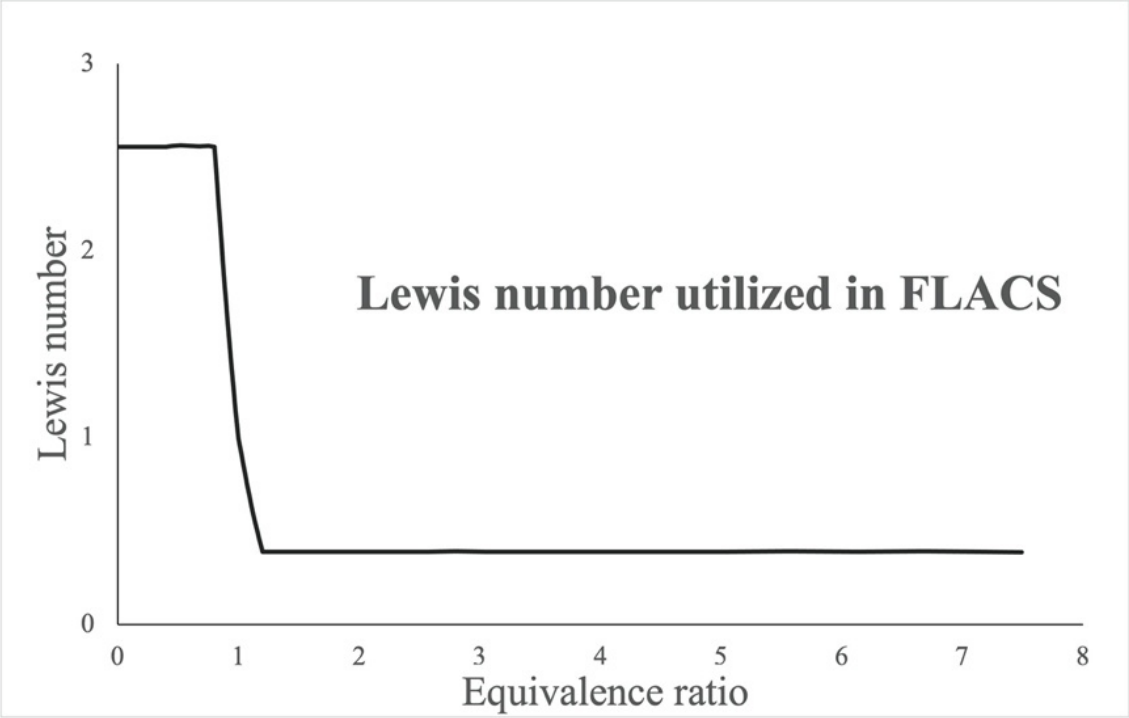

Figure 2.11: Lewis number utilized in FLACS for hydrogen-air mixtures

In general, the Le-correction enhances the turbulent burning velocities for $ER < 1$ in FLACS, and it reduces the burning velocities for $ER > 1$, as shown in Figure 2.10.

FLACS implements Markstein number-dependent turbulent burning velocity model only in the Flacs3 beta solver based on Equation (2.14), Equation (2.15), Equation (2.18), and Equation (2.19). The Markstein number-dependent burning velocity model gives improved results of turbulent burning velocities, e.g., in hydrogen-air mixtures related to the FLACS simulations done by Hiksen (2018). The Markstein number-dependent correction is not widely used in FLACS for hydrocarbons and hydrogen due to its limited amount experimental data basement and its dependence on the gas mixture, equivalence ratio, temperature, pressure, etc.

3 MODELS FOR BURNING VELOCITIES

This chapter presents numerical models for the determination of burning velocity. The laminar burning velocity prediction model presents first by implementing sub-models for the dependent parameters of thermal diffusivity, Lewis number, and chemical timescale. Every single factor related to SL estimation will be specified separately. The numerical models for the determination of turbulent burning velocity will be illustrated afterward based upon the laminar burning velocity models.

3.1 Laminar burning velocity models

Combining with the prediction equations presents in section 2.3, the expression for laminar burning velocity in term of thermal diffusivity, Lewis number, and the chemical time scale of the reaction is given as

$$S_L = \left[\alpha * Le * A * c_F^{n_F} * c_O^{n_O} * e^{(-T_a/T_P)}\right]^{1/2} \tag{3.1}$$

A simple prediction model for laminar burning velocity is desirable to utilize in FLACS. Therefore, 4 hypothesis models with less dependent parameters will be tested, and the detailed expression for hypothesis models are shown in Table 3.1.

Table 3.1: Detailed expression of 4 hypothesis models

Hypothesis model	Detailed expression
1	$S_L = (\alpha * A * e^{(-T_a/T_P)})^{1/2}$
2	$S_L = (\alpha * A * e^{(-T_a/T_P)})^{1/2}$
3	$S_L = (\alpha * Le * A * e^{(-T_a/T_P)})^{1/2}$
4	$S_L = (\alpha * Le * A * c_F^{n_F} * e^{(-T_a/T_P)})^{1/2}$

Model 1 and model 2 estimate laminar burning velocities to unity Lewis number. Constant thermal diffusivity would be used in hypothesis model 1, and its value would be equal to the mass diffusion coefficient (D). Arntzen (1998) recommended using $D \approx 2 * 10^{-5}$ for laminar

flames in FLACS. It is therefore applying this value in model 1 for testing efficiency. The thermal diffusivity in model 2, model 3, and model 4 varies according to the equivalence ratio or mole fraction of hydrogen. Model 3 and model 4 estimate laminar burning velocities to non-unity Lewis number, with which model 4 also includes dependent parameters of hydrogen concentration. All the factors involving these four models will be specified separately in this chapter's following sectors.

3.2 Modelling mixture thermal diffusivity of unburned gases

Thermal diffusivity is a measure of how quickly a system reacts to temperature changes. Thermal diffusivity is proportional to thermal conductivity. A system that is said to conduct heat efficiently must also have effective heat diffusion properties to facilitate heat transfer. On the contrary, thermal diffusivity is inversely proportional to density and specific heat capacity. A higher density can limit the speed and distance that heat can travel through the system. A smaller specific heat capacity means less heat needed to increase one unit in temperature, which means heat transferring more quickly throughout the system. Thus, all three factors should be included in the model for thermal diffusivity estimation. Furthermore, the study focuses on hydrogen-air combustion, a system involving both hydrogen and air. A mixture of thermal diffusivity will be preferable for further modelling of laminar burning velocity. Combining with the expression of thermal diffusivity in Equation (2.4), the mixture thermal diffusivity can be determined according to

$$\alpha_{mix} = \frac{\lambda_{mix}}{\rho_{u,mix} * C_{p,mix}} \tag{3.2}$$

where λ_{mix} presents the mixture´s thermal conductivity for the premixed hydrogen and air, $\rho_{u,mix}$ and $C_{p,mix}$ the mixture´s density, and specific heat capacity for the unburned hydrogen-air mixtures. Models for these three parameters will be presented separately.

Modelling mixture thermal conductivity of unburned gases

In general, there are three methods to predict the mixture thermal conductivity for gases. One is mole fraction weighted. The second one is harmonic mole fraction weighted. The last one is mass fraction weighted. For methods relative to mole fraction weighted and harmonic mole

fraction weighted, the mixture thermal conductivity can be modeled with the formulations recommended by Mathur et al. (1967), as follows

$$\lambda_{mix,1} = \sum_{i=1}^{N} x_i * \lambda_i \quad (3.3)$$

$$\lambda_{mix,2} = 1/\sum_{i=1}^{N} x_i/\lambda_i \quad (3.4)$$

$$\lambda_{mix,3} = 0.5 * (\sum_{i=1}^{N} x_i * \lambda_i + 1/\sum_{i=1}^{N} x_i/\lambda_i) \quad (3.5)$$

with x_i and λ_i present mole fraction and thermal conductivity for i^{th} species. In the meantime, the formulation for the method, as mass fraction weighted, is expressed as follows

$$\lambda_{mix,4} = \sum_{i=1}^{N} Y_i * \lambda_i \quad (3.6)$$

with Y_i present mass fraction for i^{th} species involved in the premixed gas combustion. FLACS utilizes the mass fraction weighted method in mixture thermal conductivity calculation for all kinds of simulations. Molar mass used in transferring from mole to mass for hydrogen, oxygen, and nitrogen are listed in Table 3.2.

Table 3.2: Molar masse for hydrogen, oxygen and nitrogen

Species	Molar mass $[g/mol]$
Hydrogen	2.016
Oxygen	31.999
Nitrogen	28.014

Four models can be used to predict the mixture thermal conductivity. Therefore, comparing these approaches to achieve a suitable best formulation to determine mixture thermal conductivity is necessary by comparing with experimental data. Mukhopadhyay et al. (1967) had measured the thermal conductivity of hydrogen – nitrogen mixtures at seven temperatures vary from -15 ℃ to 200 ℃. The accuracy of experiment results has a 1% margin of error. Thus, it is reliable to compare the predicted mixture thermal conductivity based on the four models and the chosen experimental data. Table 3.3 shows the experimental data for $T = 20.1$℃.

Table 3.3: Experimental data of mixture thermal conductivity for $H_2 - N_2$ mixtures ($T = 20.1$ ℃)

Temperature [℃]	x_{H2}	λ_{mix_EXP} $[cal/cm \cdot s \cdot ℃]$	λ_{mix_EXP} $[mW/m \cdot K]$
20.1	0.0000	$6.13 \cdot 10^{-5}$	25.6651
	0.1910	$9.37 \cdot 10^{-5}$	39.2303
	0.4010	$14.29 \cdot 10^{-5}$	59.8294
	0.5750	$20.11 \cdot 10^{-5}$	84.1965
	0.7780	$28.13 \cdot 10^{-5}$	117.7747
	1.0000	$42.06 \cdot 10^{-5}$	176.0968

For hydrogen mole fraction equals 0, there is no hydrogen in the gas mixtures. Meanwhile, there is no nitrogen in the gas mixtures when the hydrogen mole fraction is 1. Therefore, from these two situations, thermal conductivity for pure hydrogen and pure nitrogen can be extracted, and they are listed in Table 3.4. These two values were used in the experiment and will be used in the modelling comparison.

Table 3.4: Thermal conductivity of hydrogen and nitrogen used in comparison at $T = 20.10$ ℃

Species	λ_i $[mW/m \cdot K]$
Hydrogen	176.0968
Nitrogen	25.6651

The mixture thermal conductivity for hydrogen and nitrogen gas mixtures is calculated following the formula corresponding to the four models. Table 3.5 presents the comparison results relative to the six given hydrogen mole fractions.

Table 3.5: Mixture thermal conductivity comparison between experimental data and four models with 6 different hydrogen mole fractions

T [℃]	x_{H2}	λ_{mix_EXP} $[mW/m\cdot K]$	$\lambda_{mix\_model\,1}$ $[mW/m\cdot K]$	$\lambda_{mix\_model\,2}$ $[mW/m\cdot K]$	$\lambda_{mix\_model\,3}$ $[mW/m\cdot K]$	$\lambda_{mix\_model\,4}$ $[mW/m\cdot K]$
20.1	0.0000	25.6651	25.6651	25.6651	25.6651	25.6651
	0.1910	39.2303	54.3976	30.6692	42.5334	28.1783
	0.4010	59.8294	85.9882	39.0377	62.5130	32.5792
	0.5750	84.1965	112.1633	50.4421	81.3027	39.0121
	0.7780	117.7747	142.7010	76.5233	109.6122	55.9627
	1.0000	176.0968	176.0968	176.0968	176.0968	176.0968

Based on the values shown in Table 3.5, higher mixture thermal conductivities obtained with $\lambda_{mix\_model\,1}$. The maximum deviation between $\lambda_{mix\_model\,1}$ and experimental data is 44% resulting from hydrogen concentration equals 40 mol%. $\lambda_{mix\_model\,2}$ and $\lambda_{mix\_model\,4}$ give lower mixture thermal conductivities compared with the experimental data. The most significant deviation given by $\lambda_{mix\_model\,4}$ with hydrogen concentration equals 78%. On the contrary, $\lambda_{mix\_model\,3}$ results in more similar mixture thermal conductivity values in contrast with experimental data. Figure 3.1 visualizes the experimental data and all mixture thermal conductivities related to four estimation models for 22 hydrogen mole fractions, including six hydrogen mole fractions shown in Table 3.4.

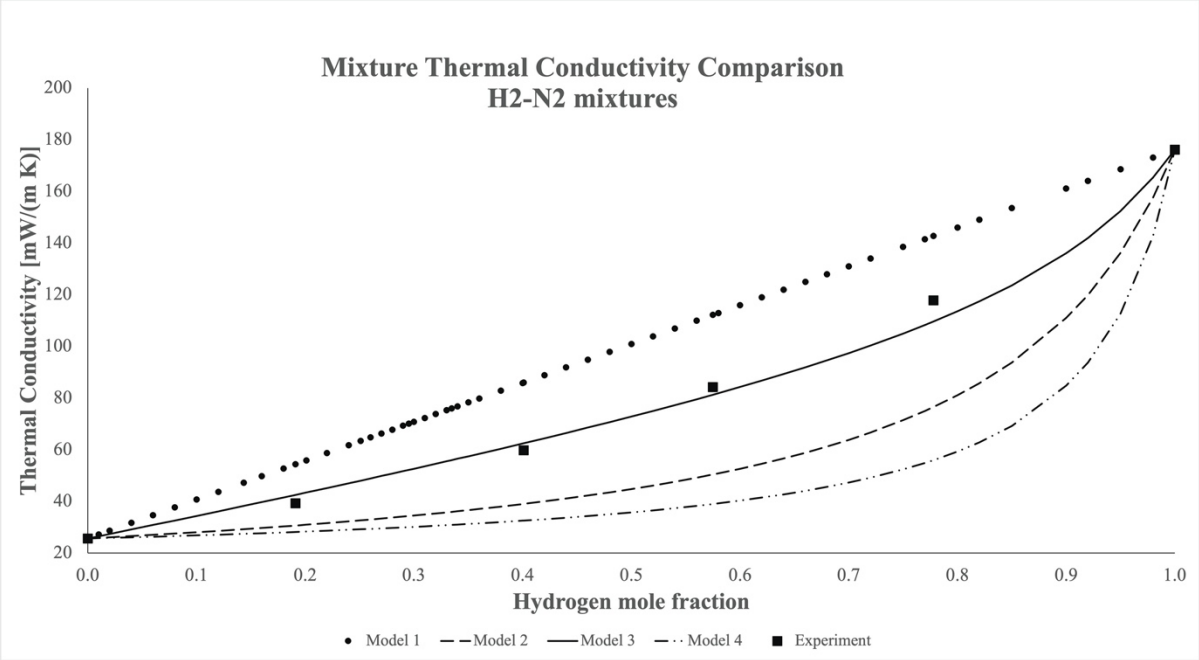

Figure 3.1: Mixture thermal conductivities of H_2- N_2 mixtures as the function of hydrogen mole fraction

The round dot line refers to $\lambda_{mix\_model\ 1}$, the dashed line is $\lambda_{mix\_model\ 2}$, the solid line presents $\lambda_{mix\_model\ 3}$, and the long dash-dot line is on behalf of $\lambda_{mix\_model\ 4}$. Six square marks represent the experimental data. All the lines and squares show that the mixture's thermal conductivity increases with increasing mole fraction of hydrogen in the mixtures with the same temperature. $\lambda_{mix\_model\ 1}$ and $\lambda_{mix\_model\ 3}$ possess similar tendency with the experimental data. Whereas the trends for $\lambda_{mix\_model\ 2}$ and $\lambda_{mix\_model\ 4}$ are more likely with each other. According to Figure 3.1 and Table 3.5, $\lambda_{mix\_model\ 3}$ is more suitable to predict mixture thermal conductivity, i.e., Equation (3.5) is recommended utilizing in modelling λ_{mix}. For the sake of prediction improvement, thermal conductivity for single species should be considered, i.e., thermal conductivity both for fuel and oxidant involving in the chemical reaction should be counted on. An equation that gives a reasonable thermal conductivity of fuel and oxidant in gas form is desired. Therefore, the normal boiling point of hydrogen, oxygen, and nitrogen will be included. *Table 3.6* lists the normal boiling point of H_2, O_2, and N_2.

Table 3.6: The normal boiling point of hydrogen, oxygen, and nitrogen (CRC Handbook Chemistry and Physics, 97th)

Species	T [℃]
Hydrogen	-252.760
Oxygen	-195.798
Nitrogen	-182.692

Determination of thermal conductivity of hydrogen, oxygen, and nitrogen

Thermal conductivity is defined as the ability of a system to transport heat energy. In gases, heat conduction occurs mainly through molecular collision. Increased molecular collisions increase the exchange of energy between molecules, which leads to the up-growing thermal conductivity of the gases. Molecular collisions are enhanced with an increase in temperature. Thus, the thermal conductivity of a gas increases with the rise of temperature. However, the pressure effect on the thermal conductivity can be negligible within a specific range. For example, Figure 3.2 shows the thermal conductivities of para hydrogen and normal hydrogen as the function of temperature and pressure. The thermal conductivities increase significantly for para hydrogen and ortho hydrogen when temperature increases from the normal boiling point of hydrogen to 750 degrees Celsius. For $T > 100$ ℃, the same thermal conductivities were observed between normal hydrogen and para hydrogen when pressure varied from 1 bar to 100 bars. At room temperature, a 1 % difference of thermal conductivity was observed between para hydrogen and normal hydrogen for $p = 1\ bar$. For para hydrogen, thermal conductivity is independent of pressure when $p = 1\ bar - 10\ bars$, and 1% difference of thermal conductivity observed for pressure increases from 10 bars to 100 bars. Therefore, it is assumed that for pressure lower than 10 bars, the thermal conductivity of hydrogen is independent of pressure.

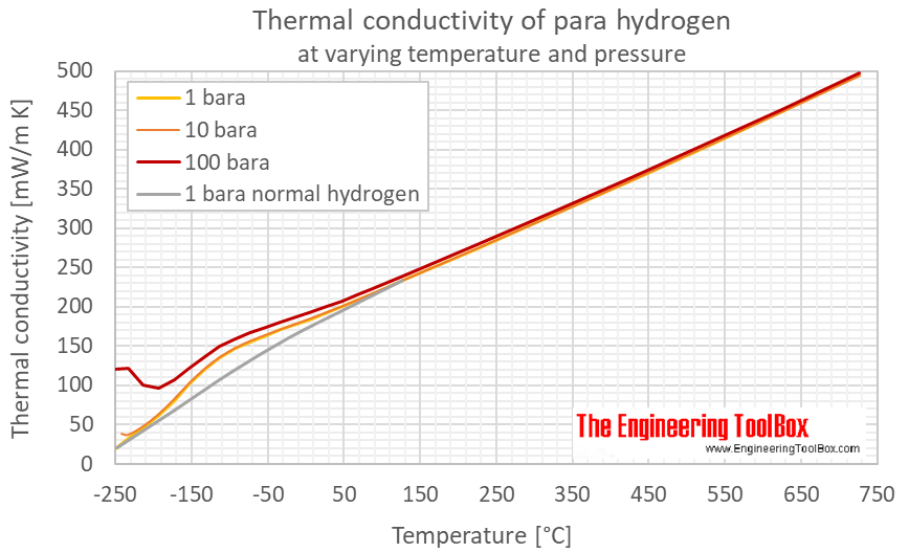

Figure 3.2: Thermal conductivities for normal- and para hydrogen as a function of temperature and pressure (Engineering toolbox, 2018)

FLACS estimates thermal conductivity of species as a function of temperature according to a second-degree polynomial (FLACS *v*10.9 User´s Manual, 2019)

$$\lambda_i = C_1 + C_2 * T \tag{3.7}$$

with C_1 and C_2 represent two constants for estimation of thermal conductivity related to given species. Ho et al. (1972) presented recommended thermal conductivities of substances at atmospheric pressure over a wide temperature range, including normal boiling point relative to each element. The constants for hydrogen, oxygen, and nitrogen can be extracted from the recommended data with the least square method. Temperature interval between normal boiling point and 300 Kelvin is selected to extract constants for hydrogen, oxygen, and nitrogen. The corresponding recommended thermal conductivities are listed in 3 tables in Appendix A. Table 3.7 shows all C_1 and C_2 for these three substances.

Table 3.7: Relative constants for calculating
thermal conductivity of hydrogen, oxygen, and nitrogen

Species	C_1 $[W/(m \cdot K)]$	C_2 $[W/(m \cdot K^2)]$
Hydrogen	$6.9107 * 10^{-3}$	$0.5970 * 10^{-3}$
Oxygen	$0.3614 * 10^{-3}$	$0.0887 * 10^{-3}$
Nitrogen	$1.1072 * 10^{-3}$	$0.0841 * 10^{-3}$

Modelling mixture density of unburned gases

The mixture density of premixed fuel and oxidant can be modelled with mole fraction-weighted formulation as follows

$$\rho_{u,mix} = \sum_{i=1}^{N} x_i * \rho_i \tag{3.8}$$

with x_i and ρ_i present mole fraction and density for i^{th} species in the mixture. the density of specific component can be estimated following the ideal gas law that applied both in FLACS and theoretical research, with the formula as follows:

$$\rho_i = \frac{p*M_i}{R*T_i} \tag{3.9}$$

here p, T_i, and R present initial pressure, initial temperature, and the universal gas constant, respectively. M_i is the molar mass of the i^{th} species. The molar mass of hydrogen, oxygen, and nitrogen used in the modelling are listed in Table 3.2.

Modelling specific heat capacity at a constant pressure of unburned gases

The specific heat capacity for an ideal gas at constant pressure is a function of temperature only for a unit mass of the gas. The mixture specific heat capacity for unburned gases is normally predicted with the mass fraction weighted formulation as follows

$$C_{p,mix} = \sum_{i=1}^{N} Y_i * C_{p,i} \tag{3.10}$$

where $C_{p,i}$, and Y_i are the specific heat capacity and mass fraction of the i^{th} species. The temperature effect dominates the varying of specific heat capacity at constant pressure. A linear dependence of specific heat capacity on temperature can be assumed. Same as thermal conductivity estimation, specific heat capacity at constant pressure can be determined with a second-degree polynomial as (FLACS *v*10.9 User´s Manual, 2019)

$$C_{p,i} = C_3 + C_4 * T \tag{3.12}$$

with C_3 and C_4 represent the two constants for estimation of specific heat capacity related to given species. C_3 and C_4 for these three substances can be extracted from the literature data of C_{p-H2}, C_{p-O2}, and C_{p-N2}. Wright Air Development Division Technical Report (1960) presented C_{p-H2} at atmospheric pressure of gaseous hydrogen for temperatures over 30 Kelvin. Therefore, a temperature interval between 30 K and 300 K is selected to extract constants for hydrogen specific heat capacity. The study of Hilsenrath et al. (1955) provided the specific heat capacity of oxygen and nitrogen for temperature over 120 K and 100 K, respectively. Therefore, a temperature interval between 120 K and 300 K is selected to extract constants for the specific heat capacity of oxygen. The temperature interval between 100 K and 300 K is selected to extract constants for the specific heat capacity of nitrogen. The corresponding literature data are listed in 3 tables in Appendix B. Figure 3.3, Figure 3.4, and Figure 3.5 show literature specific heat capacity of hydrogen, oxygen, and nitrogen respectively at atmospheric pressure as a function of selected temperature intervals.

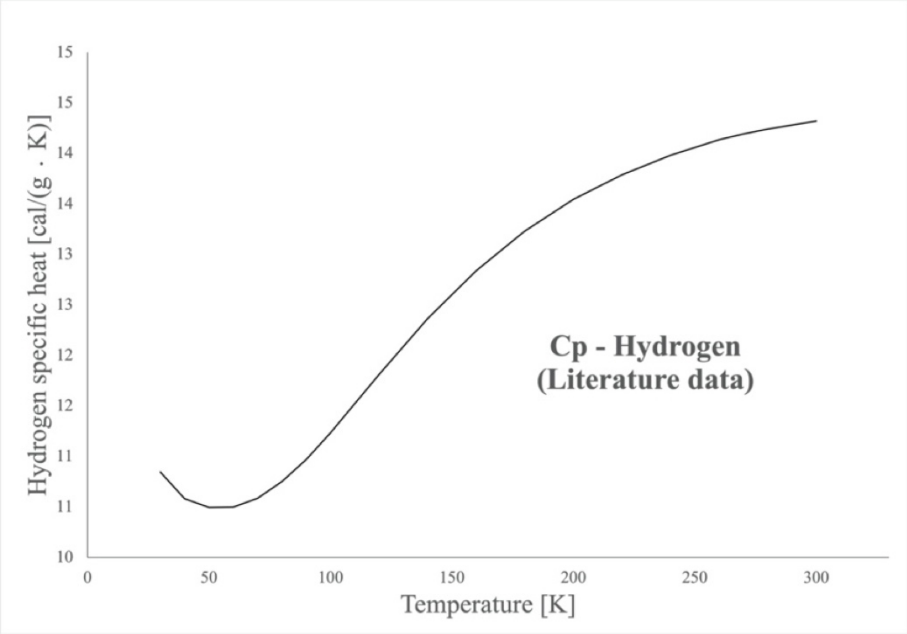

Figure 3.3: Literature specific heat capacity of hydrogen
at atmospheric pressure and selected temperature intervals

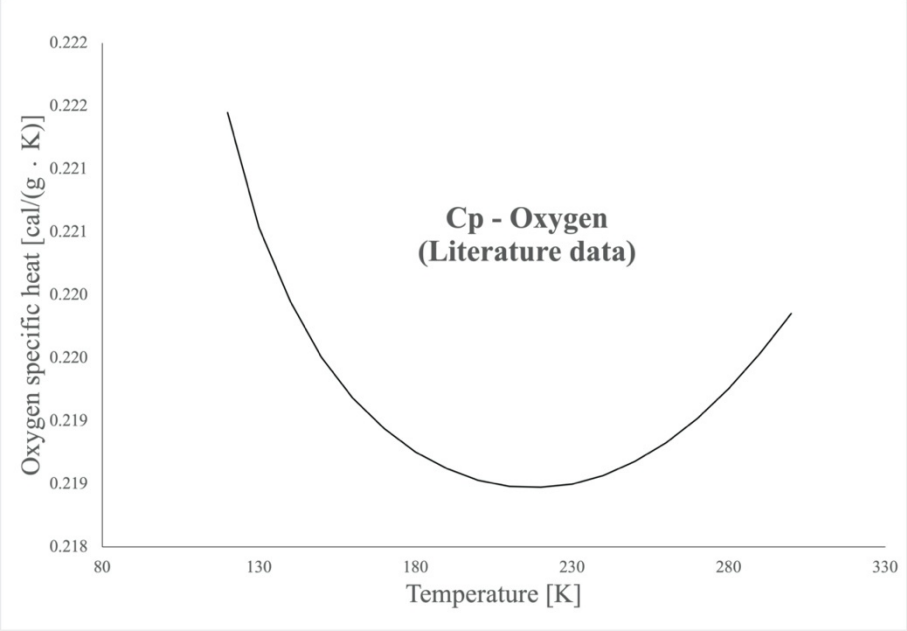

Figure 3.4: Literature specific heat capacity of oxygen
at atmospheric pressure and selected temperature intervals

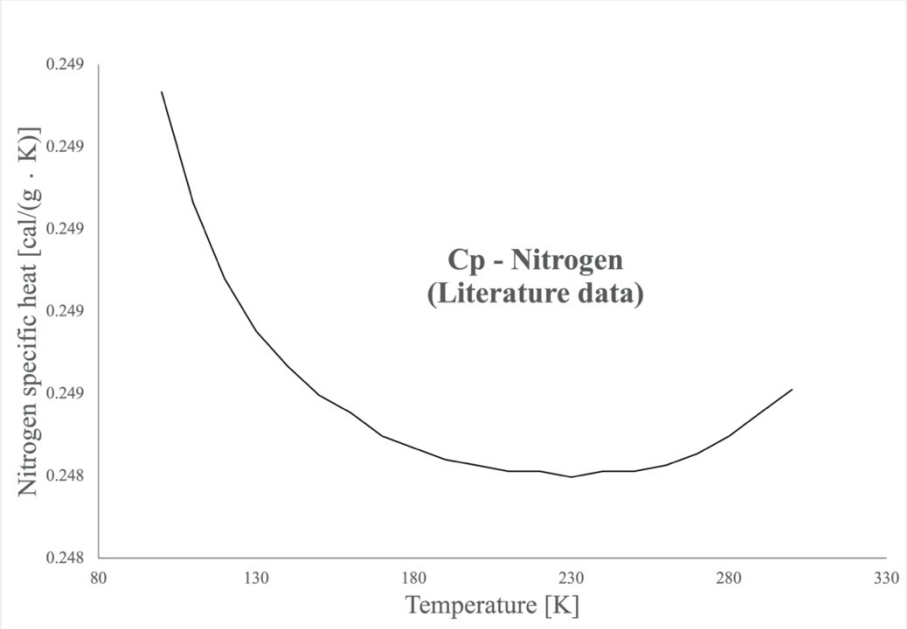

Figure 3.5: Literature specific heat capacity of nitrogen
at atmospheric pressure and selected temperature intervals

Within the selected temperature intervals, the specific heat capacity of hydrogen and oxygen decreased for lower temperatures and increased afterward. For nitrogen, C_{p-N2} varies from 0.248 to 0.249 within the selected temperature interval. Sight variation was obtained, and a linear relationship was observed with a decreasing tendency. Consequently, two equations with different C_3 and C_4 relative to hydrogen and oxygen are recommended. Based on Figure 2.2, para hydrogen concentration increases dramatically in normal hydrogen when the temperature falls to 160 K. This unique physical property of hydrogen will affect the specific heat capacity of hydrogen at constant pressure. It is, therefore, two equations relative to the estimation of C_{p-H2} will be separated by $T = 160\ K$. One equation for $T \leq 160\ K$, the other for $T > 160\ K$. Based on the trends of C_{p-O2} in Figure 3.4, two equations relative to the estimation of C_{p-O2} will be separated by $T = 190\ K$. One equation for $T \leq 190\ K$, the other for $T > 190\ K$. Equation (3.13), Equation (3.14), and Equation (3.15) are correspondingly related to estimation of specific heat capacity at atmospheric pressure for hydrogen, oxygen, and nitrogen.

$$C_{p-H2} = \begin{cases} 10.63 + 0.0142 * T & T \leq 160\ K \\ 11.62 + 0.0093 * T & T > 160\ K \end{cases} \quad (3.13)$$

$$C_{p-O2} = \begin{cases} 0.932 - 0.00001770 * T & T \leq 190\ K \\ 0.886 + 0.00000626 * T & T > 190\ K \end{cases} \quad (3.14)$$

$$C_{p-N2} = 1.0425 - 0.0000169 * T \quad T \leq 300\ K \quad (3.15)$$

3.3 Modelling the effective Lewis number of unburned gases

An effective Lewis number (Le_{eff}) for an unburned mixture is desired since both fuel and oxidant take part in the thermal and mass diffusions of a combustion process. For the exact stoichiometric mixture, all the fuel and oxidant reacted completely. Fuel and oxidant are weighted evenly for combustion. Thus, individual Lewis numbers Le_F and Le_O should be correspondingly weighted evenly, and Le_{eff} is the mean value of Lewis number for fuel and Lewis number for oxidant. For non-stoichiometric mixtures, deficient species limits the combustion, and the Lewis number corresponding to the deficient reactant should be weighted more. The weight of Lewis number for deficient reactant optimizes under conditions sufficiently far from stoichiometry, where Le_{eff} equals Lewis number for deficient species (Joulin et al., 1981; Jackson, 1987).

A transition of the effective Lewis number would be obtained when combustion goes from fuel-lean side to fuel-rich side. For lean mixtures, fuel is the deficient species, while for rich mixtures, oxidant becomes deficient. An effective Lewis number should be modelled as the function of equivalence ratio to represent this transition. Based on the study of Bechtold and Matalon (2001), the effective Lewis number can be estimated according to

$$Le_{eff} = 1 + \frac{(Le_A - 1) + (Le_D - 1) * A_{Le}}{1 + A_{Le}} \quad (3.16)$$

with subscripts, *A* and *D* present abundant reactant and deficient reactant, respectively. A_{Le} is a constant correction to adjust the weight of mixture strength. The formula for the determination of A_{Le} can be expressed as follows

$$A_{Le} = \begin{cases} 1 + \beta_z * (1/\phi - 1) & ER < 1 \\ 1 + \beta_z * (\phi - 1) & ER \geq 1 \end{cases} \quad (3.17)$$

where β_z refers to the Zeldovich number. Under the exact stoichiometric condition, A_{Le}=1 since abundant reactant and deficient reactant weighted evenly. As a measure of the temperature sensitivity of the overall reaction rate, Zeldovich number can be expressed as follows

$$\beta_z = \frac{E_a}{R} * \frac{(T_P - T_i)}{T_P^2} = \frac{T_A}{T_P} * (1 - \frac{T_i}{T_P}) \quad (3.18)$$

Lewis number for deficient reactant should be specified for sufficiently far from stoichiometry conditions. Since oxygen dominates the effect of oxidant in combustion process, in fuel rich mixtures, Le_{O2} will be used as Le_D. Thus, Le_{H2} is the effective Lewis number for the sufficiently lean side and Le_{O2} for the sufficiently rich side. The values for Le_{H2} and Le_{O2} are listed in Table 3.8.

Table 3.8: Lewis number for deficient species
(Nambauer et al., 2020)

	Hydrogen	Oxygen
Lewis number	0.3	2.1

3.4 Modelling chemical time scale

The chemical time scale is the inverse of the reaction rate and can be modelled as a function of pre-exponential factor, activation temperature, and product temperature. These three parameters are highly sensitive to the type of fuel involving in the combustion and initial conditions of the chemical reaction, such as fuel composition or equivalence ratio, initial temperature, and pressure. Individual models for each parameter should be illustrated.

Product temperature selection

Theoretically, product temperature can be calculated with assumptions, such as combustion undergoes with an adiabatic chemical reaction. The enthalpy change of the reaction is idealized equal to the heat release to the products of reaction. Thus, the heat release of the chemical reaction can be calculated from its enthalpy of formation change ($\Delta H = q, q < 0$

for exothermic reaction). Combined with the specific heat capacity of the product, its temperature change can be estimated ($dH = \int C_p * dT$) with the default of constant specific heat capacity utilizing in the system. The product temperature is the final state of product temperature if the initial state is known. It is time-consuming to calculate the product temperature of fuel-air combustion due to the complex chemical reactions undergone. The combustion involves considerable numbers of atoms and molecules. Therefore, it can be completed by computational tools, such as the chemical equilibrium calculator and FLACS.

T_P estimated by chemical equilibrium calculator:

The chemical equilibrium calculator is available online, and it uses data from the CHEMKIN thermodynamic database. It implements the STANJAN algorithm to calculate various equilibrium properties such as temperature, concentration, and pressure. To obtain accurate results that desired, initial conditions related to combustion should be specified first. Table 3.9 shows an example of the input specifications for premixed hydrogen-air combustion at room temperature and atmospheric pressure.

Table 3.9: Input specification for product temperature calculation ($ER = 1$)

<table>
<tr><th>x_i</th><th>T_0 [°C]</th><th>p [bar]</th><th>Calculation Constraints</th><th>Elements</th><th>Reactant Mixture Composition</th><th>Additional Species</th></tr>
<tr><td>H_2</td><td rowspan="3">20</td><td rowspan="3">1</td><td rowspan="3">Constant pressure and enthalpy</td><td>H</td><td>0.2953</td><td rowspan="3">H_2O, OH</td></tr>
<tr><td>O_2</td><td>O</td><td>0.1476</td></tr>
<tr><td>N_2</td><td>N</td><td>0.5571</td></tr>
</table>

Figure 3.6 reviews the input specifications mentioned above and the output of estimated product temperature for $ER = 1$ in the snapshot of green and yellow, respectively. Reactant mixture composition should be changed when the equivalence ratio varies, and the other specifications can be held if initial temperature and pressure are constants. The output product temperature for the equilibrium state fulfilled is 2396.1 Kelvin. In comparison with literature data of the product temperature for stoichiometric hydrogen-air mixtures, 2400 K.

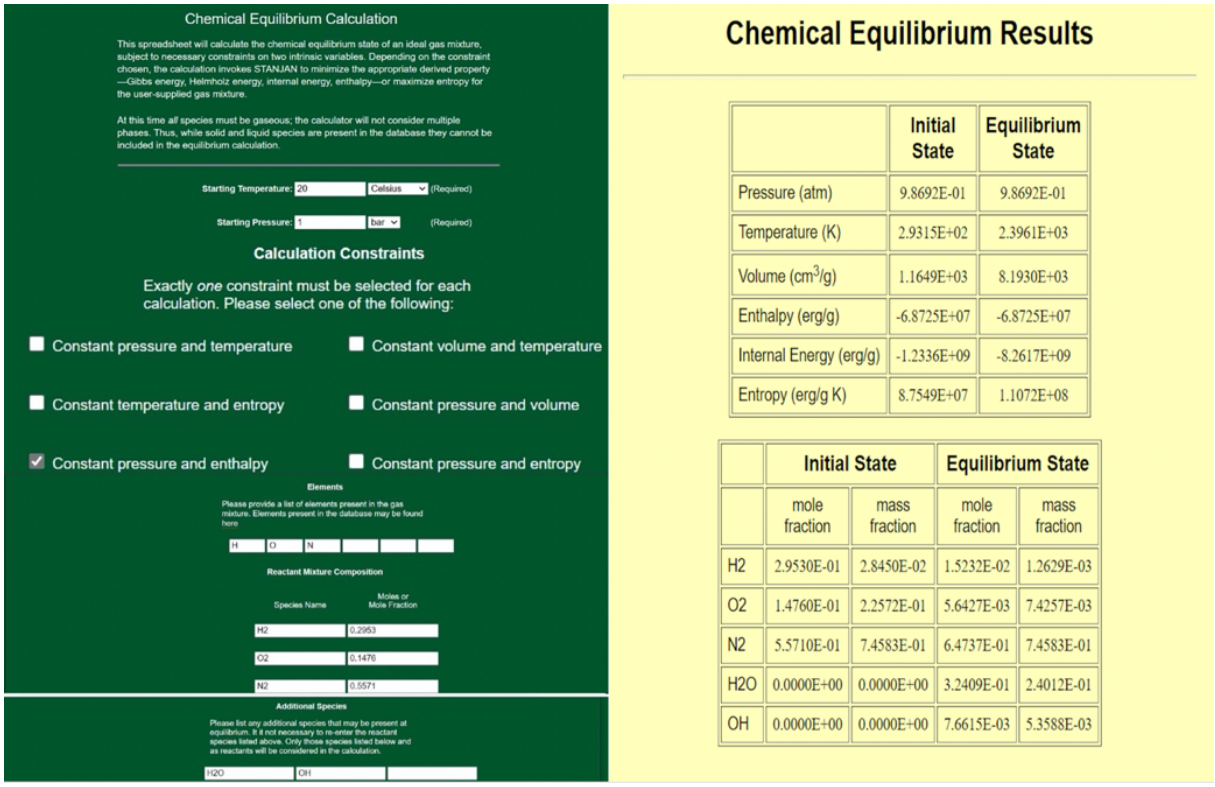

	Initial State	Equilibrium State
Pressure (atm)	9.8692E-01	9.8692E-01
Temperature (K)	2.9315E+02	2.3961E+03
Volume (cm^3/g)	1.1649E+03	8.1930E+03
Enthalpy (erg/g)	-6.8725E+07	-6.8725E+07
Internal Energy (erg/g)	-1.2336E+09	-8.2617E+09
Entropy (erg/g K)	8.7549E+07	1.1072E+08

	Initial State		Equilibrium State	
	mole fraction	mass fraction	mole fraction	mass fraction
H2	2.9530E-01	2.8450E-02	1.5232E-02	1.2629E-03
O2	1.4760E-01	2.2572E-01	5.6427E-03	7.4257E-03
N2	5.5710E-01	7.4583E-01	6.4737E-01	7.4583E-01
H2O	0.0000E+00	0.0000E+00	3.2409E-01	2.4012E-01
OH	0.0000E+00	0.0000E+00	7.6615E-03	5.3588E-03

Figure 3.6: Input specifications and outputs of product temperature with $ER = 1$

T_P simulated by FLACS:

Temperature output in FLACS simulation corresponds to the temperature in products given by once the flame has reached the monitor point (MP). Furthermore, the value of temperature output responses linearly to the production output in FLACS. With monitor points located differently, the output of temperature and production will vary from one monitor point to another. The highest temperature output value will be chosen as the product temperature used to predict laminar burning velocity. To confirm that correct T_P is chosen for later work, both the output of temperature and production for all the selected monitor points should be checked. Figure 3.7 shows an example for the output of temperatures and productions corresponding to selected monitor points with the equivalence ratio equals 1. In FLACS-CFD 20.1 the production output is shown in the form of a mass fraction. Here the mass fraction for MP No. 6 is around 0.0001, which means no flame goes through this point. Correspondingly, the temperature output in this monitor point will be the initial temperature, and this is confirmed by the figure located on the left top.

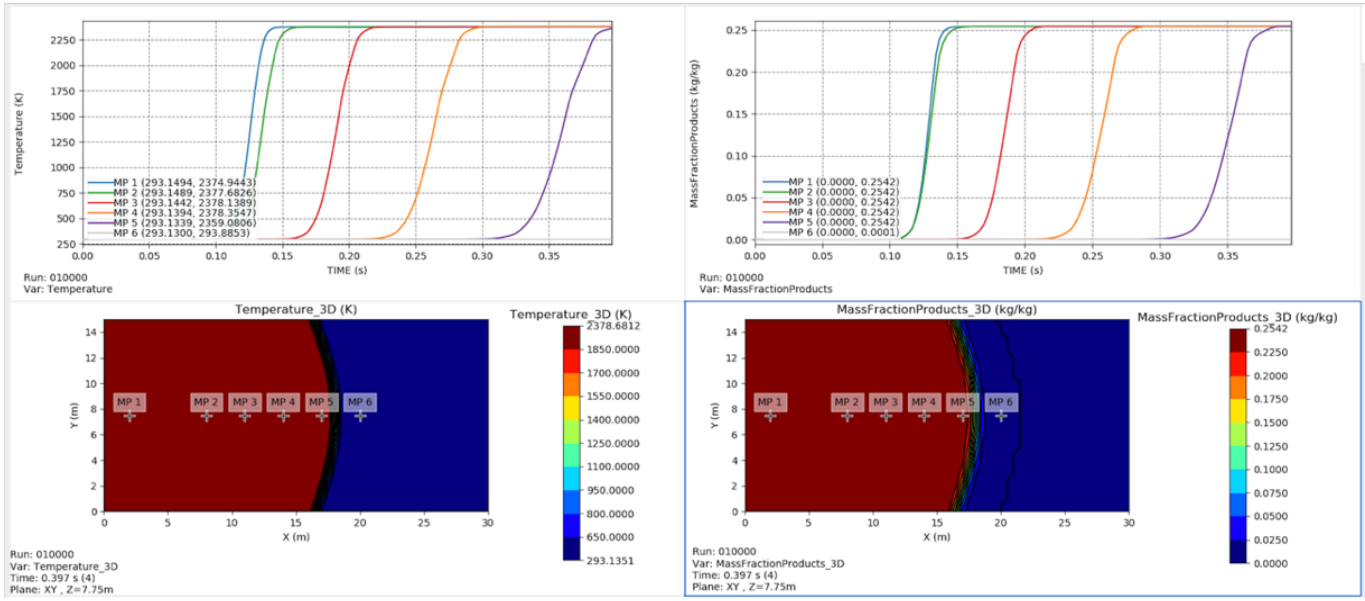

Figure 3.7: The mass fraction and temperature in products corresponding to six monitor points with $ER = 1$ (FLACS-CFD 20.1)

Since there are two different versions of FLACS available for simulation, a comparison is completed to check if there is any difference in temperature in products between these two versions. Table 3.10 shows five temperatures in products for each version of FLACS corresponding to representative equivalence ratios.

Table 3.10: Temperature in products given by two available FLACS

ER	T_p - FLACS *v*10.9 [K]	T_p - FLACS-CFD 20.1 [K]	Deviation [‰]
0.40	1428.7720	1428.7524	0.0137
1.07	2394.3782	2394.3452	0.0138
1.29	2328.2949	2329.2920	-0.0012
1.64	2186.2795	2186.2444	0.0161
7.49	1112.5574	1113.4233	-0.7783

The maximum temperature in products comes with $ER = 1.07$, both for FLACS v10.9 and FLACS-CFD 20.1. The values of T_P^{max} agree well with the maximum product temperature for hydrogen-air mixtures in the literature. Lower values of temperature in products obtained both for FLACS v10.9 and FLACS-CFD 20.1 when laminar burning velocity peaks at $ER = 1.64$. The temperature in products simulated by FLACS-CFD 20.1 is generally lower than that given by FLACS v10.9. However, higher T_P resulted from FLACS-CFD 20.1 for $ER = 1.29$ and 7.49. The deviation temperature in products between two versions of FLACS is negligible since the most significant deviation that obtained with $ER = 1.79$ is smaller than 1%.

Comparison of T_P between two approaches:

Since there are two approaches for obtaining product temperature, a comparison of T_P is completed for ensuring that proper values of product temperature using in the model comparison of laminar burning velocity prediction in Chapter 4. Figure 3.8 shows three types of T_P for hydrogen-air combustion as a function of equivalence ratio at room temperature and atmospheric pressure. Cross marks refer to product temperature estimated by chemical equilibrium calculator. The dots and circles are on behalf of temperature in products corresponding to FLACS-CFD 20.1 and FLACS v10.9.

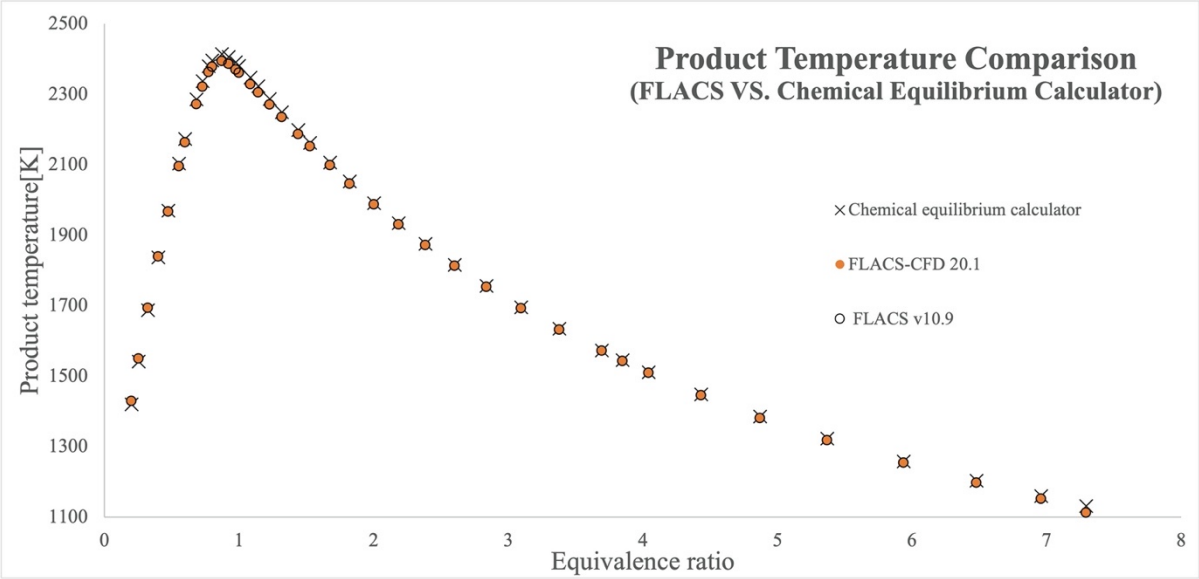

Figure 3.8: Product temperature comparison

The indistinctive difference among these three T_P observes in this figure. It is assumed that product temperature both from FLACS and online chemical equilibrium calculator can further predict laminar burning velocity. However, there is a slight difference in temperature output between the two versions of FLACS. Meanwhile, the product temperatures resulted from FLACS are sensitive to the location of monitor points. By contrast, the product temperature given by the online chemical equilibrium calculator will be used to compare laminar burning velocity prediction.

Activation temperature estimation

The activation temperature can be estimated from dependence of laminar burning velocity on product temperature according to

$$S_L^2 \propto e^{-T_A/T_P} \tag{3.19}$$

T_A can be determined by plotting $\ln S_L^2$ versus $1/T_P$. The value of T_A is inversely the slope evaluating with least square method. Dorofeev et al. (2001) commented that experimental data show good linear behaviour in $\ln S_L^2$ and $1/T_P$ variables for hydrogen-lean mixtures and stoichiometric mixtures. Therefore, T_A can be predicted by the linear relation between $\ln S_L^2$

and $1/T_P$ with lean and stoichiometric hydrogen mixtures. Arntzen (1998) assumed that a constant activation temperature can be applied for combustion under given initial temperature and pressure, independent of fuel concentration. It is, therefore, an activation temperature extracted from the plot of $\ln S_L^2$ and $1/T_P$ with lean and stoichiometric hydrogen mixtures can also be applied for prediction laminar burning velocity in hydrogen-rich mixtures.

A concrete value of activation temperature is needed for prediction model testing of laminar burning velocity. Thus, available values of T_P and S_L are required for the determination of T_A. The values of laminar burning velocities and product temperatures corresponding to the selected equivalence ratios range from 0.4 to 1 at the desired initial temperature, and pressure can be estimated with FLACS and chemical equilibrium calculator. Without the Le-dependent correction, FLACS gives more reasonable laminar burning velocities in hydrogen-air mixtures, as shown in Figure 2.10. Therefore, it is assumed that S_L resulting from FLACS simulation with no Le-dependent correction can be used to predict T_A. Figure 3.9 shows a construction of a stoichiometric hydrogen-air gas explosion in FLACS in a nonconfined gas cloud with six specific monitor points located in the middle of the cloud. Based on this method, $T_A = 13305\ K$ is obtained for hydrogen-air mixtures at 25 ℃ and 1 atm.

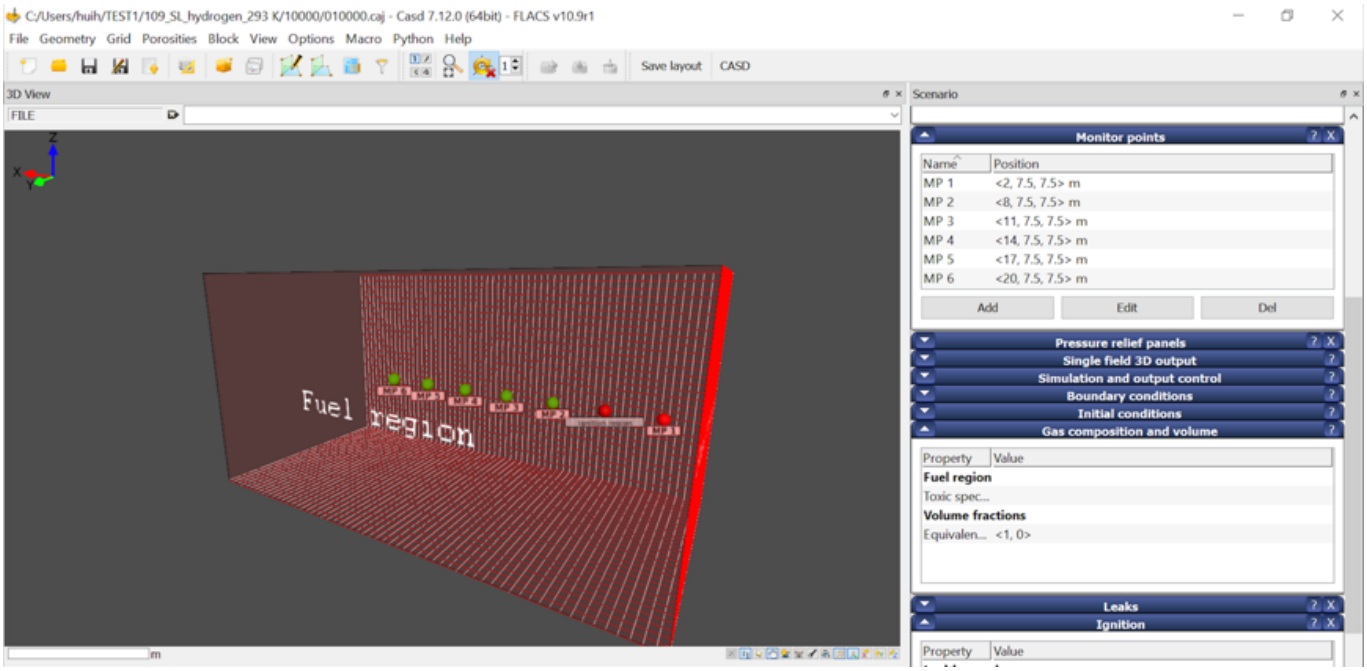

Figure 3.9: Inputs specifications for FLACS simulation of gas explosion in hydrogen-air mixtures ($ER = 1$)

The value of activation temperature varies from model to model. Therefore, various activation temperatures can be utilized in S_L model testing. Arntzen (1998) suggested that $T_A = 12000$ can be used as the activation temperature for hydrogen-air mixtures. Dorofeev et al. (1999) presented three reliable activation temperatures based on the analysis of experimental data related to hydrogen combustion at temperatures varying from 298 K to 650 K and pressure varying from 1 bar to 3 bars. For hydrogen-air lean mixtures, $T_A = 9800\ K$. For hydrogen-air rich mixtures, $T_A = 17700\ K$. For stoichiometric $H_2/O_2/N_2$ mixtures, $T_A = 10400\ K$.

Pre-exponential factor determination

The value of the pre-exponential factor varies with the model of laminar burning velocity prediction. Equations for pre-exponential factor estimation to S_L models are listed in Table 3.11.

Table 3.11: Estimation equations for pre-exponential factor

Hypothesis model	Equation for A estimation
1	$A = S_L^2 * 50000 * e^{T_A/T_P}$
2	$A = S_L^2 * \alpha_{mix}^{-1} * e^{T_A/T_P}$
3	$A = S_L^2 * \alpha_{mix}^{-1} * Le_{eff}^{-1} * e^{T_A/T_P}$
4	$A = S_L^2 * \alpha_{mix}^{-1} * Le_{eff}^{-1} * (c_F^{n_F})^{-1} * e^{T_A/T_P}$

According to the assumption of Arntzen (1998), a constant pre-exponential factor can be applied for combustion under given initial temperature and pressure, regardless of fuel concentration change. Therefore, the pre-exponential factor given by the maximum laminar burning velocity and maximum product temperature will be chosen to verify the model efficiency of laminar burning velocity prediction.

Fuel concentration determination

The chemical time scale is expressed as a function of pre-exponential factor, the molar concentration of hydrogen, activation temperature, and product temperature in hypothesis model 4. Therefore, the determination of hydrogen concentration should be specified. Since hydrogen can be regarded as an ideal gas, and the ideal gas law can be applied for estimation of the molar concentration of hydrogen with the expression as follows

$$c_{H2} = x_{H2} * \frac{p}{(R*T_i)} \tag{3.20}$$

with c_{H2} refers to the molar concentration of hydrogen in the mixtures of reactant, x_{H2} is a ratio of hydrogen in reactant by volume, p, T_i and R are initial pressure, temperature, and universal gas constant respectively. The detailed formula derivation is shown in Appendix C.

3.5 Turbulent burning velocity models

Based on the prediction equations presents in section 2.4, the turbulent burning velocity depends on turbulent fluctuation velocity, laminar burning velocity, integral length scale, kinematic viscosity, Lewis number, and Markstein number. In contrast, the laminar burning velocity can be expressed either as a function of thermal diffusivity and chemical time scale or thermal diffusivity, Lewis number, and chemical time scale. Combined all the expressions for laminar burning velocity and turbulent burning velocity, three equations can predict turbulent burning velocity, as shown in Table 3.12. The detailed formula derivation is shown in Appendix D.

Table 3.12: Prediction equations for turbulent burning velocity

	Equations for S_T prediction
1	$S_T = C_{ST} * C_K^{-\beta} * \left(u'\right)^{(1-1.5*\beta)} * \alpha^{\beta} * \tau_c^{-\beta} * l_I^{0.5*\beta} * \nu^{(-0.5*\beta)}$
2	$S_T = C_{ST} * C_K^{-\beta} * \left(u'\right)^{(1-1.5*\beta)} * \alpha^{\beta} * Le^{\beta} * \tau_c^{-\beta} * l_I^{0.5*\beta} * \nu^{(-0.5*\beta)}$
3	$S_T = C_{ST} * C_K^{-\beta} * \left(u'\right)^{(1-1.5*\beta)} * \alpha^{\beta} * \tau_c^{-\beta} * l_I^{0.5*\beta} * \nu^{(-0.5*\beta)} * Le^{(-\beta)}$

In comparison with these three equations, the differences come with the Lewis number correction and Markstein number correction corresponding to the selection of C_{ST} and β. In the view of Lewis number correction, the first equation is valid for conditions that both laminar and turbulent burning velocities either corrected or not with Lewis number. These two conditions can be distinguished by the different estimations for chemical time scales. The second equation is valid for the condition that only laminar burning velocity is corrected by Lewis number. The third equation is valid for the condition that only turbulent burning velocity is corrected by Lewis number. In the view of Markstein number, different prediction results of turbulent burning velocities would obtain either based on fixed C_{ST} and β or on C_{ST} and β varying with Markstein number for all these three equations.

All the factors involving these three equations are classified into three groups: laminar burning velocity group, turbulent Reynolds number group, and dimensionless constant number group. The laminar burning velocity group includes α, τ_c, and Le. The turbulent Reynolds number group includes $u^{'}, l_I,$ and ν. The dimensionless constant number group includes C_{ST}, C_K, and β. All these three groups will be specified separately in the following section.

The laminar burning velocity group

Different values related to $u^{'}, l_I$ and ν can be chosen for model testing. The thermal diffusivity can be a fixed value, that is $2 * 10^{-5}$ as utilized in FLACS or a constant varying with equivalence ratio, same as utilized in S_L prediction models. The chemical time scale and Lewis number would be estimated with the same approaches utilized in S_L prediction models.

The turbulent Reynolds number group

Different values related to $u^{'}, l_I$ and ν can be chosen for model testing. For example, Bradley et al. (1987) collected six different experiment data related to turbulent burning velocities in hydrogen-air mixtures. The values of $u^{'}, l_I,$ and ν differ from experiment to experiment, as shown in Table 3.13. Typically, the turbulent fluctuation velocity would be varied from 0.2 to 18 meters per second. The integral length scales would be varied from 1 mm to 10 cm. The

kinematic viscosity would be a value with a magnitude of 10^{-5}. The value of kinematic viscosity also can be estimated with an approximation of $\nu = \alpha$ (Bray, 1990), and the prediction equations for turbulent burning velocity can be updated as shown in Table 3.14.

Table 3.13: Experimental data of $u', l_I, and\ \nu$ utilized in the determination of turbulent burning velocities in hydrogen-air mixtures (Bradley et al., 1987)

	$u'\ [m/s]$	$l_I\ [mm]$	$10^6 * \nu\ [m^2/s]$
1	0.33 – 5.98	14.2 – 38.2	17.98 – 24.08
2	4.07 – 17.29	37.23 – 43.0	28.51
3	0.24 – 17.29	12.49 – 43.0	21.44 – 38.50
4	0.30 – 9.80	0.07 – 115.5	149
5	0.76 – 5.66	4.35 – 12.42	19.51
6	0.40 – 11.60	Re_T estimated	17.83 – 20.75

Table 3.14: Prediction equations for turbulent burning velocity ($\nu = \alpha$)

	Equations for S_T prediction
1	$S_T = C_{ST} * C_K^{-\beta} * \left(u'\right)^{(1-1.5*\beta)} * \alpha^{0.5*\beta} * \tau_c^{-\beta} * l_I^{0.5*\beta}$
2	$S_T = C_{ST} * C_K^{-\beta} * \left(u'\right)^{(1-1.5*\beta)} * \alpha^{0.5*\beta} * Le^{\beta} * \tau_c^{-\beta} * l_I^{0.5*\beta}$
3	$S_T = C_{ST} * C_K^{-\beta} * \left(u'\right)^{(1-1.5*\beta)} * \alpha^{0.5*\beta} * \tau_c^{-\beta} * l_I^{0.5*\beta} * Le^{(-\beta)}$

The dimensionless constant number group

Different values relative to C_{ST}, C_K, and β can be chosen for model testing. They can be fixed values as utilized in models of Bray (1990), Bradley et al. (1992) and Bradley et al. (2013). They also can be other constants fulfilling certain limitations. For example, the value of β would vary typically from 0.2 to 0.4. The value of C_K should be conformance to the specification of Karlovitz strain rate, e.g., $K < 0.3$ or $K > 0.05$ for Bray (1990) model and Brayley et al. (2013) model respectively. C_{ST} and β would vary with Markstein number

based Baredley et al. (2013). For hydrogen, the Markstein number utilized in experiments carried out by Baredley et al. (2013) ranged from -23.6 to -5.59 for $ER < 1$.

4 RESULT AND DISCUSSION

In this chapter, the laminar burning velocities relative to the 4 hypothesis models will be calculated. Results will be presented and discussed regarding comparison with different literature and FLACS model. The turbulent burning velocities relative to prediction models will be calculated. Results will be presented and discussed regarding comparison with selected literature experiments and the FLACS model.

4.1 Laminar burning velocity model

The 4 hypothesis models will be tested by comparison with the FLACS model result of the laminar burning velocities the select the most effective model for S_L prediction in hydrogen-air mixtures. The accuracy of the selecting model will be verified by the comparison of literature data. *Table 4.1* lists the corresponding initial conditions for estimation of laminar burning velocities for comparisons.

Table 4.1: Initial conditions for prediction of laminar burning velocity

T_i [K]	p [atm]	x_{H2} [vol %]	ER
298.15	1	14 – 76	0.4 – 7.5

Same as the laminar burning velocity, the determination of other parameters in this section is based on initial conditions listed in Table 4.1, unless stated otherwise.

4.1.1 Testing thermal diffusivity for fuel and oxidant

The property of thermal diffusivity distinguishes the laminar burning velocity of hydrogen-air mixtures. It is crucial to verify the accuracy of thermal diffusivity of hydrogen, oxygen, and nitrogen by comparison with corresponding literature data (CRC Handbook of Chemistry and

Physics, 71st edition). The thermal diffusivity of oxygen and nitrogen are highly similar to each other. Based on the lack of direct literature data of α_{O2}, the comparison will focus on thermal diffusivity of hydrogen and nitrogen at atmospheric pressure and $T = 300\ K$. Table 4.2 lists all the equations related to calculation of α_{H2} and α_{N2} with corresponding constants.

Table 4.2: Equations for calculation thermal diffusivity of hydrogen and nitrogen

Species	**Equation for calculation α**
Hydrogen	$\lambda = 6.9107 + 0.597 * T_i$
	$\rho = (p * 2.016)/(8.3145 * T_i)$
	$c_p = 11.62 + 0.0093 * T_i$
Nitrogen	$\lambda = 1.1072 + 0.0841 * T_i$
	$\rho = (p * 28.014)/(8.3145 * T_i)$
	$c_p = 1.0425 - 0.0000169 * T_i$

Table 4.3 shows the results of calculation and comparison for α_{H2} and α_{N2} separately.

Table 4.3: Thermal diffusivity comparison for hydrogen and nitrogen between prediction model and literature data

	λ $[W/m \cdot K]$	ρ $[g/m^3]$	C_p $[J/g \cdot K]$	α_{model} $[m^2/s]$	$\alpha_{Literature}$ $[m^2/s]$	Deviation [%]
Hydrogen	0.186	81.89	14.41	$1.58 * 10^{-4}$	$1.6 * 10^{-4}$	-1.25
Nitrogen	0.026	1137.98	1.04	$2.23 * 10^{-5}$	$2.2 * 10^{-5}$	1.36

The thermal diffusivity of hydrogen estimated by the model is 1.25% lower than the literature data. Calculated nitrogen thermal diffusivity based on the model is 1.36% higher than the literature data. The small deviations for α_{H2} and α_{N2} indicate that thermal diffusivity estimation based on thermal conductivity model results effective thermal diffusivity values both for fuel and oxidant. The hypothesis models 2, 3, and 4 for laminar burning velocity prediction depend on the mixture thermal diffusivity differing with equivalence ratio, e.g., as shown in Figure 4.1.

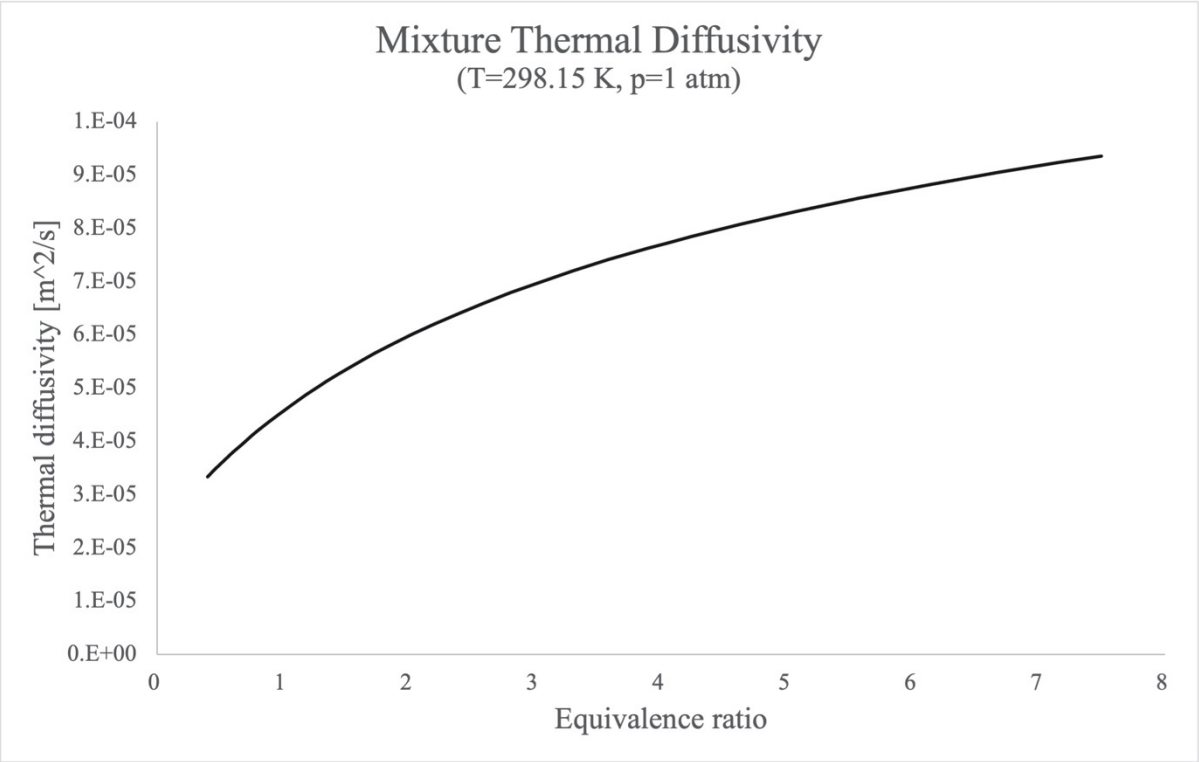

Figure 4.1: The mixture thermal diffusivities vary with ER (at NTP)

4.1.2 Testing effective Lewis number model

Specific physical and chemical properties of hydrogen enhance the flame instability resulting from hydrogen-air combustion. An effective Lewis number model is required to represent this flame instability. Based on the calculation model for effective Lewis number, Le_{eff} is dependent on an effective Zeldovich number that varies with equivalence ratio through its dependence on product temperature and Lewis number for hydrogen and oxygen. Figure 4.2 presents the effective Lewis number for hydrogen-air mixtures as a function of equivalence ratio with $T_A = 13305$ K.

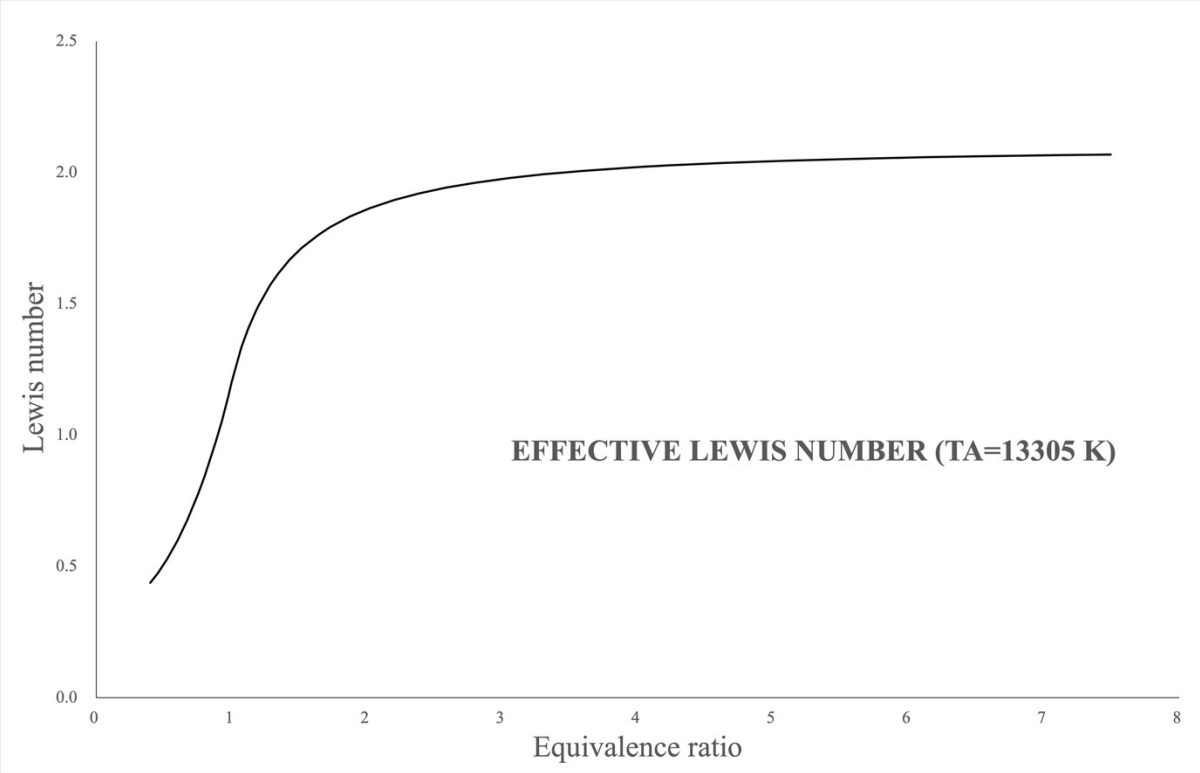

Figure 4.2: The effective Lewis number for
hydrogen-air mixtures with T_A = 13305 K

Generally, the effective Lewis number for hydrogen-air mixtures increases with increasing equivalence ratio. In the hydrogen lean mixtures, $Le_{eff} < 1$ was observed for $ER < 0.9$. The effective Lewis number increases from 0.996 to 1.20 when the equivalence ratio varies from 0.9 to 1.0. In hydrogen rich mixtures, $Le_{eff} > 1$. For most of selected equivalence ratios, the values of effective Lewis number agree well with the theoretical requirements, where $Le_{eff} < 1$ for $ER < 1$, and $Le_{eff} > 1$ for $ER > 1$.

The effective Lewis number estimation also depends on the activation temperature through Zeldovich number. As mentioned in section 3.1.3, there are multiple choices of activation temperatures to determine laminar burning velocity in hydrogen-air mixtures. Figure 4.3 shows the comparison of the effective Lewis number predicted to five different activation temperatures mentioned in section 3.1.3 for reviewing the dependence of Le_{eff} on activation temperature.

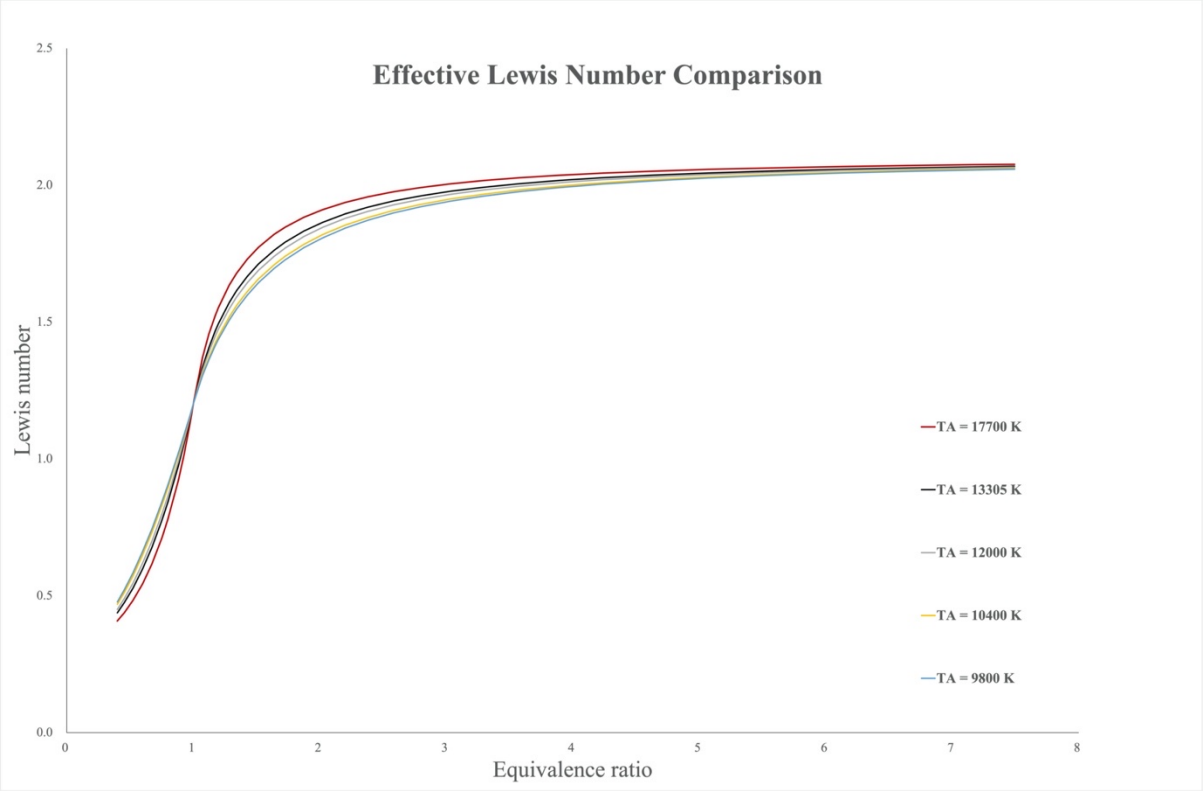

Figure 4.3: Effective Lewis number comparison
with respect to different activation temperatures

Le_{eff} decreases with increasing activation temperature for $ER < 1$, and it increases with rise of T_A for $ER > 1$. Comparatively, a smaller deviation among these five effective Lewis numbers obtained for $ER > 3$. It indicates that the effective Lewis number becomes less sensitive to the change of activation temperature for mixtures far from stoichiometry in fuel-rich side. For example, at $ER = 4.05, Le_{eff} = 2.01$ for $T_A = 9800\ K$; and $Le_{eff} = 2.04$ for $T_A = 17700\ K$. The value of Le_{eff} changes slightly comparing with larger varying of activation temperature. For $1 < ER < 2$, the deviation increases related to increase in activation temperature. Table 4.4 shows the effective Lewis numbers corresponding to activation temperatures for $ER = 1.07$ (that product temperature peaks) and $ER = 1.64$ (that laminar burning velocity peaks in FLACS simulation).

Table 4.4: The effective Lewis number corresponding to activation temperatures for $ER = 1.07$ and $ER = 1.64$

T_A [K]	$Le_{eff\ (ER=1.07)}$	$Le_{eff\ (ER=1.64)}$
9800	1.30	1.70
10400	1.31	1.71
12000	1.32	1.74
13305	1.33	1.76
17700	1.37	1.82

For T_A increases directly from 9800 K to 17700 K, the effective Lewis number increased 5.38% (from 1.30 to 1.37) when product temperature was peaking obtained. Under maximum laminar burning velocity circumstance, the effective Lewis number increased 7.06% (from 1.70 to 1.82). Therefore, a raised deviation caused by activation temperature would be obtained, as shown in Figure 4.2. The effective Lewis number increased 1.54% for T_A varies from 9800 K to 12000 K at $ER = 1.07$, and it increased 2.35% at $ER = 1.64$. Consequently, the effective Lewis number is less dependent on activation temperature for $T_A < 13305\ K$.

4.1.3 Testing 4 hypothesis models for S_L prediction

To estimate prediction accuracy of the hypothesis models listed in Table 3.1, all the calculated S_L based on these four models would be tested by comparing the FLACS model. For easy comparison, maximal laminar burning velocity for all four models is fixed to S_L^{max} given by the FLACS model. All the parameters related to calculating the pre-exponential factor corresponding to each model are listed in Table 4.5.

Table 4.5: All the parameters related to the calculation of A

S_L Model	S_L^{max} $[m/s]$	T_A [K]	T_p^{max} [K]	α_{mix} $[m^2/s]$	Le_{eff}	Power exponent for c_{H2}
1	2.9214	13305	2419.6	$2.00 * 10^{-5}$	/	0.93
2				$4.69 * 10^{-5}$		
3					1.33	
4						

The product temperature for hydrogen-air mixtures peaks at $ER = 1.07$. Therefore, the calculation values of mixture thermal diffusivity and effective Lewis number corresponding to $ER = 1.07$ are selected for models 2-4. Figure 4.4 represents all the laminar burning velocities corresponding to 4 hypothesis models and the FLACS model with the same initial conditions. The square marks refer to the laminar burning velocities given by FLACS, and four lines present correspondingly four models.

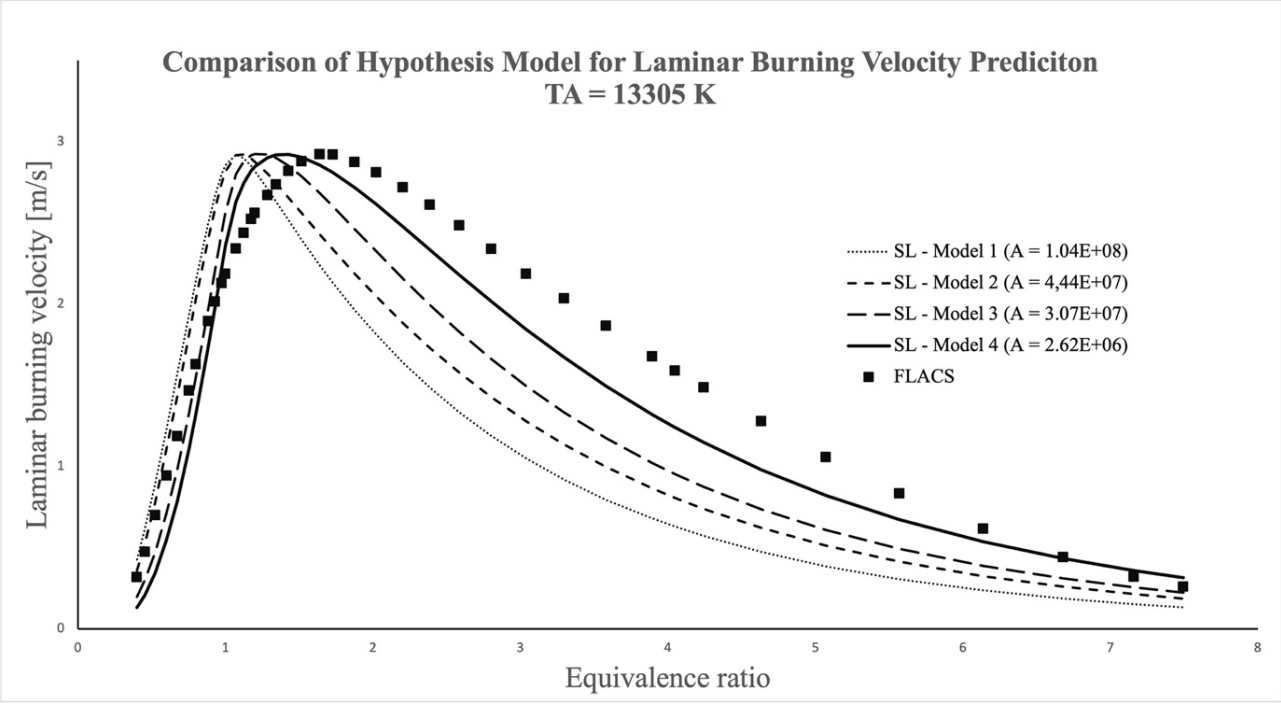

Figure 4.4: Laminar burning velocity comparison between hypothesis models and FLACS model (T_A = 13305 K)

For FLACS, the maximum laminar burning velocity comes with $ER = 1.64$. For all hypothesis models, S_L^{max} observed in hydrogen-rich mixtures, and the location corresponded to ER is gradually shift to the right. S_L for model 1 peaks at $ER = 1.07$, which is the same equivalence ratio where maximum product temperature is obtained. S_L for model 2 peaks at $ER = 1.12$. S_L for model 3 and 4 peaks at $ER = 1.20$ and $ER = 1.43$, respectively. Theoretically, the maximum product temperature for hydrogen-air mixtures comes with an equivalence ratio slightly higher than 1, and the laminar burning velocity peaks at an equivalence ratio near 1.7. Comparatively, hypothesis model 4 consists best with these two requirements. Hypothesis model 1 and 2 are more suitable for predicting the laminar burning velocity of hydrocarbon-air mixtures, such as methane-air mixtures. Same as product temperature, the maximum laminar burning velocity for methane-air mixtures will be obtained with an equivalence ratio close to stoichiometry.

The comparison between prediction models and the FLACS model shows that $S_{L-model}$ agrees well with $S_{L-FLACS}$ in hydrogen-lean mixtures. In the hydrogen-rich mixtures, a small deviation is observed when the equivalence ratio varies from 1 to 1.52. For $ER > 1.52$, the values of $S_{L-model}$ are distinctively lower than $S_{L-FLACS}$, especially the values estimated by hypothesis models 1, 2 and 3. The fitness of $S_{L-model}$ to $S_{L-FLACS}$ should be improved. The dependence of laminar burning velocity on activation temperature and the pre-exponential factor shown in section 2.3.3 can be applied for adjustment of the fitness. With a smaller activation temperature, the laminar burning velocities will rise, and deviations in hydrogen-rich mixtures between $S_{L-model}$ and $S_{L-FLACS}$ can be minimized. However, S_L^{max} will increase at the same time, and therefore, a smaller pre-exponential factor should be applied for keeping the maximum laminar burning velocity equals 2.9214. Figure 4.5 shows a new comparison of laminar burning velocity between FLACS and prediction results. Smaller activation temperature and the pre-exponential factors corresponding to all hypothesis models are used for $S_L$estimation.

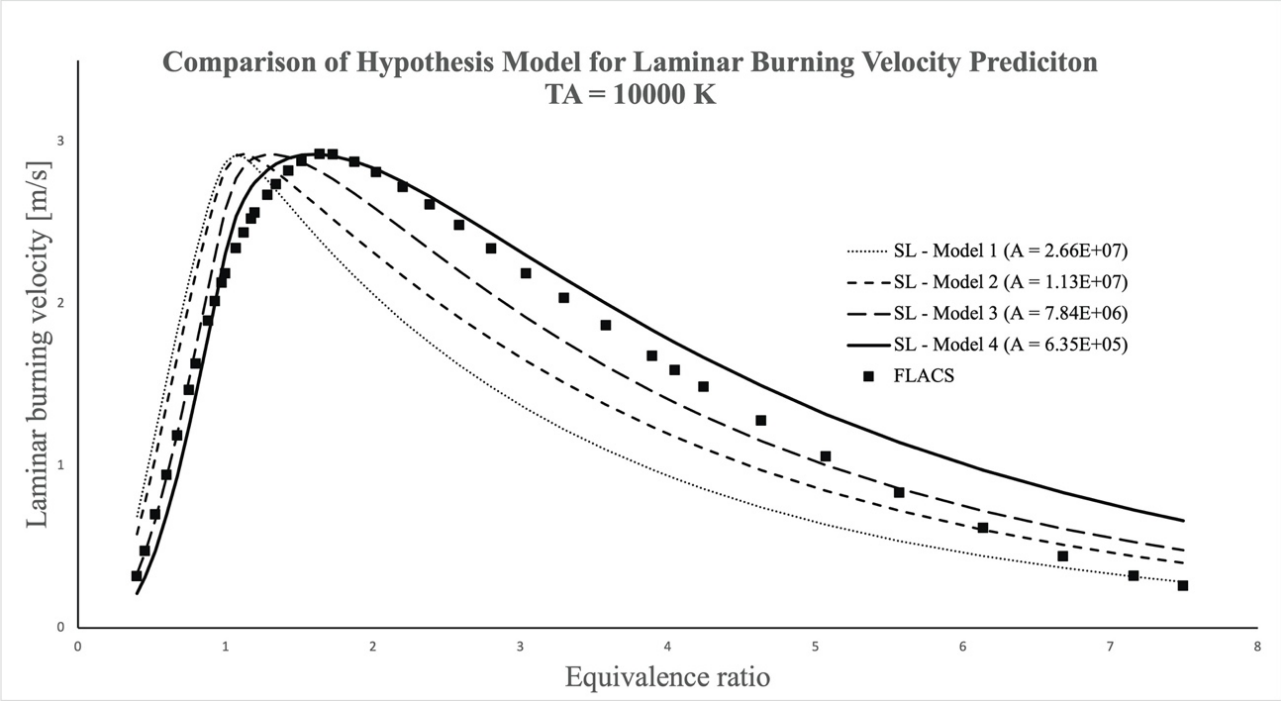

Figure 4.5: Laminar burning velocity comparison between hypothesis models and FLACS model (T_A = 10000 K)

With the adjustment of T_A and A, better fitness are observed for model 3, model 4 to FLACS. In the hydrogen-lean mixtures, $S_{L-model\,3}$ and $S_{L-model\,4}$ agree well with $S_{L-FLACS}$. In the hydrogen-rich mixtures, deviations become smaller for $S_{L-model\,3}$ and $S_{L-model\,4}$. Comparatively, laminar burning velocities estimated by the hypothesis model 4 fit the FLACS model results best. For $1 < ER < 4$, model 4 gives the most minor deviation. Although the deviation between model 4 and FLACS increases with the rise of the equivalence ratio for $ER > 4$, hypothesis model 4 gives best prediction of laminar burning velocity relative to the most selected equivalence ratios.

Selection of activation temperature, pre-exponential factor and power exponent of fuel concentration

There are multiple choices of activation temperature, pre-exponential factor, and power exponent of hydrogen concentration for the laminar burning velocity prediction. The selection of these three parameters can be narrow down for the specific requirements related to the hydrogen-air combustion theory. For example, S_L^{max} comes with $ER \approx 1.7$

theoretically. Consequently, a higher value of S_L should be obtained for $ER \approx 1.7$ than S_L for $ER \approx 1.5$. Table 4.6 shows predicted laminar burning velocities with respect to four equivalence ratios and five activation temperatures varying from 9800 K to 12000 K. Same power exponent of hydrogen concentration utilized for all activation temperatures. Pre-exponential factors are modified to get a fixed value of S_L^{max} corresponding to each activation temperature.

Table 4.6: Laminar burning velocities corresponding to the selected ERs

ER	$S_{L-FLACS}$ $[m/s]$	$S_{L\ (T_A=12000\ K)}$ $[m/s]$	$S_{L\ (T_A=11000\ K)}$ $[m/s]$	$S_{L\ (T_A=10000\ K)}$ $[m/s]$	$S_{L\ (T_A=9900\ K)}$ $[m/s]$	$S_{L\ (T_A=9800\ K)}$ $[m/s]$
1.43	2.8188	2.9214	2.9131	2.8965	2.8938	2.8912
1.52	2.8793	2.9186	2.9214	2.9158	2.9142	2.9127
1.64	2.9214	2.8929	2.9114	2.9214	2.9214	2.9214
1.73	2.9194	2.8606	2.8903	2.9119	2.9130	2.9142

Regardless of T_A change, a similar predicted S_L is obtained for each equivalence ratio. However, laminar burning velocity peaks at different equivalence ratios. The higher the activation temperature, the smaller the equivalence ratio corresponding to S_L peaking. Compared with the FLACS model, $T_A \leq 10000\ K$ gives better S_L prediction since the laminar burning velocity peaks at the same ER where $S_{L-FLACS}$ peaks. In the view of obtaining higher S_L at $ER \approx 1.7$, $T_A = 9800\ K$ would give a better prediction of S_L. Table 4.7 shows predicted laminar burning velocities with respect to three equivalence ratios and six power exponents of hydrogen molar concentration for $T_A = 9800\ K$.

Table 4.7: Laminar burning velocities as function of equivalence ratio and power exponent of c_{H2}

T_A [K]	n	$A * 10^5$ $[m^3/mol \cdot s]$	$S_{L\ (ER=1.52)}$ $[m/s]$	$S_{L\ (ER=1.64)}$ $[m/s]$	$S_{L\ (ER=1.73)}$ $[m/s]$
9800	0.90	6.15	2.9147	2.9214	2.9128
	0.91	5.98	2.9140	2.9214	2.9133
	0.92	5.81	2.9134	2.9214	2.9137
	0.93	5.65	2.9127	2.9214	2.9142
	0.94	5.49	2.9120	2.9214	2.9146
	0.95	5.34	2.9113	2.9214	2.9151

The value of S_L at $ER = 1.52$ is higher than that at $ER = 1.73$ when the power exponent smaller than 0.92. Similar S_L is obtained when the power exponent equals 0.92, and for $n \geq 0.93$, $ER = 1.73$ gives higher S_L. It is, therefore, 0.93, 0.94, and 0.95 would be better choices of power exponent for utilizing in the S_L prediction model. As mentioned in section 4.1.3, the deviation of S_L between the predicted model and the FLACS model increases with the rise of ER in hydrogen-ich mixtures. With the higher value of exponent coefficient of the molar concentration of hydrogen utilized in the model, the deviation will be slightly enlarged.

To sum up, it is recommended to utilize 0.93 as the exponent coefficient of the molar concentration of hydrogen in the prediction model for S_L.

4.1.4 S_L model comparison with selected literature data

Combined with specific hydrogen combustion theory, activation temperature that is smaller than 11000 Kelvin and power exponent of hydrogen concentration varying from 0.93 to 0.95 would enhance the effectiveness of the prediction model. Figure 4.6 compares the laminar burning velocities results from the prediction model 4, the FLACS model, and literature data at room temperature and atmospheric pressure. All the laminar burning velocities in this figure are plotted against the equivalence ratio. Figure 4.7 reviews the same comparison among prediction results, FLACS model and literature data, and the values of S_L plotted versus mole fraction of hydrogen. The dash lines in Figure 4.6 and Figure 4.7 represent the predicted values of S_L following the Equation Equation (4.1) as

$$S_L = \left[\alpha_{mix} * Le_{eff} * 9.52 * 10^5 * c_{H2}^{0.93} * e^{-(11000/T_P)}\right]^{1/2} \quad (4.1)$$

The solid lines in Figure 4.6 and Figure 4.7 represent the predicted values of S_L following the and Equation (4.2) as

$$S_L = \left[\alpha_{mix} * Le_{eff} * 5.65 * 10^5 * c_{H2}^{0.93} * e^{-(9800/T_P)}\right]^{1/2} \quad (4.2)$$

The square marks refer to the FLACS model results of S_L for both figures, and all other symbols represent the literature data relating to 8 experiments carried out between 1997 and 2013 with different experimental methods or data processing.

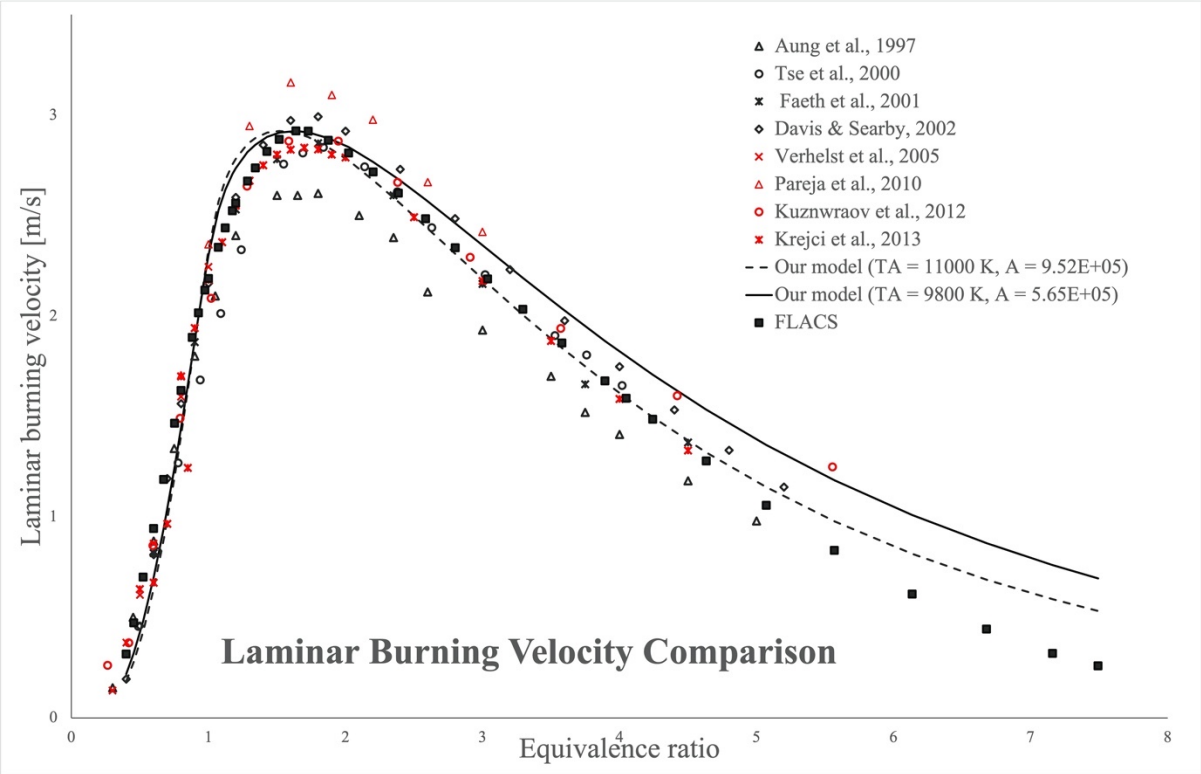

Figure 4.6: Laminar burning velocity in hydrogen-air mixtures as a function of ER

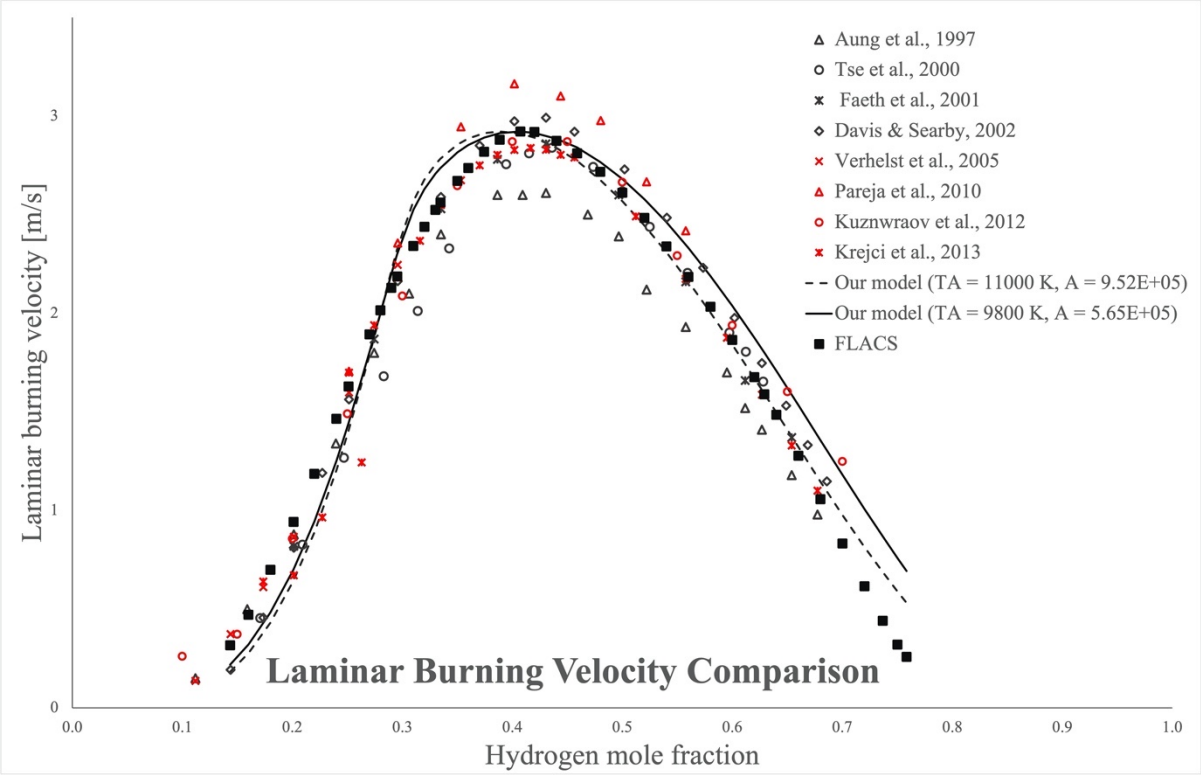

Figure 4.7: Laminar burning velocity in hydrogen-air mixtures as a function of x_{H2}

The predicted laminar burning velocities based on two sets of activation temperatures and pre-exponent factors are similar for $ER < 1.73$. For $ER > 1.73$, the deviation increases with the rise of hydrogen concentration in the mixtures. All predicted laminar burning velocities agree well with the selected literature data, especially in hydrogen-lean mixtures. Compared with the FLACS model results, the laminar burning velocities predicted with $T_A = 11000\ K$ gives the best fitness. Comparatively, the prediction model with $T_A = 9800\ K$ gives higher values of S_L in hydrogen-rich mixtures. Two possible reasons for enhancement of S_L prediction is listed as follows:

1. The mixture thermal diffusivity is dominated by the thermal diffusivity of hydrogen, which is much higher than oxygen and nitrogen. More hydrogen in mixtures, higher thermal diffusivity of mixture results which further leading to a larger value of laminar burning velocity.

2. The effective Lewis number becomes a fixed value as Lewis number for deficient substances in an equivalence ratio far from stoichiometry. The adjustment of Le_{eff} to S_L is weakened for $ER > 3$.

To sum up, a model resulting better prediction of laminar burning velocity in hydrogen-air mixtures dependents on parameters:

1. The thermal diffusivity given by an effective thermal conductivity estimation model that varies with mole fraction of hydrogen through the combination of mole fraction weighted, and harmonic mole fraction weighted approaches.

2. Effective Lewis number based on an effective Zeldovich number varies with equivalence ratio through its dependence on product temperature and Lewis number corresponding to hydrogen and oxygen.

3. Chemical time scale expressed as a function of fuel concentration, product temperature, activation temperature, and pre-exponential factor.

4.1.5 Testing S_L model for mixtures with different oxygen concentration in the air

Dilution of air with the insertion of extra nitrogen reduces the burning velocity and thereby the pressure in a hydrogen explosion. How well this effect is modelled is therefore studied below. Figure 4.8 – Figure 4.11 represent the comparison of the laminar burning velocities in H_2 / O_2 / N_2 mixtures with four different O_2 contents in the air, respectively. All the laminar burning velocities are plotted against the hydrogen mole fraction. The cross marks refer to the literature data extracted from the work of Lewis and von Elbe (1987). The solid square marks present the FLACS model results extracted from the work of Jon Tolaas (2017). The present burning velocity correction in FLACS due to other O_2/N_2 ratios is based on the data of Lewis and von Elbe (1987), with focus on higher oxygen concentrations. The FLACS model is not very accurate, as shown in fthe igures below. The black lines are on behalf of model prediction results based on the Equation (4.3) as follows

$$S_L = \left[\alpha_{mix} * Le_{eff} * 5.65 * 10^5 * c_{H2}^{0.93} * e^{-(9800/T_P)}\right]^{1/2} \quad (4.3)$$

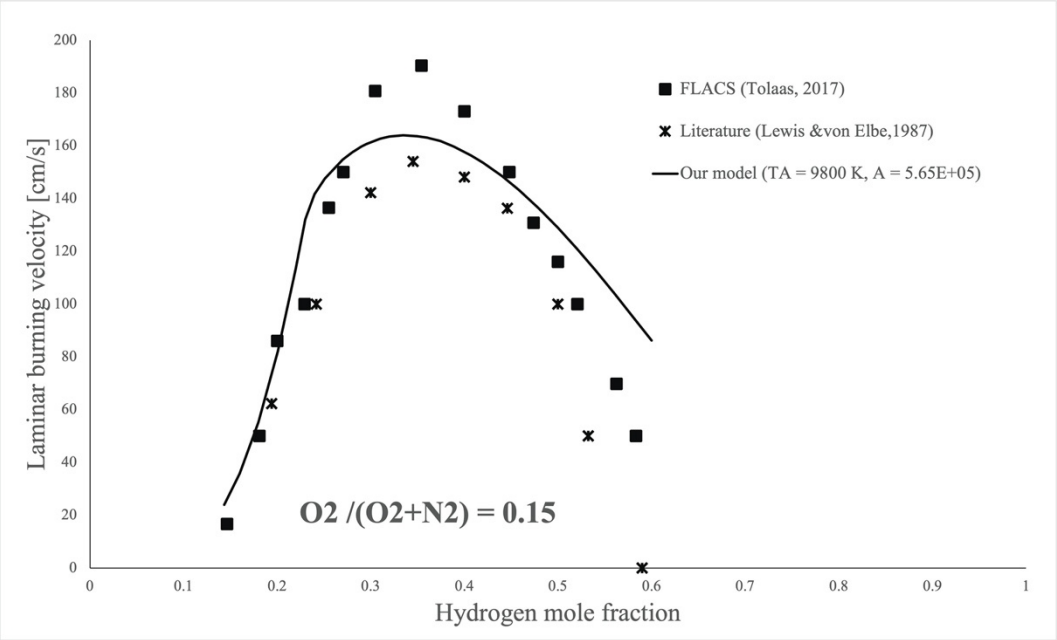

Figure 4.8: The laminar burning velocities as a function of x_{H2} in H_2 / O_2 / N_2 mixtures with $x_{O2} = 0.15$ vol% in the air

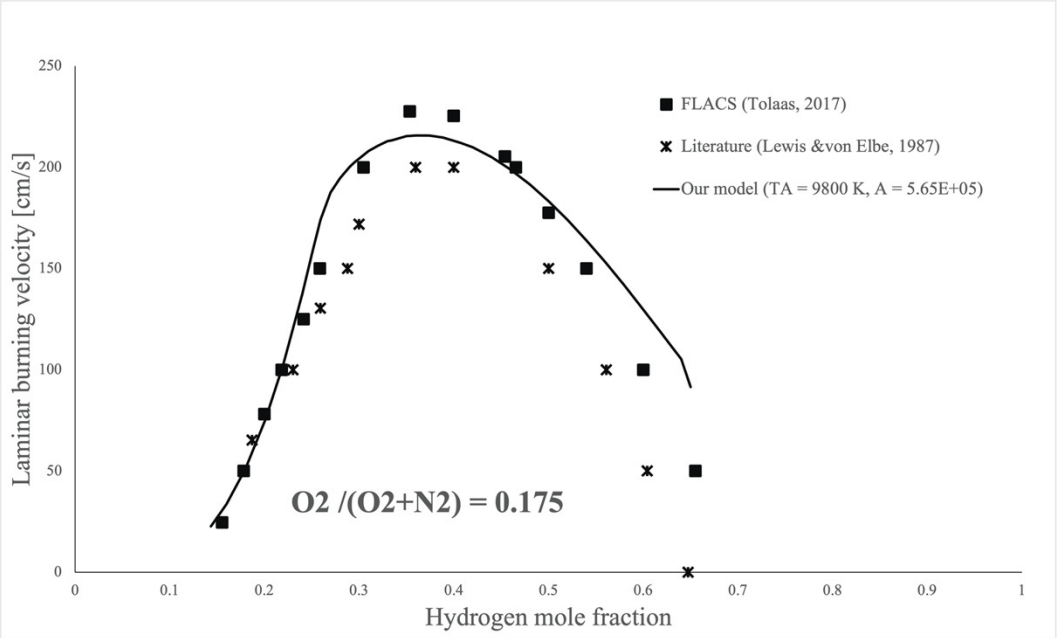

Figure 4.9: The laminar burning velocities as a function of x_{H2} in H_2 / O_2 / N_2 mixtures with $x_{O2} = 0.175$ vol% in the air

Figure 4.8 andFigure 4.9 present laminar burning velocities in hydrogen and nitrogen diluted air mixtures. Although the tendency for predicted values of laminar burning velocities is slightly tilted to the left, it agrees well both with literature data and the FLACS model results in hydrogen-lean mixtures. The prediction model results in higher value of laminar burning velocities with respect to a higher mole fraction of hydrogen comparing with literature data and FLACS model results. S_L^{max} comes with $x_{H2} = 33\ mol\%$ in Figure 4.8 and S_L^{max} comes with $x_{H2} = 36\ mol\%$ in Figure 4.9. Theoretically, the laminar burning velocity for hydrogen and normal air mixtures peaks at $x_{H2} \approx 42\ mol\%$. Less oxygen involved in the combustion and the chemical reaction will reach equilibrium in the lower hydrogen mole fraction. Therefore, the laminar burning velocity peaks at a lower hydrogen mole fraction correspondingly.

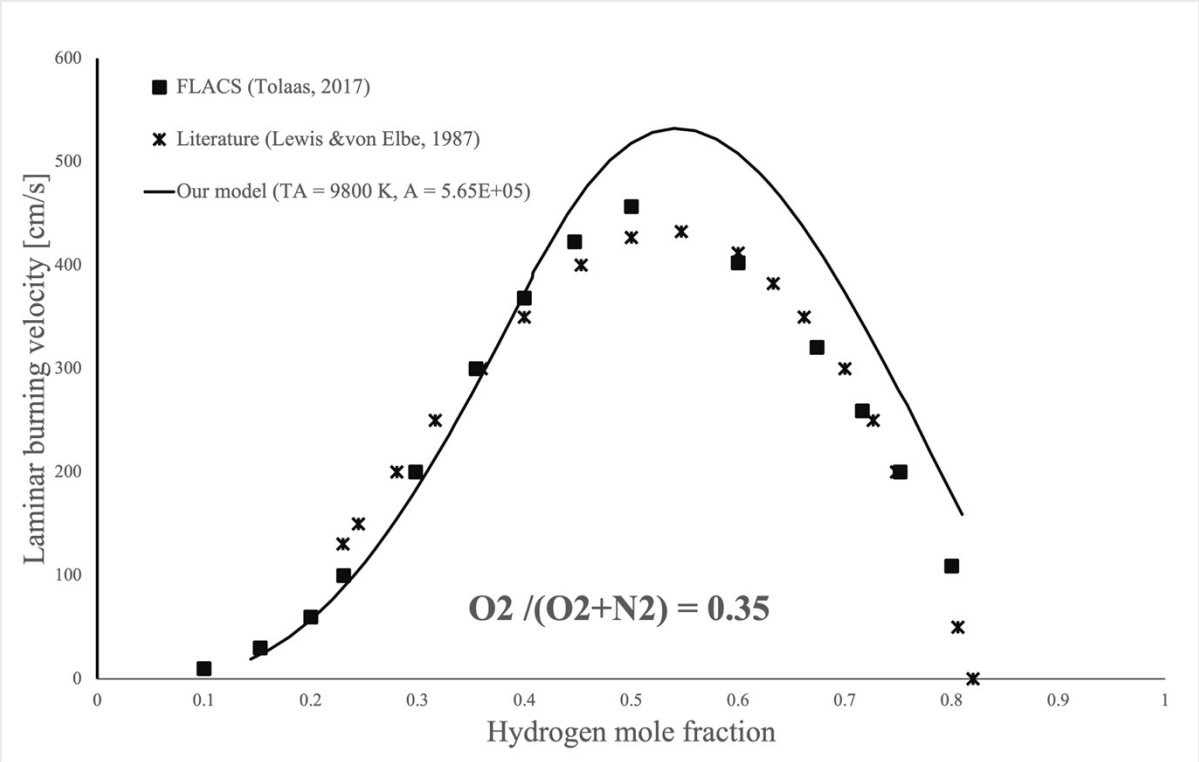

Figure 4.10: The laminar burning velocities as a function of x_{H2} in H_2 / O_2 / N_2 mixtures with $x_{O2} = 0.35$ vol% in the air

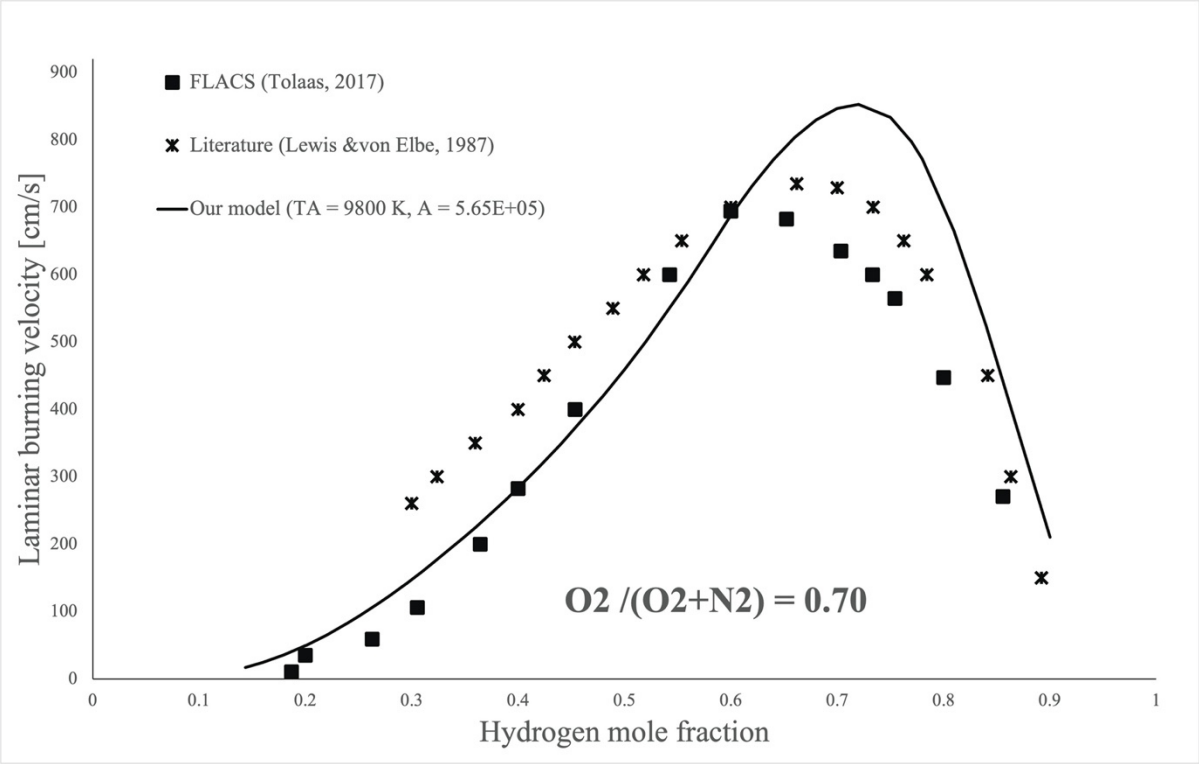

Figure 4.11: The laminar burning velocities as a function of x_{H2} in H_2 / O_2 / N_2 mixtures with $x_{O2} = 0.70$ vol% in the air

Figure 4.10 and Figure 4.11 presents laminar burning velocities in hydrogen and oxygen-enriched air mixtures. The predicted laminar burning velocity peaks at a higher hydrogen mole fraction compared with theoretical data for hydrogen and normal air mixtures. S_L^{max} comes with $x_{H2} = 54\ mol\%$ in Figure 4.10, and S_L^{max} comes with $x_{H2} = 72$ mol% in Figure 4.11. More oxygen involved in the combustion and the chemical reaction will reach the state of equilibrium in the higher hydrogen mole fraction. Therefore, the laminar burning velocity peaks at a higher hydrogen mole fraction correspondingly. The prediction model results in higher values of laminar burning velocities in hydrogen-rich mixtures comparing with literature data and the FLACS model results and lower values of laminar burning velocities predicted in hydrogen-lean mixtures. The prediction model gives the best agreement both with the FLACS model and the literature data for hydrogen-air mixtures with 35 $mol\%$ oxygen, as shown in Figure 4.10.

Therefore, it is recommended that oxygen concentration correction should be account for in the laminar burning velocity prediction model for hydrogen and oxygen-enriched air

mixtures. Figure 4.12 and Figure 4.13 show the laminar burning velocities comparison among FLACS model, literature data, prediction results based on Equation (4.3) and Equation (4.4). The cross and square marks refer to the literature data and FLACS model results of S_L. The black lines refer to the laminar burning velocities predicted with Equation (4.3). The red lines are on behalf of new model prediction results based on the Equation (4.4) as follows

$$S_L = \left[\alpha_{mix} * Le_{eff} * 2.14 * 10^5 * c_{H2}^{0.5} * c_{O2}^{1} * e^{-(9800/T_P)}\right]^{1/2} \qquad (4.4)$$

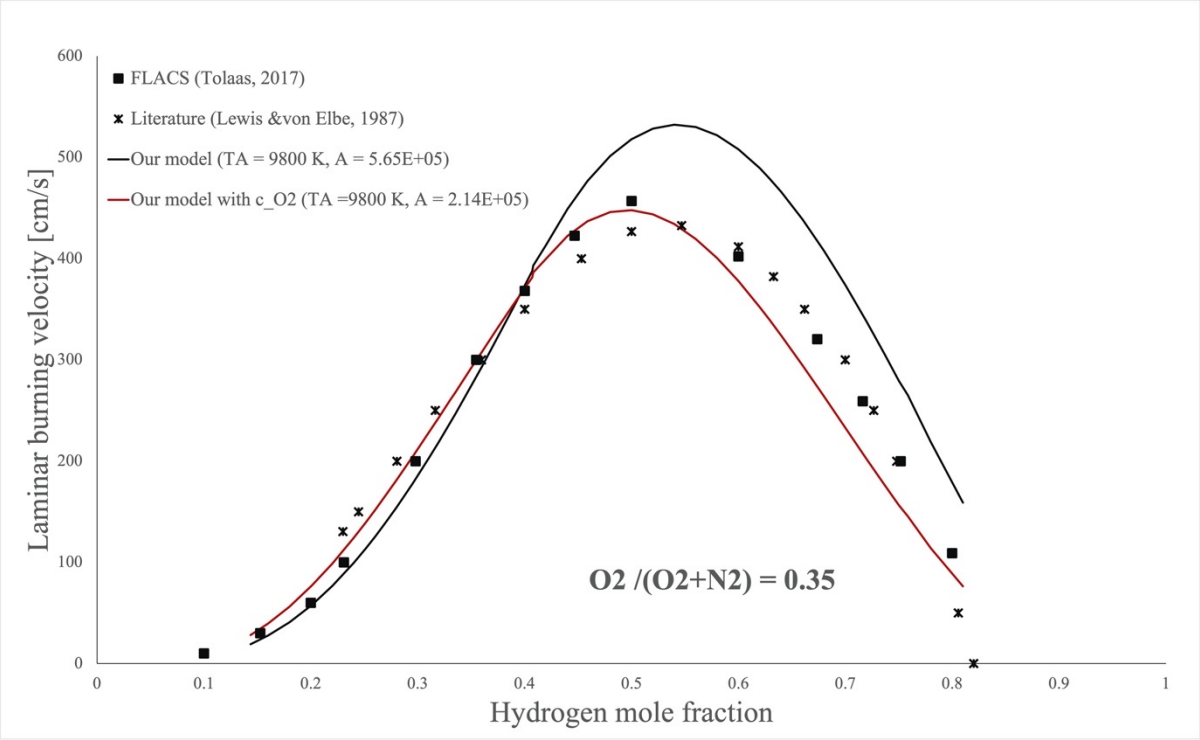

Figure 4.12: S_L comparison among literature data,
FLACS model and two prediction models
($x_{O2} = 0.35$ vol%)

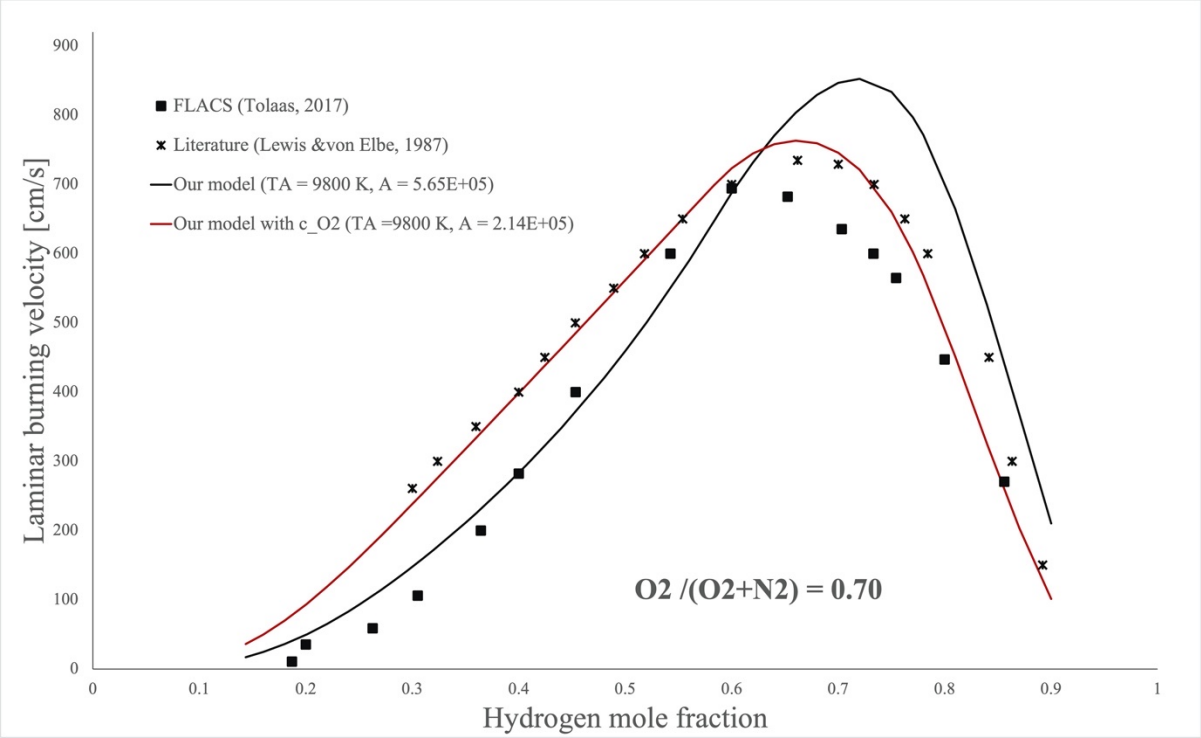

Figure 4.13: S_L comparison among literature data,
FLACS simulation and two prediction models
($x_{O2} = 0.70$ vol%)

In general, better agreement is observed both in Figure 4.12 and in Figure 4.13 between literature data and the prediction values of laminar burning velocity based on the new model, both in hydrogen lean mixtures and hydrogen-rich mixtures. Although lower values of predicted S_L are obtained in these two figures in hydrogen-rich mixtures compared with corresponding literature data, the deviation decreases with the increase of the molar concentration of oxygen in the air.

Figure 4.14 and Figure 4.15 show the predicted laminar burning velocities in mixtures of hydrogen and nitrogen diluted air in comparison with the FLACS model and the literature data. The predicted values result from Equation (4.3) for black lines and Equation (4.4) for red lines.

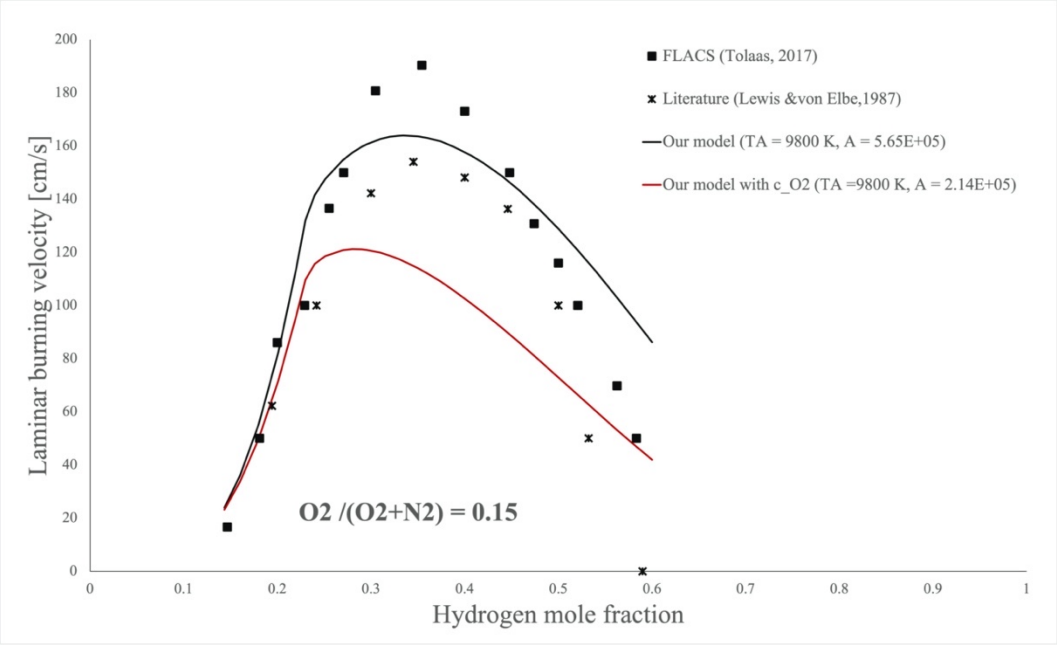

Figure 4.14: S_L comparison among literature data,
FLACS model and two prediction models
($x_{O2} = 0.15$ vol%)

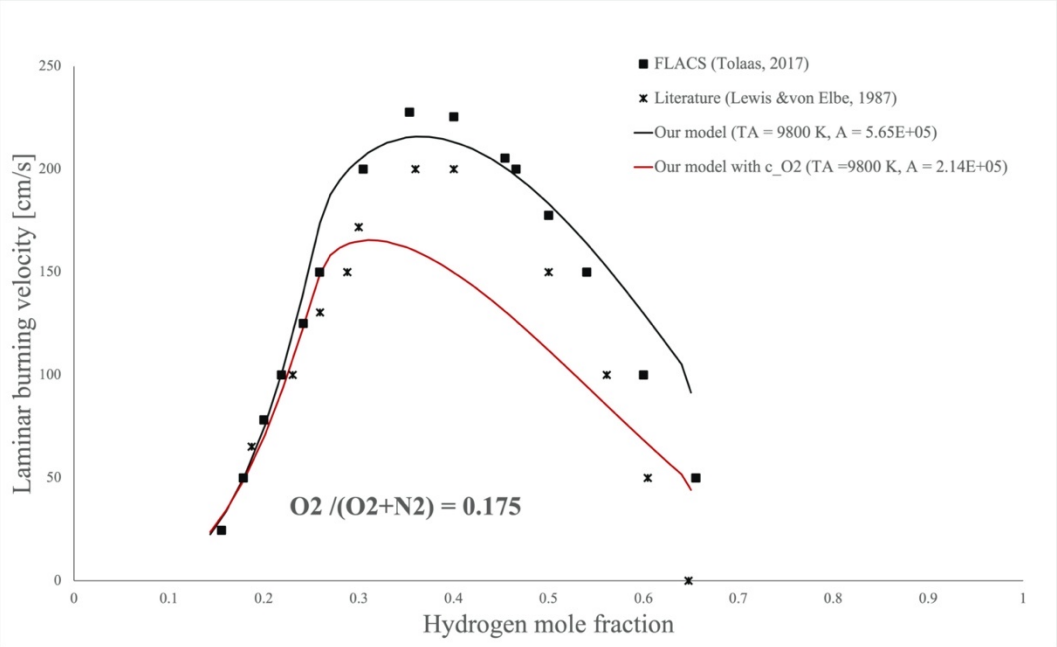

Figure 4.15: S_L comparison among literature data,
FLACS model and two prediction models
($x_{O2} = 0.175$ vol%)

In hydrogen-lean mixtures, the predicted laminar burning velocities resulting from the new model agree well both with the FLACS model and literature data as shown in these two figures. Distinctive deviation observed in hydrogen-rich mixtures among prediction values, FLACS model, and literature data due to the rapid decrease of oxygen concentration in the air.

To sum up, Equation (4.3) can be used to predict laminar burning velocities in hydrogen-air mixtures generally. Oxygen concentration is also recommended to improve prediction accuracy of laminar burning velocity in mixtures of hydrogen and oxygen-enriched air.

4.2 Turbulent burning velocity model

The laminar burning velocity model comparison results that combining with thermal diffusivity, Lewis number correction, and chemical time scale, the model of S_L give a higher accurate prediction. Consequently, the turbulent burning velocity model study below will focus on the prediction model involving Lewis number correction. The second equation listed in Table 3.14 is not valid in this study since the Lewis number correction is excluded from the prediction model of turbulent burning velocity. The third equation listed in Table 3.14 also is not valid here since the Lewis number correction is excluded from the prediction of laminar burning velocity. Therefore, the prediction model for turbulent burning velocity in hydrogen-air mixtures can be as follows

$$S_T = C_{ST} * C_K^{-\beta} * \left(u´\right)^{(1-1.5*\beta)} * \alpha^{0.5*\beta} * \tau_c^{-\beta} * l_I^{0.5*\beta} \quad (4.5)$$

S_T model comparison

To evaluate the effectiveness of the turbulent burning velocity model as expressed by Equation (4.5), the S_T prediction model is compared with the FLACS model and the experimental data from Kitagawa et al. (2008) at two turbulent fluctuation velocities and four equivalence ratios shown in Table 4.8. The turbulent length scale is 10 mm for experimental data and 1mm of length scale will be utilized in the S_T prediction model and the FLACS model.

Table 4.8: Experimental data of S_T for model comparison (Kitagawa et al., 2008)

ER	0.4	0.6	0.8	1.0
$u' = 0.8$	1.30	1.77	2.42	2.66
$u' = 1.59$	2.0	2.66	3.19	3.45

Table 4.9 shows the specification of parameters related to the FLACS model with expression as follows

$$S_T = C_{ST} * C_K^{-\beta} * u'^{(1-1.5*\beta)} * \left(\frac{S_L}{\sqrt{Le}}\right)^{2*\beta} * \sqrt{\frac{l_I}{\nu}}^{(0.5*\beta)} \quad (4.6)$$

Table 4.9: Parameters specification for FLACS model

Model	**Specification of parameter involving in the estimation of S_T**
FLACS	$C_{ST} = 0.875,\ \beta = 0.392$ $C_K = \sqrt{1/15}$, $\nu = \alpha = 2 * 10^{-5}$ Le varies with ER, as shown in Figure 2.10 and Figure 2.11

FLACS simulation includes temperature and pressure dependence factor when initial temperature and pressure differ from reference conditions, which are 293.15 K and 1 bar. S_T model comparison carries out at 298.15 K and 1 atm. Therefore, the effects of temperature and pressure on predicted turbulent burning velocity would also take into account the calculation based on the new prediction model. Assuming the temperature and pressure dependence dominated by chemical time scale since the magnitude of thermal diffusivity is 10^{-5}. Relevant constants for predicting turbulent burning velocity are listed in Table 4.10.

Table 4.10: Parameters specification for the prediction model

	C_{ST}	C_K	β	T_A	A
New model	2.5	$\sqrt{1/15}$	0.2	11000	$9.52 * 10^5$

The comparison results are shown in Figure 4.16 where the turbulent burning velocities are plotted with the equivalence ratio. The hollow symbols refer to burning velocities given by $u^{'} = 0.8\ m/s$, and the solids are S_T relative to $u^{'} = 1.59\ m/s$. The triangle, diamond, and circle represent turbulent burning velocities from the experiment, FLACS and prediction models.

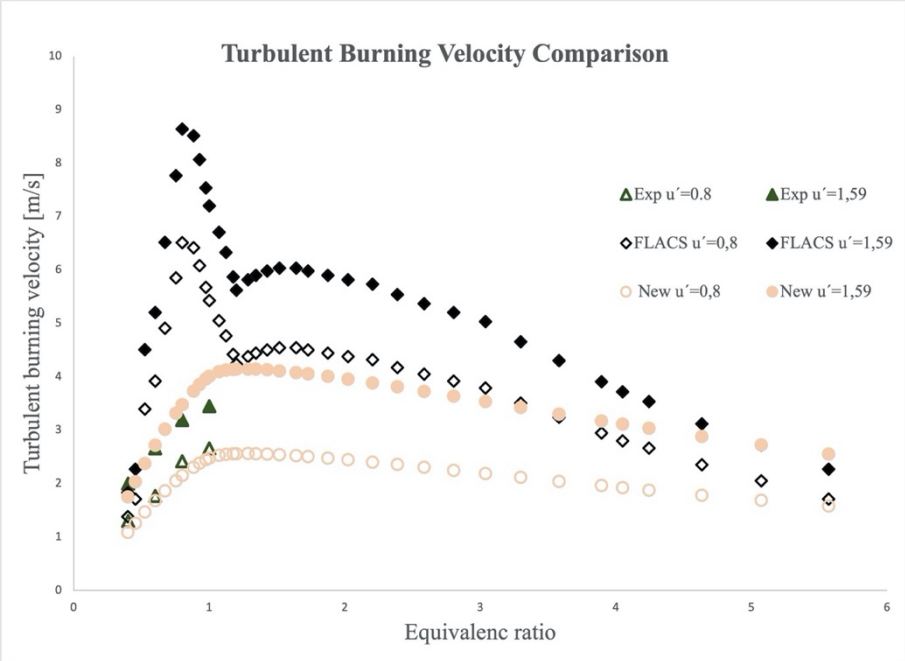

Figure 4.16: Turbulent burning velocity comparison among the new prediction model, the FLACS model and the experimental data

Compared with the present FLACS model results, better agreement is obtained between predicted turbulent burning velocities and experimental data. Three possible reasons for the distinct deviation between the FLACS model, experiments, and the new prediction model are listed below:

1. Inappropriate fixed value of thermal diffusivity utilized in FLACS for hydrogen. The thermal diffusivity for hydrogen-air mixtures is 2 to 4 times higher than the fixed value utilized in FLACS. As can be seen from equation (4.5), correct values will give lower burning velocity. The thermal diffusivity minimizes the thermal-diffusive effect on burning velocity. For hydrogen-air combustions, the thermal diffusive effect is crucial since it represents cellular flame formation related to increase of burning velocity resulting from flame instability. The new prediction model is a function of

thermal diffusivity, and it varies with equivalence ratio. As shown in Figure 4.1, it increases in lean mixtures. The burning rate increases since more gas mixtures are preheated, diffused into the lame front, and burned. In rich mixtures, it gradually stabilized, leading to stabilization of the flame and burning velocity decreases.

2. Inappropriate values for Lewis number correction are utilized in FLACS, as shown in Figure 2.10 and Figure 2.11. Le-correction enlarges burning velocity in hydrogen-lean mixtures and reduces burning velocity in hydrogen-rich mixtures. However, the Lewis number effect is avoided in the new prediction model for turbulent burning velocity.

3. The experiment values are from a small scale, and the turbulent flame may not be fully developed. The experimental values will then be lower than the fully developed flame.

Pressure dependence of prediction model for S_T

Kitagawa et al. (2008) also investigated the pressure dependence of turbulent burning velocity in their experiments. The experimental values of pressure exponent are positive for hydrogen, for example, 0.38 for $ER = 0.6$ and 0.18 for $ER = 1.0$. The new prediction model for turbulent burning velocity depends on thermal diffusivity and chemical time scale. The thermal diffusivity is inversely proportional to pressure with an exponent of -1, and the chemical time scale is proportional to pressure with an exponent of 0.93. Combined with exponent β shown in Equation (4.5), the new model results in positive pressure dependence of 0.086 for $\beta = 0.2$, 0.129 for $\beta = 0.3$, and 0.172 for $\beta = 0.4$ respectively. They are close to experimental values. Theoretically, laminar burning velocity increases with the rise of pressure, as described in section 2.3.3. Therefore, a positive pressure exponent seems more reasonable. However, the pressure exponent utilized in FLACS for hydrogen is -0.035 for laminar burning velocity. The pressure exponent for the turbulent burning velocity is a function of the pressure exponent of laminar burning velocity. The pressure exponent for the turbulent burning velocity is therefore -0.027 for hydrogen (from Equation 4.6), which is negative. Compared with the present FLACS model, better pressure dependence is obtained with the new prediction model. To sum up, Equation (4.5) can be used to predict turbulent burning velocities in hydrogen-air mixtures.

5 CONCLUSION

This chapter presents the conclusions and suggestion for the future works.

5.1 Conclusions

This thesis focuses on numerical models for predicting burning velocities especial in hydrogen-air mixtures. In the views of laminar burning velocity prediction, the numerical model for hydrogen-air combustion strongly depends on:

- Thermal diffusivity based on an effective thermal conductivity estimation model that varies with mole fraction of hydrogen through the combination of mole fraction weighted, and harmonic mole fraction weighted approaches.

- Lewis number correlation based on an effective Zeldovich number that varies with equivalence ratio through its dependence on product temperature and Lewis number related to hydrogen and oxygen.

- Chemical time scale based on fuel concentration, product temperature, activation temperature, and preexponential factor. In hydrogen-lean mixtures, the chemical time scale depends strongly on hydrogen concentration. In hydrogen-rich mixtures, oxygen concentration should also be accounted for to improve prediction accuracy.

In the view of turbulent burning velocity prediction, the Lewis number dependence can be avoided with the new prediction model. The chemical composition effect on the turbulent burning velocity is modelled with the reaction rate and thermal diffusivity instead of laminar burning velocity and Lewis number. This is a great improvement since it is very difficult to estimate the Lewis number for mixtures of hydrogen and hydrocarbons and at elevated pressures.

5.2 Future Directions

The following are recommendations or future improvements on the current work and recommendations for future study areas based on results presented in this thesis.

- An accurate power exponent for oxygen concentration should be found and utilized in the prediction model for laminar burning velocity in hydrogen-rich mixtures to improve the accuracy of S_L prediction.

- The prediction model for laminar burning velocity should be utilized in hydrocarbon-air mixtures, especially with thermal diffusivity and Lewis number varying with equivalence ratio. To see whether the model can be extended to all hydrocarbons for S_L prediction.

- The estimation model´s effectiveness for Lewis number related to hydrocarbons should be tested and utilized both in S_L and S_T prediction models aiming at disposing of Lewis number effect relative to turbulent burning velocity prediction.

- A good mixture rule should be found for mixtures of hydrogen and hydrocarbons. To see whether the model can be extended to hydrocarbon-air mixtures diluted with hydrogen.

BIBILOGRAPHY

Abdel-Gayed, R. G., Bradley, D., & Lawes, M. (1987). Turbulent burning velocities: A general correlation in terms of straining rates. *Proceedings the Royal of Society A: Mathematical and Physical Sciences*, 414(1847): 387-413.
DOI: https://doi.org/10.1098/rspa.1987.0150

Abdel-Gayed, R. G., Bradley, D., Lawes, M., & Lung, F. K. K. (1988). Premixed turbulent burning during explosions. *Symposium (International) on Combustion*, 21 (1): 497-504.
DOI: https://doi.org/10.1016/s0082-0784(88)80278-9

Arntzen, B. J. (1998). Modelling of Turbulent and Combustion for Simulation of Gas Explosions in Complex Geometries. PhD Thesis, The Norwegian Univeristy of Science and Technology.

Astbury, G. R., & Hawksworth, S. J. (2007). Spontaneous ignition of hydrogen leaks: A review of postulated mechanisms. *International Journal of Hydrogen Energy*. 32(13): 2178-2185. DOI: https://doi.org/10.1016/j.ijhydene.2007.04.005

Astbury, G.R. (2008). A Review of the Properties and Hazards of Some Alternative Fuels. *Process Safety and Environmental Protection*, 86(6): 397-414.
DOI: https://doi.org/10.1016/j.psep.2008.05.001

Bechtold, J. K., & Matalon, M. (2001). The Dependence of the Markstein Length on Stoichiometry. *Combustion and Flame*. 127 (1-2): 1906-1913.
DOI: https://doi.org/10.1016/50010-2180(01)00297-8

Bradley, D., Gaskell, P. H., Gu, X. J., & Sedaghat, A. (2005). Premixed flamelet modelling: Factors influencing the turbulent heat release rate source term and the turbulent burning velocity. *Combustion and Flame*, 143(3): 227-245.
DOI: https://doi.org/10.1016/j.combustflame.2005.05.014

Bradley, D., Haq, M. Z., Hicks, R. A., Kitagawa, T., Lawes, M., Sheppard, C. G. W., & Woolley, R. (2003). Turbulent burning velocity, burned gas distribution, and associated flame surface definition. *Combustion and Flame*, 33 (4): 415 – 430. DOI: https://doi.org/10.1016/S0010-2180(03)00039-7

Bradley, D., Lau, A. K.C., Lawes, M., & Smith, F.T. (1992). Flame stretch rate as a determinant of turbulent burning velocity. *Philosophical Transactions of the Royal Socirty A: Mathematical, Physical and Engineering Sciences*, 338(1650): 359-387. DOI: https://doi.org/10.1098/rsta.1992.0012

Bradley, D., Lawes, M., & Mansour, M. S. (2011b). Measurement of turbulent burning velocities in implosions at high pressures. *Proceedings of the Combustion Institute*, 33(1): 1269-1275. DOI: https://doi.org/10.1016/j.proci.2010.06.032

Bradley, D., Lawes, M., Kexin, L., & Mansour, M. S. (2013). Measurements and correlations of turbulent burning velocities over wide ranges of fuels and elevated pressures. *Proceedings of the Combustion Institute*, 34 (1): 1519-1526. DOI: https://doi.org/10.1016/j.proci.2012.02.060

Bjerketvedt, D., Bakke, J. R., & von Wingerden, K. (1993). Gas Explosion Handbook. Version 1.2. Bergen: Christian Michelsen Research. 225 p. (Report CMR-93-a25034).

Bjerketvedt, D., Bakke, J. R., & van Wingerden, K. (1997). Gas Explosion Handbook. Christian Michelsen Research AS. Bergen: *Journal of Hazardous Materials*, 52: 1-150.

Biennial Report on Hydrogen Safety. (2007). Combustion of Hydrogen. [online]: http://www.hysafe.org/BRHS

Chemical equilibrium calculator - colorado state university. [Online]: http://navier.engr.colostate.edu/code/code-4/index.html

Cracknell, R. F., Alcock, J. L., Rowson, J. J., Shirvill, L. C., & Ungut, A. (2002). Safety Considerations in Retailing Hydrogen. *Journal of Fuels and Lubricants*, pp. 922-926.

CRC Handbook of Chemistry and Physics. (1999). Thermal Physics. Cambridge, UK: Cambridge University Press. 71st edition, pp.372.

CRC Handbook of Chemistry and Physics. (2016-2017). Thermal Physics. Cambridge, UK: Cambridge University Press. 97th edition.

Davis S.G., & Searby, G. (2002). The use of counterflow flames for the evaluation of burning velocities and stretch effects in hydrogen/air mixtures, *Comb. Sci. Tech.*, 174(11-2): 93-110. DOI: https://doi.org/10.1080/13712944

Dahoe, A. E. (2005). Laminar burning velocities of hydrogen-air mixtures from closed vessel gas explosions. *Journal of Loss Prevention in the Process Industries*, 18(3): 152-166. DOI: https://doi.org/10.1016/j.jlp.2005.03.007

Dirrenberger P., Gall H. L., Bounaceur, R., et al. (2011). Measurements of Laminar Flame Velocity for Components of Natural Gas. *Energy and Fuels, American Chemical Society*, 25(9): 3875-3884. DOI: https://doi.org/10.1021/ef200707h

Dorofeev, S. B., Kuznetsov, M. S., Alekseev, V. I., Efimenko, A. A., & Breitung, W. (1999). Evaluation of Limits for Effective Flame Acceleration in Hydrogen Mixture. Scientific Report, Karlsruhe Research Center, FZKA 6349, IAE-6150/3, 1999.

Dorofeev, S. B., Kuznetsov, M. S., Alekseev, V. I., Efimenko, A. A., & Breitung, W. (2001). Evaluation of Limits for Effective Flame Acceleration in Hydrogen Mixture. [Online]: https://core.ac.uk/download/pdf/197567091.pdf

Eckhoff, R. K. (2016). Explosion hazards in the process industries. Elsevier: Amsterdam.

Egolfopoulos F. N., Hansen N., Ju Y., Kohse-höinghaus K., Law C. K., Qi F. (2014). Advances and Challenges in Laminar Flame Experiments and Implications for Combustion Chemistry. *Progr. Energy Combust Sci*, 43:36-67.

Engineering ToolBox, (2018). Hydrogen - Thermal Conductivity. [online]: https://www.engineeringtoolbox.com/hydrogen-H2-thermal-conductivity-temperature-pressure-d_2106.html

Frisch, U. (1996). Turbulence: The Legacy of A. N. Kolmogorov. *Cambridge University Press*, Cambridge.

Forman A. W. (1984). Combustion Theory. Princeton, New Jersey: The Benjamin/Cummings Publishing Company. 2nd ed.

Gasse, A. (1992). Experimentelle Bestimmung und Simulation von Explosionsgrenzen, untersucht an wasserstoffhaltigen Brenngasgemischen, Dissertation. Uni/GH Paderborn, Germany.

Glassman I, Richard A. Y., & Glumac, N. G. (2014). Combustion. Chapter 1 & Chapter 4, 5th edition, ISBN 978-0-12-407913-7.

Gexcon AS. (2019). FLACS v10.9 User´s Manual.

Gulder, O. (2007). Contribution of small scale turbulent to burning velocity of flamelets in the thin reaction zone regime. Proc. Combust. Inst. 31 (I): 1369-1375.

Helene Hisken. (2018). Investigation of instability and turbulence effects on gas explosions: experiments and modelling. PhD Thesis. University of Bergen.

Hermanns, R. T. E. (2007). Laminar burning velocities of methane-hydrogen-air mixtures. Figure 4.1 & Figure 4.2. Technische Universiteit Eindhoven.
DOI: https://doi.org/10.6100/IR630126

Hilsenrath, J., Beckett, C. W., Benedict, W. S., Fano, L., Hoge, H. J., et al. (1955). Tables of Thermal Properties of Gases. National Bureau of Standards Circular 564.

Ho, C. Y., Powell, R. W., & Liley, P. E. (1972). Thermal Conductivity of the Elements. *Journal of Physical and Chemcial Reference Data*, 1(2), 279-421.
DOI: https://doi.org/10.1063/1.3253100

Iijima, T., & Takeno, T. (1986). Effects of temperature and pressure on burning velocity. *Combustion and Flame*, 65:35-43.

International Energy Agency (IEA). (2019). The Future of Hydrogen – Seizing today´s opportunities. Japan. [online]: https://www.iea.org/reports/the-future-of-hydrogen

Joulin, G., & Mitani, T. (1981). Linear stability analysis of two-reactant flames. *Combustion and Flame*, 40, 235-246. DOI: https://doi.org/10.1016/0010-2180(81)90127-9

Jackson, T. L. (1987). Effect of Thermal Expansion on the Stability of Two-Reactant Flames. *Combustion Science and Technology*, 53(1), 51-54.
DOI: https://doi.org/10.1080/00102208708947018

Jim Farris. (2010). A simple image of spin isomers of molecular hydrogen.
[online]: https://commons.wikimedia.org/wiki/File:Spinisomers_of_molecular_hydrogen.png

Kitagawa, T., Nakahara, T., Maruyama, K., Kado, K., Hayakawa, A., & Kobayashi, S. (2008). Turbulent burning velocity of hydrogen-air premixed propagating flames at elevated pressures. International Journal of Hydrogen Energy, 33(20): 5842–5849
DOI: https://doi.org/10.1016/j.ijhydene.2008.06.013

Krejci, M. C., Mathieu, O., Vissotski, A. J., Ravi, S., Sikes, T. G., & Petersen, E. L. (2013). Laminar Flame Speed and Ignition Delay Time Data for the Kinetic Modelling of hydrogen and Syngas Fuel Blends. Journal of Engineering for Gas Turbines and Power.
DOI: https://doi.org/10.1115/1.4007737

Kwon, O.C., & Faeth, G.M. (2001). Flame stretches interactions of premixed hydrogen-fuelled flames: measurements and predictions, *Comb. Flame*, 124(4), 590-610.

Kuznetsov, M., Kobelt, S., Grune, J., & Jordan, T. (2012). Flammability limits and laminar flame speed of hydrogen-air mixture at sub-atmospheric pressures. International Journal of Hydrogen Energy, 37:17580-17588.

Law, C. K. (2006). Combustion Physics. Cambridge University Press.

Law, C. K. (2010). Combustion Physics. Cambridge University Press.

Lewis B., & von Elbe, G. (1934). Determination of the Speed of Flames and the Temperature Distribution in a Spherical Bomb from Time-Pressure Explosion Records. *J Chem Phys*, 2(5): 283–90.

Lewis, B. & von Elbe, G. (1987). Combustion, Flames and Explosions of Gases, Academic Press, INC., 3rd ed., pp. 396.

Liu, D., & MacFarlane, R. (1983). Laminar burning velocities of hydrogen-air and hydrogen-air-steam flames. *Combustion and Flame*, 49 (1-3): 59-71.
DOI: https://doi.org/10.1016/0010-2180(83)90151-7

Maha Ibrahim Ahmed Eleryan. (2020). Methodology Options for Hydrogen Safety Analysis. Master Thesis. University of Stavanger.

Maher Al-baghdadi. (2020). An Overview of hydrogen as an Alternative Fuel. [online]: https://www.researchgate.net/publication/342067663_An_Overview_of_Hydrogen_as_an_Alternative_Fuel/stats

Mathur, S., Tondon, P. K., & Saxena, S. C. (1967). Thermal conductivity of binary, ternary and quaternary mixtures of rare gases. *Molecular Physics: An International Journal at the Interface Between Chemistry and Physics*, 12(6): 569-579.

Middha, P. (2010). Development, use and validation of the CFD tool FLACS for hydrogen safety studies. PhD Thesis. University of Bergen.

Mukhopadhyay, P., Gupta, A. D., & Barua, A. K. (1967). Thermal conductivity of hydrogen-nitrogen and hydrogen-carbon-dioxide gas mixtures. *British Journal of Applied Physics*, 18(9), 1302-1306. DOI: https://doi.org/10.1088/0508-3443/18/9/312

Nambauer, M., Hasslnerger, J., Chakraborty, N., & Klein, M. (2020). Vortex Dynamics and Fractal Structures in Reactive Richtmyer-Meshkov Instability. Conference proceedings.

Patankar, S. V., & Spalding, D. B. (1972) A Calculation Procedure for Heat, Mass and Momentum Transfer in Therr-Dimensional Parabolic Flows. International Journal of Heat and Mass Transfer, 15 (10): 1787-1806. DOI: https://doi.org/10.1016/0017-9310(72)90054-3

Pareja, J., Burbano, H. J., & Ogami, Y. (2010). Measure of the laminar burning velocity of hydrogen-air premixed flames. International Journal of Hydrogen Energy, 35: 1812-1818. DOI: https://doi.org/10.1016/j.ijhydene.2009.12.031

Rallis, C. J., & Garforth, A. M. (1980). The Determination of Laminar Burning Velocity. Prog. Energy Combust. Sci. 6:303-329.

Risto Lautkaski. (1997). Understanding vented gas explosions. VTT Research Notes 1812. [online]: https://www.osti.gov/etdeweb/servlets/purl/591688

Schroeder, V. (2003). Explosionsgrenzen vo Wasserstoff und Wasserstoff/Methan-Gemischen. BAM Research Report No.253, NW-Verlag, Bremerhaven.

Sivashinsky, G. I. (1983). Instabilities, pattern formation, and turbulence in flames. *Ann. Rev. Fluid Mech.*, 15(1): 179-199.

Taylor, S. C. (1991). Burning Velocity and The Influence of Flame Stretch. PhD Thesis. The University of Leeds.

Tolaas, J. (2017). Construction and Evaluation of a Temperature Dependent Laminar Burning Velocity Model for Inerted Hydrogen, Methane and Carbon Monoxide Mixtures. Master Thesis, University of Bergen.

Tse, S. D., ZHU, D. L. & Law. C. K. (2000). Morphology and Burning Rate of Expanding Spherical Flames in H2/O2/N2 Inert Mixture up to 60 Atmospheres. *Proceedings of the Combustion Institute*, 28: 1793-1800.

Turns, S. R. (1999). An Introduction to Combustion. ISBN 0-07-230096-5.

Verhelst, S., Woolley, R., Lawes, M., & Sierens, R. (2005). Laminar and unstable burning velocities and Markstein lengths of hydrogen-air mixtures at engine-like conditions. *Proceedings of the Combustion Institute*, 30: 209-216.
DOI: https://doi.org/10.1016/j.proci.2004.07.042

Versteeg, V., & Malalasekera, W. (2007). An introduction to computational fluid dynamics: The finite volume method. Pearson Education Limited, 2nd edition, Chapter 2.8.

Veynante, D., & Vervish, L. (2002). Turbulent combustion modelling. *Progress in Energy and Combustion Science*, 28:193-266.

Woolley, H., Scott, R. B., and Brickwedde, F. (1948). Compilation of thermal properties of hydrogen in its various isotopic and ortho-para modifications. *Journal of research of the National Bureau of Standards*, 41(5): 379-475.

Wright Air Development Division Technical Report. (1960).

Appendix A

Literature data for thermal conductivity of hydrogen, oxygen, and nitrogen present in this section.

T [K]	λ_{H2} $[mW/m \cdot K]$
20	15.9
25	19.3
30	22.7
35	26.1
40	29.4
45	32.8
50	36.1
60	42.6
70	48.9
80	55.2
90	61.4
100	67.6
110	73.8
120	80.1
130	86.4
140	92,6
150	98.6
160	104.6
170	110.5
180	116.4
190	122.2
200	128.0
210	133.8
220	139.5
230	145.1
240	150.6
250	156.0
260	161.3
270	166.5
280	171.7
290	176.7
300	181.5

T [K]	λ_{O2} $[mW/m \cdot K]$
90	8.13
100	9.05
110	9.98
120	10.92
130	11.87
140	12.81
150	13.76
160	14.66
170	15.56
180	16.46
190	17.35
200	18.24
210	19.11
220	19.97
230	20.83
240	21.68
250	22.54
260	23.39
270	24.24
280	25.09
290	25.92
300	26.74

T [K]	λ_{N2} $[mW/m \cdot K]$
77.24	7.17
78	7.45
80	7.62
90	8.52
100	9.41
110	10.30
120	11.19
130	12.08
140	12.96
150	13.85
160	14.74
170	15.62
180	16.51
190	17.39
200	18.26
210	19.08
220	19.89
230	20.67
240	21.45
250	22.22
260	22.98
270	23.74
280	24.49
290	25.24
300	25.98

Appendix B

Literature data for specific heat capacity of hydrogen, oxygen, and nitrogen present in this section.

T [K]	C_{p-H2} $[cal/g \cdot K]$
30	2.5904
40	2.5274
50	2.5067
60	2.5076
70	2.5283
80	2.5678
90	2.6200
100	2.6831
120	2.8211
140	2.9532
160	3.0665
180	3.1602
200	3.2351
220	3.2933
240	3.3396
260	3.3761
270	3.3899
280	3.4017
300	3.4204

T [K]	C_{p-O2} $[cal/g \cdot K]$
120	0.22145
130	0.22054
140	0.21995
150	0.21950
160	0.21919
170	0.21894
180	0.21875
190	0.21862
200	0.21853
210	0.21848
220	0.21847
230	0.21850
240	0.21857
250	0.21868
260	0.21883
270	0.21902
280	0.21926
290	0.21954
300	0.21985

T [K]	C_{p-N2} $[cal/g \cdot K]$
100	0.24887
110	0.24873
120	0.24864
130	0.24858
140	0.24853
150	0.24850
160	0.24848
170	0.24845
180	0.24843
190	0.24842
200	0.24841
210	0.24841
220	0.24841
230	0.24840
240	0.24841
250	0.24841
260	0.24841
270	0.24843
280	0.24845
290	0.24848
300	0.24851

Appendix C

Detailed formula derivation for calculation of molar concentration of H_2 in air in this section.

In general, molar concentration is a measure of the concentration of a chemical species in a solution, in terms of amount of this species in moles per unit volume of solution. Thus, hydrogen molar concentration in air can be expresses as follows

$$c_{H2} = \frac{amount\ of\ H_2\ in\ moles}{total\ volume\ of\ solution} = \frac{n_{H2}}{V_{total}} \quad \text{(A.1)}$$

with n_{H2} refers to the amount of hydrogen in moles, and it defined as the ratio of the amount of hydrogen in mass to molar mass of hydrogen. Thus, the expression of hydrogen molar concentration can be updated as follows

$$c_{H2} = \frac{m_{H2}/M_{H2}}{V_{total}} = \frac{m_{H2}}{V_{total}} * \frac{1}{M_{H2}} \quad \text{(A.2)}$$

Combined with $m_{H2} = \rho_{H2} * V_{H2}$, the hydrogen molar concentration can be expressed as function of its density, its molar masse, and its volumetric fraction as follows

$$c_{H2} = \frac{\rho_{H2} * V_{H2}}{M_{H2} * V_{total}} = \frac{\rho_{H2}}{M_{H2}} * \frac{V_{H2}}{V_{total}} = \frac{\rho_{H2}}{M_{H2}} * x_{H2} \quad \text{(A.3)}$$

The ideal gas law is often written in an empirical form as follows

$$p * V = n * R * T \quad \text{(A.4)}$$

Assuming that the ideal law is valid for hydrogen, and therefore

$$p * V_{H2} = n_{H2} * R * T \rightarrow \frac{p}{(R*T)} = \frac{n_{H2}}{V_{H2}} = \frac{\rho_{H2}}{M_{H2}} \quad \text{(A.5)}$$

Combined with Equation (A.3) with (A.5), molar concentration of hydrogen in the air can be calculated with the formula as follows

$$c_{H2} = x_{H2} * \frac{p}{(R*T)} \quad \text{(A.6)}$$

Appendix D

Detailed formula derivation for estimation of turbulent burning velocity in hydrogen-air mixtures present in this section.

Combined with Equation (2.15) and Equation (2.16), the Karlovitz strain rate can be expressed as function of turbulent fluctuation velocity, laminar burning velocity, integral length scale, and kinematic viscosity as follows

$$K = C_K * \left(\frac{u'}{S_L}\right)^2 * \left(\frac{u' * l_I}{\nu}\right)^{-0.5} = C_K * u'^{1.5} * S_L^{-2} * l_I^{-0.5} * \nu^{0.5} \quad \text{(A.7)}$$

Setting Equation (A.7) into Equation (2.14), the turbulent burning velocity can be expressed, based on Bray (1990) model, as follows

$$\begin{aligned} S_T &= C_{ST} * u' * (C_K * u'^{1.5} * S_L^{-2} * l_I^{-0.5} * \nu^{0.5})^{-\beta} \\ &= C_{ST} * C_K^{-\beta} * (u')^{(1-1.5*\beta)} * S_L^{2*\beta} * l_I^{0.5*\beta} * \nu^{(-0.5*\beta)} \end{aligned} \quad \text{(A.8)}$$

Setting Equation (A.7) into Equation (2.17), the turbulent burning velocity can be expressed, based on Bradley et al. (1992) model, as follows

$$\begin{aligned} S_T &= C_{ST} * u' * (C_K * u'^{1.5} * S_L^{-2} * l_I^{-0.5} * \nu^{0.5} * Le)^{-\beta} \\ &= C_{ST} * C_K^{-\beta} * (u')^{(1-1.5*\beta)} * S_L^{2*\beta} * l_I^{0.5*\beta} * \nu^{(-0.5*\beta)} * Le^{(-\beta)} \end{aligned} \quad \text{(A.9)}$$

The laminar burning velocity can be expressed either as function of thermal diffusivity and chemical time scale or as function of thermal diffusivity, Lewis number and chemical time scale. Equation (2.6) describes the former relation among S_L, α and τ_c. Combined with Equation (A.8), the equation for estimating turbulent burning velocity can be updated, based on Bray (1990) model, as follows

$$S_T = C_{ST} * C_K^{-\beta} * (u')^{(1-1.5*\beta)} * \alpha^{\beta} * \tau_c^{-\beta} * l_I^{0.5*\beta} * \nu^{(-0.5*\beta)} \quad \text{(A.10)}$$

Combined Equation (2.6) and Equation (A.9), the equation for estimating turbulent burning velocity can be updated, based on Bradley et al. (1992) model, as follows

$$S_T = C_{ST} * C_K^{-\beta} * \left(u^{'}\right)^{(1-1.5*\beta)} * \alpha^{\beta} * \tau_c^{-\beta} * l_I^{0.5*\beta} * \nu^{(-0.5*\beta)} * Le^{(-\beta)} \qquad \text{(A.11)}$$

Equation (2.10) describes the latter relation among S_L, α, Le and τ_c. Combined with Equation (A.8), the equation for estimating turbulent burning velocity can be updated, based on Bray (1990) model, as follows

$$S_T = C_{ST} * C_K^{-\beta} * \left(u^{'}\right)^{(1-1.5*\beta)} * \alpha^{\beta} * Le^{\beta} * \tau_c^{-\beta} * l_I^{0.5*\beta} * \nu^{(-0.5*\beta)} \qquad \text{(A.12)}$$

Combined Equation (2.10) and Equation (A.9), the equation for estimating turbulent burning velocity can be updated, based on Bradley et al. (1992) model, as follows

$$S_T = C_{ST} * C_K^{-\beta} * \left(u^{'}\right)^{(1-1.5*\beta)} * \alpha^{\beta} * \tau_c^{-\beta} * l_I^{0.5*\beta} * \nu^{(-0.5*\beta)} \qquad \text{(A.13)}$$

Equation (A.13) equals Equation (A.10). Therefore, there are totally three equations related to predict turbulent burning velocity.